TITLE PAGE

Report Title: LOW-ENGINE-FRICTION TECHNOLOGY FOR ADVANCED NATURAL-GAS RECIPROCATING ENGINES

Annual Technical Progress Report

Reporting Period: June 1, 2004 – June 30, 2005

for

DoE Cooperative Agreement No. DE-FC26-02NT41339

Submitted by

Victor Wong, Tian Tian, Luke Moughon, Rosalind Takata, Jeffrey Jocsak

Massachusetts Institute of Technology
Room 31-155, 77 Massachusetts Avenue
Cambridge, MA 02139

September 30, 2005

Sub-Contractor
Colorado State University
Fort Collins, CO 80523
Brian Willson, Rudy Stanglmaier, Ted Bestor, Kirk Evans, Kris Quillen

Submitted to:

NETL AAD Document Control Building 921
Department of Energy
National Energy Technology Laboratory
P.O. Box 10940
Pittsburgh, PA 15236-0940

DISCLAIMER

ABSTRACT

This program aims at improving the efficiency of advanced natural-gas reciprocating engines (ANGRE) by reducing piston and piston ring assembly friction without major adverse effects on engine performance, such as increased oil consumption and wear. An iterative process of simulation, experimentation and analysis is being followed towards achieving the goal of demonstrating a complete optimized low-friction engine system. To date, a detailed set of piston and piston-ring dynamic and friction models have been developed and applied that illustrate the fundamental relationships between design parameters and friction losses. Low friction ring designs have already been recommended in a previous phase, with full-scale engine validation partially completed.

Current accomplishments include the addition of several additional power cylinder design areas to the overall system analysis. These include analyses of lubricant and cylinder surface finish and a parametric study of piston design. The Waukesha engine was found to be already well optimized in the areas of lubricant, surface skewness and honing cross-hatch angle, where friction reductions of 12% for lubricant, and 5% for surface characteristics, are projected. For the piston, a friction reduction of up to 50% may be possible by controlling waviness alone, while additional friction reductions are expected when other parameters are optimized. A total power cylinder friction reduction of 30-50% is expected, translating to an engine efficiency increase of two percentage points from its current baseline towards the goal of 50% efficiency.

Key elements of the continuing work include further analysis and optimization of the engine piston design, in-engine testing of recommended lubricant and surface designs, design iteration and optimization of previously recommended technologies, and full-engine testing of a complete, optimized, low-friction power cylinder system.

Table of Contents

LIST OF FIGURES

LIST OF TABLES

LOW-ENGINE-FRICTION TECHNOLOGY FOR ADVANCED NATURAL-GAS RECIPROCATING ENGINES

Annual Technical Progress Report
Reporting Period: June 1, 2004 – June 30, 2005
Massachusetts Institute of Technology
DoE Cooperative Agreement No. DE-FC26-02NT41339

EXECUTIVE SUMMARY

This program aims to improve the efficiency of advanced natural-gas reciprocating engines (ANGRE) by reducing piston and piston ring assembly friction without major adverse effects on engine performance, such as increased oil consumption and wear. The approach is to apply or adapt existing computer models to evaluate the friction reduction potential of power-cylinder component design, surface treatment, and lubrication concepts. The promising low-friction candidate design concepts are validated experimentally on a full-size large-bore natural-gas engine at Colorado State University (CSU). Waukesha Engine Dresser, Inc. provides the engine, parts, and engineering support for the program.

The program has several major tasks, as shown in the Milestones chart, summarized as follows. Two of the tasks were previously reported. (1) The assessment of friction reduction opportunities, and design and recommendation of friction-reducing ring-pack designs. (2) Testing of these designs, which is currently being completed with an improved test rig. Remaining tasks include: (3) Analyze piston design parameters and recommend friction-reduction techniques; (4) Analyze lubricant and surface finish effects in the power cylinder, for friction reduction possibilities; (5) Test and demonstrate recommended concepts in Waukesha engine; (4) Analyze test results and iterate on initial recommendations; (6) Analyze test results and iterate on initial recommendations; (7) Demonstrate complete low-friction system, incorporating all recommendations. This reporting period focused primarily on tasks (3) and (4), with analyses completed in all areas.

Three analyses have been completed in this reporting period: an analysis of the effects of lubricant viscosity on ring-pack friction, one on the effects of liner surface texture on ring-pack friction, and one on the effects of several piston design parameters on piston friction losses. The lubricant and surface finish analyses initially focused on the ring-pack, and will be expanded to include the piston. The lubricant analysis studied the effects of mean viscosity as well as viscosity variation during the engine cycle. It was found that a reduced viscosity lubricant can reduce frictional losses in the Waukesha engine, with controlled viscosity variation further reducing losses for a total reduction of ~12%. Specific recommendations from the liner finish study were reductions in both skewness and honing cross-hatch angle. Although the Waukesha engine is already well optimized in surface skewness and cross-hatch angle, further friction reduction of ~5% is expected. In the case of the piston, a friction reduction of up to 50% is predicted for reducing skirt waviness alone. Further reductions are expected when the skirt profile, skirt/liner clearance, and other parameters are optimized.

The modeling and analysis efforts were on schedule. Existing friction, ring dynamics, and lubrication models have been adapted to the large-engine configurations. The analyses were applied to a Waukesha F18 VGF engine, in-line 6-cylinder [152 mm bore, 165 mm stroke], 18-liter natural gas SI engine. These detailed studies illustrated the fundamental relationships between design parameters and friction losses. Results indicate that a combined power cylinder friction reduction of 30-50% is possible, corresponding to ~2% increase in engine efficiency. As planned, strategies and guidelines have been developed for optimized lubricant, surface finish, and piston parameters.

The project team participated in the following conferences: The ASME-ICED 2004 Fall and 2005 Spring Conferences in Long Beach (Oct 2004) and in Chicago (April 2005), respectively, in which specific ARES/ARICE tracks were held. In addition, we initiated an Industry-University Workshop on Low-Engine Friction in collaboration with Purdue University, in which all major manufacturers of ARES engines participated with strongly supporting feedback. The Principal Investigator also participated in the 2nd Annual Advanced Stationary Reciprocating Engines Conference, organized by ARES/ARICE. Five technical papers have been peer-reviewed and published: at CIMAC Congress 2004 (1 paper), ASME-ICED Fall 2004 (2), SAE Powertrain and Fluid Systems Conference Oct 2004 (1), and ASME-ICED Spring 2005 (1). MIT, CSU and Waukesha also continue to hold monthly conference calls to maintain communication on testing progress and procedures as well as gain guidance from industry experts. Semi-annual meetings between MIT, CSU and Waukesha also help to maintain contact and communication between research, testing and industry groups. We aim at even further enhancing our interactions with industry and others in the ARES community, including universities and national laboratories in the coming year.

This current Annual Report covers progress through June 2005 and focuses on the three analyses described: lubricant and cylinder liner surface properties, with respect to the piston rings, and piston design parameters.

For the next reporting period, through June 2006, further analysis, in-engine testing, and design iteration will be continued. Team discussions will be held to ensure that the potential for power cylinder improvements will be fully and practically explored. Key elements of the continuing work include further analysis and optimization of the engine piston design, in-engine testing of recommended lubricant and surface designs, design iteration and optimization for previously recommended technologies, and full-engine testing of a complete, optimized, low-friction power cylinder system. Specifically, tasks will include (1) Expanded analysis of piston friction, including the effects of piston skirt material, rigidity (material compliance or stiffness matrix) and lubricant parameters (2) Combined piston and ring analysis of liner surface effects and recommendation of low-friction liner texture (3) System analysis of lubricant effects and recommendation and testing of optimized lubricant (4) Analysis of ring-pack testing (currently being completed at CSU) results and possible design iteration (5) System analysis of lubricants, mechanical design, and materials as an integrated system for overall friction reduction, and (6) Experimental validation and demonstration of the next phase of a low-friction system.

LOW-ENGINE-FRICTION TECHNOLOGY FOR ADVANCED NATURAL-GAS RECIPROCATING ENGINES
Annual Technical Progress Report
(June 1, 2004 – June 30, 2005)
DoE Cooperative Agreement No. DE-FC26-02NT41339

I. INTRODUCTION

A. Objectives

Parasitic losses of advanced natural gas reciprocating engines (ANGRE) will be lowered, by reducing friction in the power cylinder (piston and ring-pack). Computer models will be evolved to assess the opportunities of piston and piston ring-pack design, surface finish, and lubrication strategies aimed at friction minimization. Fundamental design parameters and performance relationships will be investigated to reduce friction, without causing adverse effects such as increased wear and oil consumption. The analysis will be accompanied by experimental validation. This will be accomplished through systematic analysis of experimental data sets, providing recommendations of promising low-friction piston/ring-pack/lubricant options, and actual testing and demonstration in an ANGRE engine.

B. Scope of Work

A combined analytical and experimental program is undertaken. The scope of work includes evaluating the performance and design of current large-bore natural gas engine and power cylinder components, and modifying or adapting existing analytical tools for ANGRE applications. Computer modeling and analysis will be used to understand and to optimize friction reduction concepts. Concept validation will be conducted experimentally on a Waukesha VGF engine; concurrent computer parametric studies on design parameters will be performed and validated by engine tests. Testing will be done at Colorado State University.

C. Tasks to Be Performed

The program has several major tasks, as shown in the following Milestones chart, two of which have been completed and presented in the previous reporting period. These tasks related to the assessment of friction reduction opportunities, and to the design and recommendation of friction-reducing ring-pack designs. Testing of these designs has been partially completed. Remaining tasks include: (1) Analyze piston design parameters and recommend friction-reduction techniques; (2) Analyze lubricant and surface finish effects in the power cylinder, for friction reduction possibilities; (3) Test and demonstrate recommended concepts in a Waukesha engine; (4) Analyze test results and iterate on initial recommendations; (5) Demonstrate complete low-friction system, incorporating all recommendations. This reporting period focused primarily on tasks (1) and (2), with analyses completed in all areas (see sections 4-6 of this report).

D. Major Accomplishments

In brief, the major accomplishments to date include the following:

- Developed/adapted computer simulations for piston and ring-pack friction applicable to ANGRE engines.
- Improved liner roughness model to better assess friction reduction potential through changes in liner design.
- Liner texture model shows a friction reduction of ~5% for the Waukesha engine ring-pack, with reduced skewness and honing cross-hatch angle
- Lubricant analysis shows friction reduction of ~12% for the Waukesha engine ring-pack, for optimum lubricant parameters
- Piston analysis shows possible friction reductions of 50% or more, with control of piston profile and other piston design parameters.

E. Current Status

Three studies focusing on reducing friction in the Waukesha power cylinder have been completed: one on the effects of lubricant properties, one on cylinder liner finish, and one on piston parameters. Recommendations are made for engine and lubricant parameters based on these studies, which will be validated in actual engine testing during the next phase, and then followed by design iterations. A cooperative partnership has been begun with a large lubricant manufacturer to design and provide lubricants for future testing.

Opportunities to further reduce friction have also been identified. Additional piston parameters will be considered, including the skirt stiffness, as well as surface and lubricant effects. Also, surface textures that have not yet been considered may be of interest, possibly including micro-dimples which may have the potential to greatly reduce engine friction. Combining mechanical design of the piston, rings, lubricant and material selection in a systems approach will produce multiplicative benefits and further improve engine efficiency. These opportunities will be addressed in the next phase of the program.

F. Report Outline

This report presents three parallel investigations of sources of friction in the power cylinder of a reciprocating engine - lubricant formulation, liner surface finish (with respect to the rings), and piston design. The next section of this report, RESULTS AND DISCUSSION contains 7 subsections, beginning with an overview of the power cylinder system in Section 1, and an introduction to the fundamentals of friction and lubrication in the piston and ring pack in Section 2. Section 3 presents a brief description of the Waukesha engine under study, and of major sources of friction within that particular engine. Section 4 presents an analysis of the effects of lubricant viscosity on ring friction, including temperature and shear-rate dependence, and several idealized cases. Section 5 presents an analysis of several liner surface textures and their effect on friction, surface parameters studied include roughness, skewness, and honing cross-hatch angle. Section 6 presents a parametric analysis of piston/liner friction and the effects of several piston design parameters. Section 7 presents experimental results of low-friction ring designs proposed in the previous reporting period.

PROJECT MILESTONE PLAN DoE Form 4600.3

(Low Engine Friction Technology for Advanced Natural Gas Reciprocating Engines)

Milestone Plan Period: October 1, 2004 – September 30, 2006

#	MAJOR TASKS
3	Design & Performance Analysis
3.1	(a) Piston analyses for improved piston friction reduction
3.2	(b) Perform parametric and system analyses to include effects of material, surface characteristics such as roughness, wear trends, and lubricant
3.3	(c) Recommend low-friction design options for ring/piston, material, and lubricant systems.
4	**Demonstrate Optimal Design Concepts**
4.1	Establish Baseline Tests (Done)
4.2	Validate effects of individual component design parameter changes to include piston, material, &
4.3	Demonstrate complete low-friction engine system with aggregate improvements
5	**Analyze Test Results of Additional System Parameters (Piston, Material, & Lube); Iterate**
6	**Manage Reporting & Education**
6.1	Prepare periodic reviews and reports
6.1.1	- Monthly team telephone conferences
6.1.2	- Deliver annual reports
6.1.3	- Deliver final report

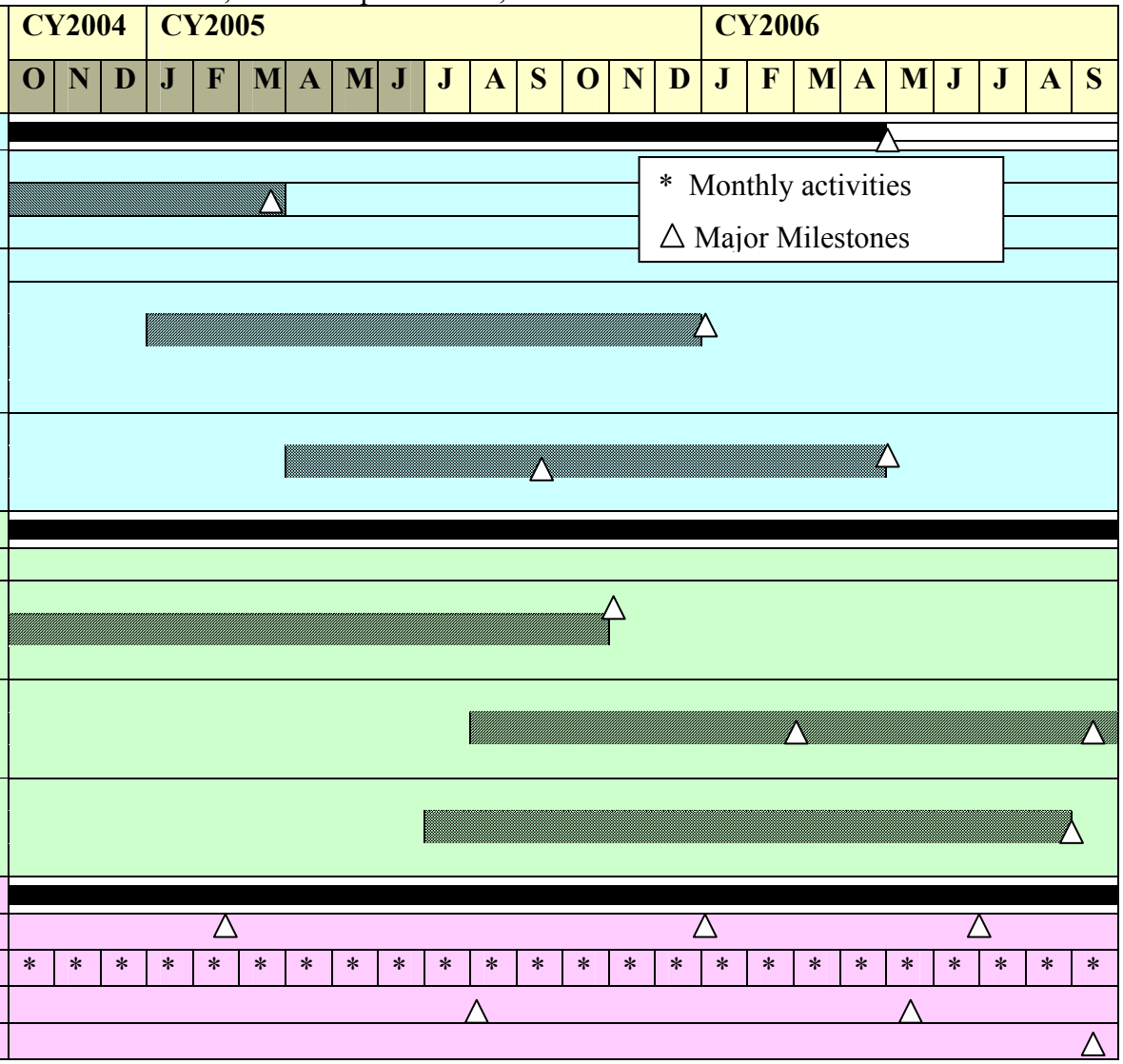

II. RESULTS AND DISCUSSION

(A) MODEL CONCEPTS: DESIGN AND PERFORMANCE ANALYSIS

1. Introduction to the Model Concepts

1.1. Overview

MIT's computer models [1,2,3,4,5] have been applied to target the most important contributors to friction in the piston-cylinder assembly of the engine. The specific models used to analyze the behavior of the piston and piston rings are described in some detail in the section that follows. Previous results from using the models resulted in recommendations for piston-ring geometry, to reduce ring friction [6,7]. In this stage, the models have been used for parametric studies on lubricant and surface parameters for the rings, as well as for piston design parameters. Strategies for design changes to reduce friction contributions from these sources are suggested in the sections that follow. In the months ahead, more friction reduction strategies will be explored. Also, the limits of these strategies will be established, and the results translated into low-friction design guidelines.

Section 2 presents an overview of the fundamentals of friction and lubrication in the piston and ring pack, and introduces the modeling tools that were used in this study. Section 3 presents a parametric analysis of the effect of lubricant parameters on ring friction, and recommendations for friction reduction via lubricant in the Waukesha engine. In Section 4, a study of surface parameters is presented, with roughness, skewness, and honing cross-hatch angle the focuses of the study. Section 5 presents several studies on piston design parameters, and the relative importance of each in contributing to piston friction reduction.

1.2. Methodology

1. Existing computer models have been modified, and applied to investigate the fundamental behavior of piston rings, lubricant, and surface texture. Substantial progress has been made in analyzing the piston rings for both hydrodynamic and boundary lubrication, and the interaction between rings, lubricant, and surface finish.
2. Other existing models have been modified and applied to investigate the behavior of the piston, and the effects of several parameters including piston profile, lubricant availability, and lubricant viscosity.
3. Results from the parametric studies on the piston and rings have been used to make recommendations for friction reduction in the Waukesha engine power cylinder.
4. We are working with a lubricant supplier to furnish lubricant for experimental verification of lubricant analysis. Also, we are working with ring and piston manufacturers to furnish prototype component designs.
5. Tests of low-friction ring designs are currently being performed, on an 18L Waukesha VGF engine, at Colorado State University. When these are completed, lubricant testing will begin.

1.3. Sources of Friction in Modern Internal Combustion Engines

Mechanical losses due to friction account for between 4 and 15% of the total energy consumed in modern internal combustion engines [8]. 40-55% of those total mechanical losses occur in the power cylinder [9], and approximately half of the power cylinder friction losses come from friction generated by the piston rings, and half from the piston (with only a small fraction of the losses due to the connecting pin) [8,10,11]. As a result, reducing both piston and piston ring friction has the potential to improve engine efficiency, lower fuel consumption and reduce emissions. These are important objectives for today's engine manufacturers, who are striving to improve engine performance while trying to meet increasingly stringent emissions standards.

1.4. Overview of the Piston Ring-Liner System

1.4.1. Description of the Piston Ring-Liner System

The piston ring pack in an internal combustion engine typically consists of three rings located in grooves in the piston, as shown in Figure 1-1. The primary purpose of the ring pack is to prevent high-pressure gases from leaking out of the combustion chamber, which would result in power losses. The rings must also prevent excessive leakage of oil from the crank case to the combustion chamber, while themselves remaining sufficiently lubricated. A third function of the piston rings, particularly for the top ring, is the dissipation of heat from the piston to the cylinder liner. The rings should perform all of these functions without introducing excessive frictional losses into the system, and while keeping wear of both the rings and the cylinder liner to a minimum.

The system achieves these three objectives by using three specialized piston rings, each with a specific function. The top ring seals the ring-liner interface in order to prevent high-pressure gas from escaping from the cylinder into the lower parts of the ring pack. The top ring also dissipates heat from the piston to the cylinder liner. The oil control ring controls the amount of oil that flows towards the combustion chamber to lubricate the upper rings, regulating both the lubrication of the top two rings and oil consumption. The second ring scrapes down any excessive oil that passes the oil control ring, further controlling oil consumption while maintaining adequate lubrication. In some cases the second ring is deemed unnecessary (as in racing engines, where light weight is more important than oil consumption), while in others extra scraper rings are added, as in large diesel engines with long life and low oil consumption requirements.

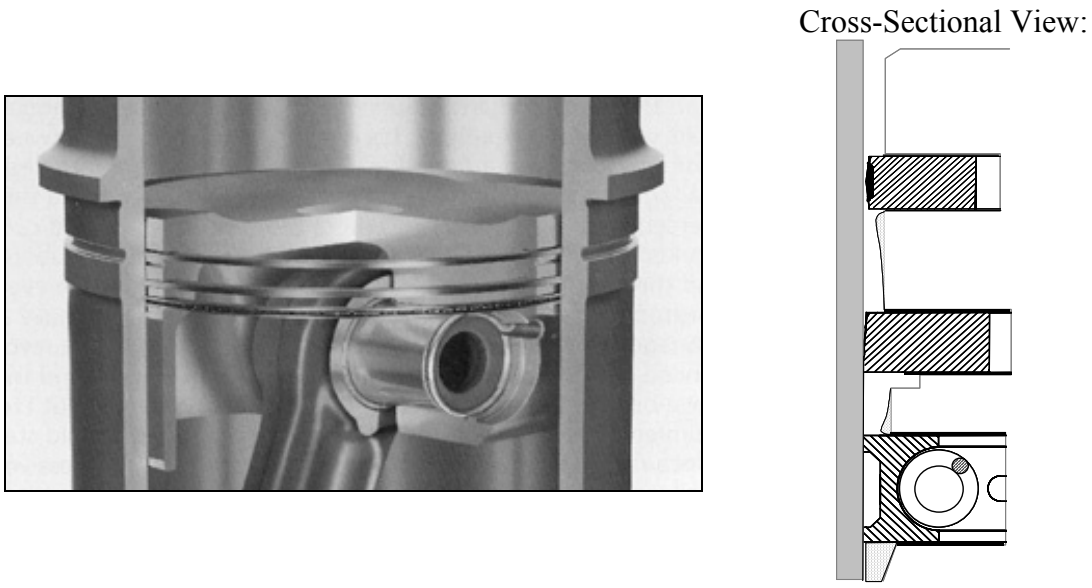

Figure 1-1: The Piston Ring Pack

1.4.2. Typical Piston Ring Designs

The designs of the three piston rings reflect their different purposes. The top ring, both far from the lubricant supply and exposed to harsh conditions, is designed to retain, and use to maximum effect, any available oil. The second ring, also called the scraper ring, is designed to scrape excess oil down the liner (towards the crank case) on down-strokes, but not transport oil back up the liner, which can increase oil consumption. The oil control ring must conform to the liner, so that excessive leakage does not occur, and adequately control the oil supply to the top two rings under all engine conditions.

The top ring is the closest to the combustion chamber, so that it is exposed to very harsh conditions and rapidly changing loads. High combustion chamber gas pressures, in particular, can put high radial loads on the top ring, causing the ring to push into the liner at high force. When lubrication is insufficient, this high contact force can lead to high friction and wear. Ring/liner friction increases the mechanical loss of the engine, while wear results in the increase of the ring gap over time, increasing leakage of combustion chamber gases and further reducing engine efficiency. The barrel-shaped face profile of the top ring has been shown to be most effective for lubrication [12], and thus reduces this friction and wear to a minimum.

The second ring has a tapered face that very effectively accumulates oil on its lower edge, for downward scraping, but it cannot accumulate oil on its upper edge to scrape upward towards the combustion chamber. This allows the second ring to reduce oil consumption and provide as a secondary control on oil flow. The scraper ring's unidirectional scraping profile is illustrated below in Figure 1-2.

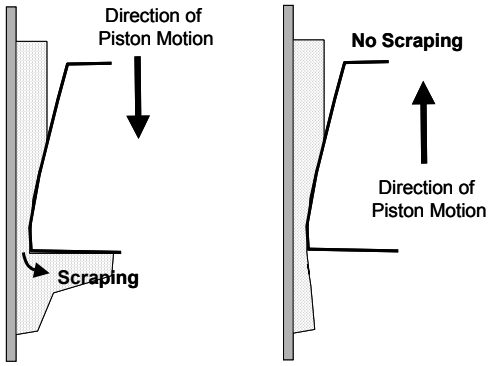

Figure 1-2: Effect of Taper Face Profile on Oil Transport

The oil control ring's purpose is to control the supply of oil traveling to the top two rings, making conformability to the liner a key design criteria. Several different oil control ring designs are in use, for different engine types. The focus of this study was the twin-land oil control ring, which is typically used in large diesel engines. The TLOCR consists of a spring mounted inside two rails, where the circumferential length of the spring determines the ring tension. The high ring tension provided by the spring produces adequate ring-liner conformability, accommodating the thermal and mechanical deformation of the cylinder bore that occurs during engine operation. The two lands effectively control oil flow by exerting a high pressure on the oil film, where the high ring tension can create a very high pressure on the oil film because of the thinness of the lands. A single land may be sufficient to control oil flow if it always conforms well, but oil ring tilt can cause one land to tilt away from the liner. Two lands are used because it is believed that at least one of the lands will control oil at any given time in the engine cycle, depending on the relative angle between the ring and the liner.

The rings are manufactured in different materials depending on the type of engine in which they are to be installed. In larger diesel engines, the rings are typically made of ductile cast iron, whose high thermal stability makes it desirable in the high operating temperatures in these engines. Cast iron ring faces are typically coated with a chrome layer for wear reduction, and considerable research is currently being devoted to the identification and development of other materials and face coatings for reduced friction and wear [9,11]. Steel is the more popular material for rings to be used in smaller gasoline engines because it is stronger than cast iron, and, therefore, the size of the rings can be reduced and conformability improved without a reduction in ring life. Some studies have been conducted in which steel rings were investigated for larger diesel engines [13]. These rings showed promise for use in larger engines, except for temperature limitations and some significant wear observed with certain steel materials used in articulated pistons.

1.4.3. Dynamic Phenomena in the Piston Ring-Liner System

The external conditions operating on the rings (temperatures, pressures, etc.) change throughout the engine cycle, causing the rings to displace and twist relative to their ring grooves. The small (order of 100 microns) clearances between the rings and their grooves can allow significant gas flow, so that pressure balances across the rings change throughout the cycle. This dynamic movement of the rings significantly affects

the performance of the rings, including oil flow, ring/liner and ring/groove friction and blow-by (gas leakage). Integral to addressing the general criteria discussed above, the piston rings must perform well dynamically, throughout the engine cycle.

Several other factors also affect ring-liner lubrication as well as the ability of the rings to seal the ring-liner interface. Bore distortion occurs because of mechanical stresses and thermal expansion due to the temperature gradient along the liner in the direction of piston motion. This overall bore distortion is comprised of radial expansion and circumferential out-of-roundness, and it is therefore a complex 3-D phenomenon that can significantly affect the conformability of the piston rings to the liner. Ring-liner lubrication is also significantly affected by the asymmetric geometry of the crank and connecting rod. As a result of this asymmetry and the various forces encountered during the engine cycle, the piston will tend to tilt about the axis of the piston pin throughout the engine cycle, which will affect angle between the ring and the liner.

The dynamics that arise due to the clearances between the ring and the grooves, combined with bore distortion and piston tilt, ultimately determine the ring-liner relative angle. This angle significantly affects the lubrication between the ring and the liner, and the friction generated by their interaction. The link between these dynamic phenomena and piston ring friction and lubrication is discussed in more detail in Section 2.

1.5. Overview of the Piston/Liner System

1.5.1. Description of the Piston/Liner System

The main function of the piston is to transmit the combustion gas pressures in the combustion cylinder to the crankshaft. The oscillating motion of the connecting rod causes an oscillating side force, between the piston and liner, to be generated as the piston moves through the engine cycle. The piston must support this force, while sliding, with a minimum of friction generation. Other considerations for the piston include noise and vibration generation – sufficient oil must be present to cushion the piston "slap" as it moves from one side of the liner to the other – and wear.

1.5.2. Typical Piston Designs

In general, the piston consists of an upper region, containing grooves for the piston rings, and a lower region known as the "skirt". The skirt supports the piston/liner contact pressures, and is the site of friction generation and wear. Thus, this is the main region of interest in this study. Skirt friction and wear are affected by three design characteristics, the skirt profile, the waviness, and the surface roughness. The skirt profile is of the largest scale, and describes the large-scale variation in piston radius in the axial direction. The waviness results from the piston machining process and results in circumferential surface grooves on the scale of 10μ. The roughness is on yet a smaller scale, on the order of 1μ or less, and is controlled by the skirt material and the surface finishing techniques used. All of these piston characteristics affect friction, although the amount and the manner in which they affect friction depend on several other factors, including lubricant formulation and the extent of piston wear.

Pistons are produced with many different profiles, including tapered, barrel, and others, each offering advantages and disadvantages. This study focuses on barrel-profile pistons, such as the one shown schematically in Figure 1-3. The barrel shape of the skirt maintains a small piston diameter near the upper land, which allows for thermal expansion, while maintaining a relatively large wetted skirt area, which helps to reduce wear. The barrel shape also assists in creating a hydrodynamic oil film, and improves stability and reduces clearances by allowing for the natural secondary motion of the piston. The proportions of the barrel shape – i.e., the curvature of the bulge – have a large effect on piston/liner surface generation.

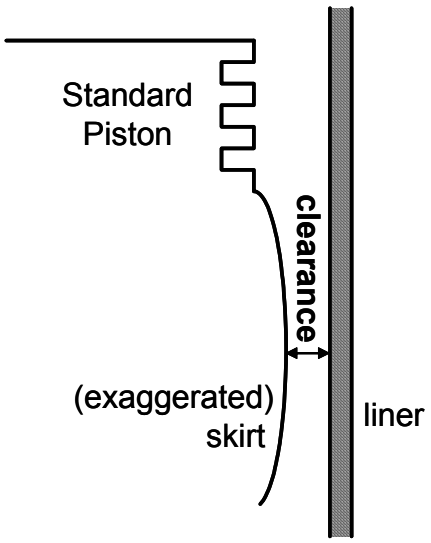

Figure 1-3: Piston with a barrel-shaped skirt

The waviness and roughness of the skirt also affect friction. Figure 1-4 shows a schematic of worn and unworn piston surfaces. For an unworn piston, the affect of the waviness dominates any roughness affects, because the waviness is on a larger scale. In this case, friction is dominated by the contact of the peaks of the waviness with the cylinder liner, causing boundary friction to occur. Contact occurs only at the high points of the machining grooves, with the height of those points determining when and how much contact occurs. As this type of contact continues, however, the peaks are worn down, as shown in the figure. In the worn case, the texture of the flat "plateaus" that has replaced the waviness peaks may become dominant. In this case, the height of flat surface roughness determines the extent of any asperity contact.

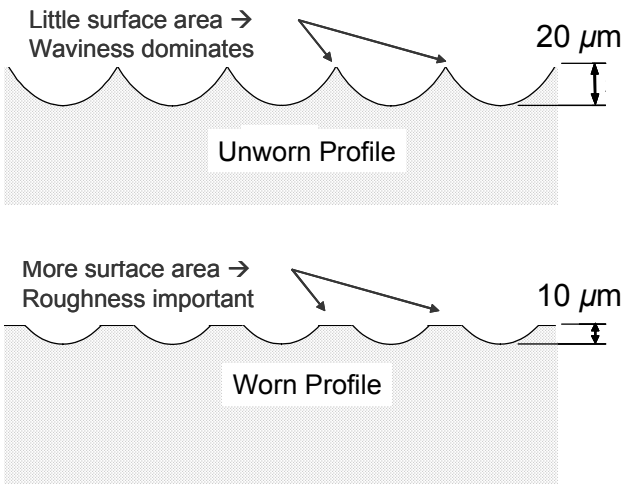

Figure 1-4: A side view of skirt waviness, worn and unworn cases.

1.5.3. Dynamic Phenomena in the Piston-Liner System

The piston is subject to different temperatures, pressures, and reaction forces over the course of the engine stroke. The asymmetric geometry of the crank and connecting rod result in cyclic side-forces between the piston skirt and liner which, together with cylinder gas forces, cause the piston to displace within the cylinder, and also tilt about the pin axis. The major feature of this secondary motion is its tendency to hug one side of the cylinder for most of a stroke, then transfer quickly to the other side, resulting in a "slap" as it contacts the opposite surface. This slap can contribute to engine noise and vibration, as well as friction. The slap and subsequent motion on the major thrust side of the piston, following combustion (and thus under high gas pressure conditions) is responsible for a large portion of the piston/liner friction.

Other dynamic phenomena contribute to piston friction and motion. The bore distortion of the cylinder, due to gas forces and thermal gradients, can have a large effect. Also, other secondary motions of the piston can affect both friction and noise. For example, after the slap, the piston continue to vibrate/oscillate until the oscillations are damped out. The extent of this oscillation depends on the contact velocity as well as the amount of damping (usually from an oil film) present, and can affect the friction, noise, and vibration of the engine.

1.6. Objectives and Approach used in the Present Study

The goal of the present study is to develop designs, surface finishes, and lubricants to reduce piston and piston ring friction, without increasing oil consumption, blow-by, and wear. Low-friction piston ring designs were developed in a previous stage (2003-2004) and are currently being tested in a full-engine test in the Engine and Energy Conversion Laboratory at Colorado State University. In the current research, optimized surface finishes and lubricants are considered for reducing ring friction, while a comprehensive analysis of piston geometry, surface properties, and lubrication is also performed.

Achieving these objectives was facilitated to a great extent by the use of extensive modeling tools, developed at MIT over the past decade, and still under development in the current study. An experimental evaluation of the designs has been/will also be conducted to validate the model predictions and to evaluate certain effects that could not be predicted quantitatively by the model. The use of this combined approach with the goal of developing an optimized piston and ring pack is what distinguishes this work from many of the previous studies that have been conducted in this area.

The following approach was used in this study. For the ring pack, low-friction ring designs, considering ring geometry and tension, have already been completed and are currently being tested in full-scale engine conditions. Further analytical study was conducted in the areas of ring lubrication, ring/liner surface finishes, and piston design, using the modeling tools developed at MIT. Parametric studies were conducted considering various surface finish and lubricant parameters, and piston designs, and a preliminary review considering advanced surface finishing techniques, such as dimpling, was conducted. A cooperative partnership with Exxon/Mobil has been formed for lubricant development and production of test oils. Once design recommendations are made, optimized designs will be manufactured and tested at CSU.

2. Fundamentals of Sliding Friction and Lubrication

2.1. Modes of Sliding Lubrication

The piston and piston rings both experience different lubrication modes during different parts of the cycle. When sufficient lubricant is available and piston speed is sufficiently high, pure hydrodynamic lubrication occurs – the radial load is fully supported by oil film pressure and there is no metal-to-metal contact. When this is not the case, and radial forces cannot be supported fully on the oil film, some asperity contact is required to partially support the load. If lubricant supply becomes very small or piston speeds get very low, such that virtually none of the load is supported by the lubricant, full boundary contact conditions occur. As will be seen in later sections, these modes of lubrication have a profound effect on the magnitude of the friction force generated by the motion of the piston and rings along the liner.

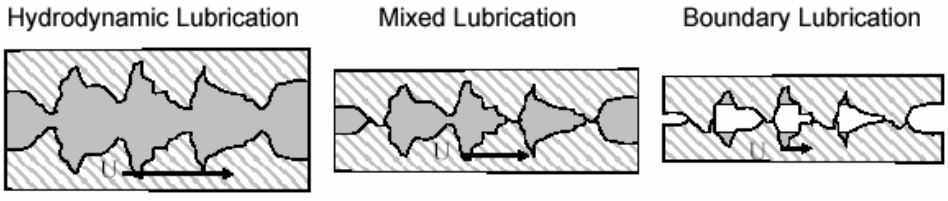

Figure 2-1: **Different modes of lubrication**

Figure 2-1 shows the typical lubrication conditions encountered by both the piston and rings. Typically, all surfaces are rough, so that asperity contact begins to occur when the oil film is thin enough that the largest asperities can touch. For the purposes of modeling, initial contact is defined by stochastic surface parameters, which are based on

the distribution of height of a surface. The surface mean is a flat surface defining the mean of the surface heights, shown in Figure 2-1 as dotted lines. A nominal separation between surfaces is then defined as the separation between the mean surfaces, and referred to as "h". The surface "roughness" is the standard deviation of the surface heights, and referred to as "σ".

For two surfaces, a combined roughness is defined in equation 2.1. Then, initial contact is modeled to occur when the nominal separation between surfaces is smaller than 4*(combined roughness), or less than four standard deviations of the combined surface heights, as given in equation 2.2:

$$\sigma \quad \sqrt{\sigma_1^2 \quad \sigma_2^2} \tag{2.1}$$

$$\frac{h}{\sigma} \quad 4 \tag{2.2}$$

where h is the nominal separation between the ring and liner, σ_1 and σ_2 are the standard deviations of the distribution of surface heights for the two surfaces [1]. The hydrodynamic-to-mixed transition condition is a statistical condition: asperity contact is said to begin occurring when there is a 95% chance that asperities whose combined height is taller than the film thickness, h, exist.

The transition from mixed to boundary lubrication occurs when there is no longer any hydrodynamic support for the load between two surfaces. There may be several causes for the loss of hydrodynamic pressure. In the power cylinder, the two main causes are low/no relative speed between surfaces – because of its reciprocating motion the piston speed goes go zero at top and bottom dead-centers, and lack of sufficient lubricant.

Based on this criteria, ring and piston lubrication states can be one of three conditions:

a) Pure Hydrodynamic Lubrication $\frac{h}{\sigma} \quad 4$

b) Mixed Lubrication $\frac{h}{\sigma} \quad 4$, some hydrodynamic support

c) Pure Boundary Lubrication $\frac{h}{\sigma} < 1$, no hydrodynamic support

The method for the determination of the friction force in each of these lubrication conditions is outlined in the sections that follow.

2.1.1. Pure Hydrodynamic Lubrication

Hydrodynamic lubrication occurs when pressure is generated between two non-parallel plates, moving relative to each other. The relative velocity and angle between the plates results in a "wedge" effect in the oil, leading to the generation of

hydrodynamic pressure which has the ability to support load, as shown in Figure 2-2. Both the piston and most rings have a barrel shape, resulting in the wedging effect and pressure generation at the inlet side of the barrel, and a reduction in pressure at the outlet. This reduction in pressure may cause cavitation in the lubricant, a condition which is dealt with in various ways in different lubrication models. A common assumption is to assign the liquid/gas equilibrium pressure to any areas that are believed to be in cavitation.

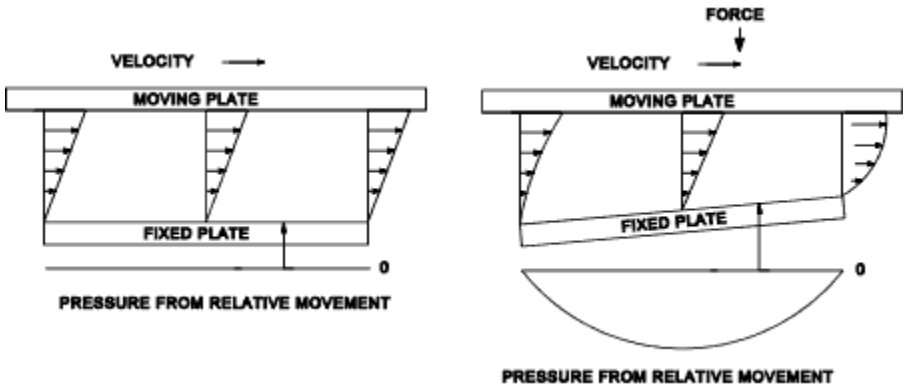

Figure 2-2: Hydrodynamic lubrication between two plates [14]

The lubricant flow and pressure generation within the lubricant is described by conservation of mass and momentum relationships. For the case of the rings and piston, several simplifying assumptions can be made, reducing these relationships to the Reynolds equation (see Appendix A for derivation):

$$\frac{\partial}{\partial x}\left(\frac{h^3}{\mu}\frac{dp}{dx}\right) = 6U\frac{\partial h}{\partial x} + 12\frac{\partial h}{\partial t} \tag{2.3}$$

where h is the nominal surface spacing, μ is the lubricant viscosity, p is the pressure in the lubricant, and U is the relative speed of the surfaces. The x-direction is the direction of fluid flow, while the y-direction is perpendicular to it. The 1-dimensional Reynolds equation is given in equation 2.3, and will be used below, for simplicity. The 1-D equation is appropriate for use with the piston rings, while a 2-D approach is necessary for the piston (see section 2.6.2).

The hydrodynamic friction force results from shear stress between the oil film and solid surfaces. Using conservation of mass and momentum (see Appendix A), a relationship for the lubricant velocity distribution can be derived (again, the 1-D form is presented, for simplicity):

$$u(y) = \frac{1}{2\mu}\frac{dp}{dx}(y^2 - hy) + \frac{Uy}{h} \tag{2.4}$$

then, shear stress at the wall is given by:

$$\tau(x) \quad \mu \frac{u}{y}\bigg|_{y\ 0} \qquad \frac{\mu U}{h} \quad \frac{h}{2}\frac{dp}{dx} \tag{2.5}$$

Hydrodynamic friction is directly dependent on this shear stress:

$$F_f \quad \int_{x1}^{x2} \tau dx \qquad \int_{x1}^{x2} \frac{\mu U}{h} \quad \frac{h}{2}\frac{dp}{dx}\ dx \tag{2.6}$$

where x_1 and x_2 are the boundaries of the wetted area.

These equations must be solved concurrently with the piston or ring dynamics, which affect the clearance and relative angle between hydrodynamic surfaces. In the case of the piston, skirt deformation must also be taken into account. The details of how this is carried out in the MIT models are described further below.

2.1.2. Pure Boundary Lubrication

Pure boundary lubrication occurs when no hydrodynamic oil pressure is generated between two surfaces, and therefore the load between the two is completely supported by asperity contact. Since there is no hydrodynamic force generated, the asperity contact pressure is fully defined by a radial force balance.

In this case, the friction force is given by the following expression:

$$F_f \qquad \int_{xc1}^{xc2} a_{asp} p_c dx \tag{2.7}$$

where a_{asp} is the friction coefficient governed by the surface properties, x_{c1} and x_{c2} define the boundaries of the portion of the surfaces that are in asperity contact according to Eq. (2.2), and p_c is the contact pressure between the two surfaces. For the purposes of modeling, the boundary friction coefficient between surfaces is assumed to be constant, and is defined as an input value. Values between 0.1-0.4 are assumed to be within realistic boundaries for this parameter.

The contact pressure, p_c, is given by the following empirical fit used by Hu [15] based on Greenwood-Tripp's theory [16].

$$P_c(x) \quad K_c \ \ 4 \quad \frac{h(x)}{\sigma}^{\ z} \tag{2.8}$$

where K_c depends on asperity and material properties and z is a correlation constant described in [15].

2.1.3. Mixed Lubrication

The friction between the ring and the liner in mixed lubrication is the sum of the contributions from pure hydrodynamic and pure boundary friction. Mixed friction is thus calculated as follows:

$$F_f = \int_{x1}^{x2} \tau dx + \int_{xc1}^{xc2} a_{asp} p_c dx \tag{2.9}$$

2.2. Governing Equations for Piston Ring Friction and Lubrication

In this section, the governing equations describing piston ring friction and lubrication that were introduced briefly in the previous section will be developed in detail. The method of solution of these equations will then be outlined for the different wetting conditions that can be present throughout the engine cycle. The solution of the governing equations yields the unknowns that are required to determine the friction force between the ring and the liner according to the equations derived in the previous section.

The system under consideration is shown in Figure 2-3. In the most general case, the unknowns are the minimum oil film thickness h_0, the inlet wetting coordinate x_1 and the outlet wetting coordinate x_2 (the profile of the ring surface is assumed to be known, and the ring tilt and radial displacement must be solved using a ring dynamics model - then once h_0 is known, h(x) is also known). That is, the wetting condition of the ring is unknown, and depends on forces acting on the ring and external conditions. The ring forces, in turn, depend partially on wetting conditions, so that an iterative solution is required. It should be noted that although there appears to be a transitional region in which oil attaches to the ring and detaches from the ring at x_1 and x_2, respectively, it was shown in [1] that if viscous diffusion is the method of attachment, this region is of negligible axial width compared to the axial width of the ring, B, and can thus be neglected.

The relationships that must be solved, iteratively, to describe the ring wetting and friction are the Reynolds equation, which describes the lubricant pressure and flow, and force and momentum balances on the ring, which describe the ring dynamics. Four wetting conditions, at the leading and trailing edges of the ring running surface, can exist. The wetting condition describes the point on the ring running surface at which the oil attaches and detaches. The following possible wetting conditions exist:

a) Fully-flooded inlet and outlet
b) Fully-flooded inlet and partially-flooded outlet
c) Partially-flooded inlet and fully-flooded outlet
d) Partially-flooded inlet and outlet

Fully-flooded conditions occur when there is an excess of oil available to fit under the ring, as illustrated in Figure 2-4 (for fully-flooded inlet).

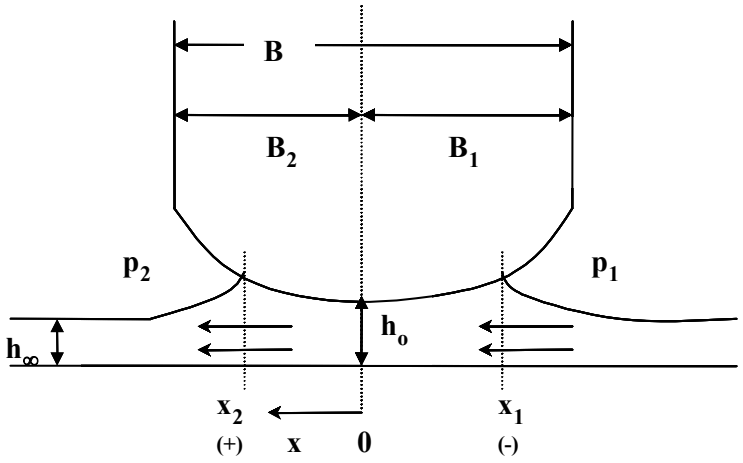

Figure 2-3: Hydrodynamic lubrication between ring and liner

For this condition, $x_1 = -B_1$. The fully-flooded outlet condition is defined analogously. In partially-flooded conditions, there is an insufficient amount of oil supplied to the ring to completely fill the space between the ring and the liner, so that the point of attachment (or detachment) of the oil film is somewhere underneath the ring running surface rather than at its edge.

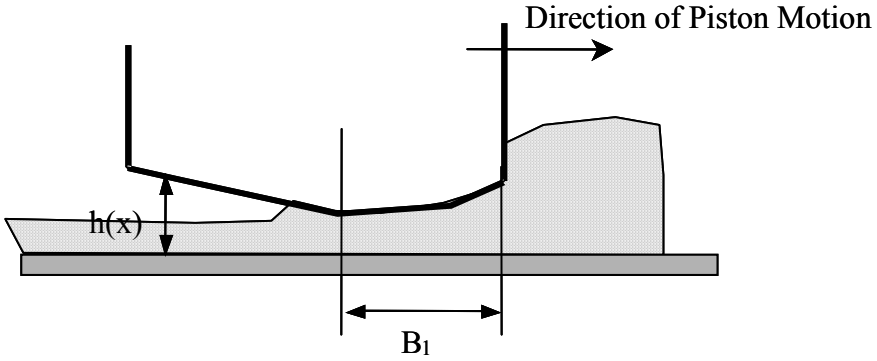

Figure 2-4: Illustration of the Fully-Flooded Inlet Condition

The wetting condition of the ring must be found iteratively, using appropriate boundary conditions as well as the Reynolds equation and ring dynamics.

2.2.1. The Reynolds Equation

The Reynolds Equation relates the height, width and shape of the oil film between the ring and the liner with the pressure gradient that is generated therein. A detailed derivation of the Reynolds Equation for incompressible lubricants can be found in Appendix A. In the present study, a quasi 2-D approach is used in which the parameters defining ring-liner lubrication are determined at specific circumferential locations on the piston, and the Reynolds Equation thus reduces to a 1-D form at each of these locations,

as given in equation 2.3.

For ease of illustration, the Reynolds equation can be simplified for certain conditions to show the effects of lubricant viscosity and piston speed on oil pressure. In mid-stroke conditions, the radial displacement of the ring over time is much smaller than the change in displacement in the axial direction due to ring face curvature and piston speed. This can be seen in scaling the Reynolds equation terms:

$$U\frac{h}{x} \sim LN\ \frac{h}{B}$$

$$\frac{h}{t} \sim hN$$

where L is the piston stroke, N is the engine speed, and B is the axial height of the ring. Then:

$$\frac{\frac{h}{t}}{U\frac{h}{x}} \sim \frac{B}{L} \qquad 1$$

Then, when the piston speed, U, is large, the second term on the right side of the Reynolds equation, known as the "squeeze term" can be ignored, simplifying the calculation. The Reynolds equation then becomes:

$$\frac{}{x}\ \frac{h^3}{\mu}\frac{dp}{dx} \qquad 6U\frac{h}{x} \tag{2.10}$$

and can be solved as:

$$\frac{dp}{dx} \quad 6\mu U\ \frac{x}{h^2} \quad C \tag{2.11}$$

From this simplified equation, the dependency of hydrodynamic pressure generation on viscosity and piston speed can be seen. The pressure, p, will be proportional to both the piston speed and viscosity, for a given film thickness, h. In reality, h is itself dependent on U and μ, but the general trend remains: hydrodynamic pressure tends to increase with relative speed and lubricant viscosity, and decrease with increasing film thickness, h.

In the converse case, near top and bottom centers, piston speed, U, approaches zero, and the squeeze term becomes dominant. In this situation, the squeeze term accounts for almost all of the hydrodynamic pressure generated in the oil film, and prevents the piston rings from losing all hydrodynamic support near dead centers.

2.2.2. Ring Dynamics – Radial Force Balance and Momentum Balance

When the gas pressures acting on the ring are known, a simple radial force balance on the ring shown in Figure 2-3 yields the radial force that must be supported by the ring/liner interface:

$$F_r \quad p_1(B_1 \quad x_1) \quad p_2(B_2 \quad x_2) \quad \int_{x1}^{x2} (p_{bdy}(x) \quad p_{hyd}(x))dx \quad p_b(B) \quad T \quad 0 \tag{2.12}$$

where p_1 and p_2 are the gas pressures at the top and bottom of the ring, p_b is the gas pressure acting on the back of the ring (usually either p_1 or p_2, depending on whether the ring is against the top or bottom of its groove), T is the ring tension, and displacements are measured from the minimum point location of the ring, so that x_1 is negative and x_2 is positive. P_{bdy} and P_{hyd} are the pressures resulting from boundary contact and hydrodynamic pressure, respectively. These pressures are non-zero when there is asperity contact, in the case of P_{bdy}, or hydrodynamic pressure generated in the oil wetting the ring, in the case of P_{hyd}. Setting Eq. (2.7) to zero assumes that the system is quasi-static in the radial direction, which has been shown to be a reasonable assumption in previous work in this area [1].

Equation 2-7 shows a simplified radial force balance, with only the largest forces shown. Several other radial forces act on the ring, such as ring/groove friction, are included in the model but not further discussed here, because of their complexity and relatively small contribution to the radial force balance.

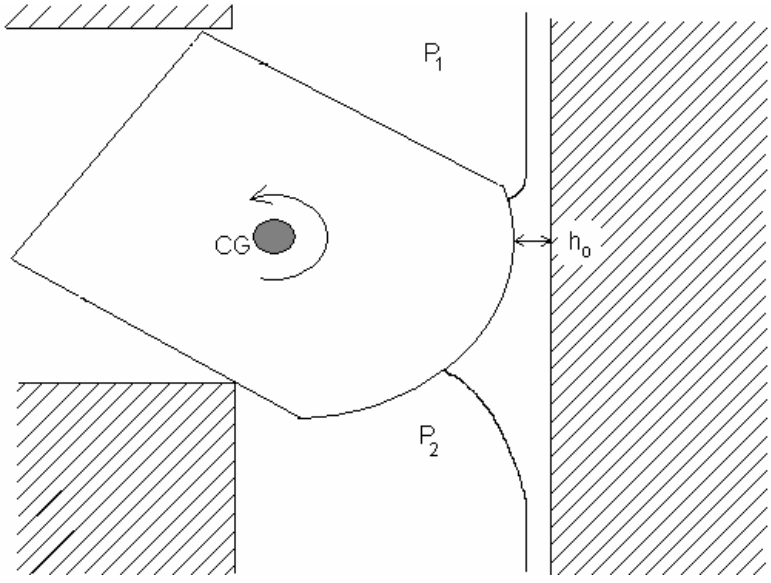

Figure 2-5: Exaggerated diagram of ring twist and dynamic minimum point

A momentum balance is also required to define the ring twist, which affects the profile of the ring relative to the oil flow direction, and, thus, the hydrodynamic pressure generation. As shown in Figure 2-5, (which is greatly exaggerated, actual twists are on the order of a few minutes) when the ring rotates the effective profile changes, and a new "dynamic" minimum point emerges. The twist/dynamics of the ring are also used to

assess gas blow-by and oil leakage behind the rings, both of which should be reduced in an optimum ring system.

A simplified momentum balance on the ring (including only the major forces, and not smaller and more complicated terms such as ring/groove friction), gives:

$$M \quad \frac{p_b \quad B_1^2}{2} \quad \frac{p_b \quad B_2^2}{2} \quad \frac{p_2 \quad (B_2^2 \quad x_2^2)}{2} \quad \frac{p_1 \quad (B_1^2 \quad x_1^2)}{2}$$
$$\int_0^w P_{top} \quad ydy \quad \int_0^w P_{bot} \quad ydy \quad \int_{x_1}^{x_2} (p_{bdy}(x) \quad p_{hyd}(x)) \quad xdx \tag{2.13}$$

where w is the radial width of the ring, and P_{top} and P_{bot} are the normal pressure on the top and bottom of the ring, respectively, due to ring/groove contact. For most of the cycle, the ring tends to be pressed against either the top or bottom of the groove, so that the groove angle and thermal deformation are large contributors to the ring twist.

2.2.3. Boundary Conditions

In the most general case, five boundary conditions are required to fully define the ring/lubricant/liner system, where there are three unknowns describing the wetting condition and two integration constants arising from use of the Reynolds equation.

The two boundary conditions required to define the integration constants define the pressures at the boundaries of the wetted area. Values for the pressures at the inlet and outlet of the oil film are assumed to be known. Then:

$$\begin{aligned} p(x_1) \quad & P_1 \\ p(x_2) \quad & P_2 \end{aligned} \tag{2.14}$$

The oil film pressures at inlet and outlet are taken to be equal to the gas pressures at those locations.

Conditions at the inlet and outlet govern the oil attachment and detachment points (the wetting boundaries). The inlet boundary condition is determined by conservation of mass for the oil, except for the case when the inlet is fully-flooded. When the ring is fully-flooded, the thickness of the oil entering the ring is assumed to fill the region between the ring and liner at the ring entrance. In partially-flooded conditions, the thickness of oil film entering the ring is assumed to be the same as that existing on the liner at some distance ahead of the ring, h_∞. In the model, this thickness is taken as the amount of oil that was left by the previous ring (in the case of the top ring moving towards the combustion chamber, the "previous" ring is the top ring itself, in its previous downward stroke). The oil control ring is assumed to be fully-flooded on its down-stroke.

Conservation of mass applied to the oil at the inlet of the ring surface gives:

$$Q(x_1) \quad Uh \tag{2.15}$$

where Q is the oil flow rate at x_1 (ring inlet wetting point) and h_∞ is the thickness of the oil on the liner before the ring boundary. $Q(x_1)$ is derived in Appendix A:

$$Q(x) = -\frac{h^3}{12\mu}\frac{dp}{dx} + \frac{Uh}{2} \tag{2.16}$$

This equation is not valid for the fully-flooded cases because not all oil on the liner will flow under the ring, some will build up on the forward ring face, as shown in Figure 2-4.

Several outlet boundary conditions have been considered. The Reynolds outlet condition has been shown to be valid in most cases [1]

$$\frac{dp}{dx}(x_2) \quad 0 \tag{2.17}$$

This equation does not apply at the end strokes because of the small piston velocity. In these regions of the cycle another exit condition is needed, which accounts for the unsteadiness of the inlet or exit point of oil attachment. A film-non-separation condition is used, which assumes that oil flowing out at x_2 accumulates between ring and liner, and no oil separates from the ring. This condition is only applicable a few crank degrees from the end-stroke regions, and is discussed in detail in [1].

2.2.4. Iteration Method and Solution in the Ring-Pack Model

The model solves the governing equations derived in the previous section at each crank angle of the engine cycle, for each of the rings. The relationships are solved iteratively to arrive at a final description of the ring/lubricant/liner interaction. Newton's method is used – a solution is found when values for the pressure distribution within the oil converge.

It should be noted that the governing equations derived above and the equations used to solve for the unknowns in the model are slightly different. In the model, the volumetric flow rate of the oil at the trailing edge of the ring is introduced as an additional unknown. This allows the use of a volumetric flow rate relationship instead of the Reynolds Equation. The two methods are entirely equivalent, and the introduction of the flow rate as an additional unknown replaces the additional integration constant that would need to be determined if the Reynolds Equation were used.

Another difference in the model is that the effects of surface roughnesses are taken into account (this is not shown in the derivations above, for simplicity). Surface textures are modeled using flow factors, along with averaged lubricant flow relationships. Flow factors are described in further detail in section 5.2.2.

2.3. Effect of Dynamic Phenomena in the Piston Ring Pack

As discussed in Section 1.4.3, the dynamics of the piston ring-liner system have a considerable effect on the lubrication conditions between the ring and the liner, and the friction generated by their interaction. Several dynamic phenomena have a significant impact on the relative angle between the ring and the liner, which alters the position of the point on the ring running surface that is closest to the liner (hereafter referred to as the minimum point). If the position of the minimum point changes, the amount of space available for oil to fit between the ring and the liner will change, and therefore the friction and lubrication conditions will also change.

In general, the ring-liner relative angle is the sum of the contributions due to ring static twist, ring dynamic twist, piston tilt, groove tilt, and bore distortion. These effects vary around the circumference of the ring due to the asymmetry introduced by the presence of the ring gap. All of these effects must be taken into account in order to determine the lubrication and friction between the ring and the liner.

2.4. Effect of Lubricant Properties on Piston Ring Pack Friction

The main lubricant property that effects ring pack friction is the viscosity. Lubricant additives such as surface friction modifiers can alter the boundary friction coefficient between ring and liner, (while other additives can have other, unintended, effects on friction). In this study, additive effects were not considered in detail, nor were other lubricant properties such as surface tension and that may affect ring/liner friction less strongly.

Lubricant viscosity directly affects only hydrodynamic friction, as indicated in the Reynolds equation (2.3) – in boundary friction conditions, very little lubricant is present, so lubricant properties can have only a small effect. However, the lubricant viscosity does govern, in part, the oil film thickness, which determines when asperity contact is initiated. Thus increasing viscosity can indirectly reduce boundary friction by decreasing the amount of boundary contact that takes place, in cases where reducing boundary friction will reduce overall friction. In general, an increase in lubricant viscosity increases film thickness, which will cause an increase in hydrodynamic friction, but may also reduce boundary contact (and vice versa). Optimization of the lubricant viscosity is a matter of balancing these two effects, minimizing the sum of hydrodynamic and boundary friction. A more detailed discussion and analysis of lubricant effects is given in section 3.

2.5. Effect of Surface Properties on Piston Ring Pack Friction

The ring and liner surfaces cannot be completely smooth, both have a surface texture that affects both oil flow and the film thickness at which asperity contact begins. Asperity heights and shapes and the distribution of asperity heights about the mean all effect ring pack friction, as do larger scale surface features such as honing marks.

In general, boundary friction increases with the combined roughness (the average height of surface asperities) of the two surfaces, because taller peaks contact at a larger film thickness, causing boundary friction to increase. Boundary friction also tends to decrease with decreasing skewness, a measure of the distribution and shape of asperities about the average surface, where a low skewness indicates a flatter, more plateau surface with deep valleys.

Other surface effects are more subtle. For example, liner textures that tend to impede oil flow increase hydrodynamic pressure generation in the lubricant. This increases the film thickness, which may either increase friction, if hydrodynamic friction is dominant, or decrease friction, if the increase in film thickness results in a decrease in asperity contact. Surface texturing may also affect oil consumption and ring/liner wear.

This study considers the effects of surface roughness and skewness, as well as honing cross-hatch angle, in more detail in section 4. Also, a brief review of promising surface textures to be considered in future studies is included.

2.6. Modeling and Governing Equations for Piston Friction and Lubrication

Several aspects of the piston/liner system make its analysis more complicated than the ring analysis. First, the piston is assumed to be always starved – that is, a fully-flooded condition does not exist, the piston is always only wetted over a portion of its surface. Also, the piston must be treated as a 2-dimensional system, a 1-D approximation like that used for the rings cannot be used, because of the spreading of lubricant in the tangential as well as the axial direction during wetting. In the model, the entire surface of the piston is taken into account, so that the changes in the locations of applied forces and lubricant wetting during the cycle are accounted for.

The flexibility of the piston also makes its analysis complex. In addition to tilting and displacing, as a unit within the cylinder liner, the piston skirt also deforms, in response to various applied forces. This skirt deformation is due in large part to the pressures applied by the oil film, which are in turn highly influenced by the skirt geometry. This phenomenon adds yet another iteration step to the analysis of the piston lubrication and friction.

2.6.1. Force and Momentum Balances

Simple force and momentum balances are used to model the dynamics of the piston. Vertical and lateral force balances are applied, taking into account gas pressures, piston inertia, ring forces, friction forces and thrust forces, as indicated in Figure 2-6. In the figure, the y-axis is in the vertical direction (positive up) and the x-axis is in the horizontal direction (positive to the right). Balances of forces and moments about the wrist-pin yield [17]:

$$\Sigma F_y: \quad F_g \quad F_{IP} \quad F_{IC} \quad \tilde{F}\cos\phi \quad F_{qj} \quad F_f \quad 0 \tag{2.18}$$

$$\Sigma F_y: \quad F_s\delta_s \quad F_{IP} \quad F_{IC} \quad \tilde{F}\sin\phi \quad F_{rj} \quad 0 \tag{2.19}$$

$$\Sigma M_p: \quad F_s y_s \delta_s \quad M_{IP} \quad M_{IC} \quad M_{PP} \quad F_{IC}(a \quad b) \quad F_{IC} C_g \quad F_g C_p \quad M_f \quad C_p \quad F_{qj} \quad F_{rj} Ij \quad 0 \tag{2.20}$$

where the terms in the above equations are:

Table 2-1: Definition of terms in piston equilibrium equations

Parameter	Definition
F_g	combustion gas force acting on top of the piston
F_{IP} ,F_{IP}	inertia force due to wrist-pin mass, x and y-directions
F_{IC} ,F_{IC}	inertia force due to piston mass, x and y-directions
F_q	vertical/normal force between piston and rings
F_r	horizontal/shear forces between piston and rings
F_f	total friction acting on the skirt, thrust and anti-thrust sides
F_s	side force, either F_1 or F_2 in the figure, depending on where contact occurs
δ	1 if contact occurs, 0 if it does not
$\tilde{F}$	connecting rod force
ϕ	connecting rod angle
M_{IC}	inertia moment of piston
M_{IP}	inertia moment of wrist-pin
M_{pp}	moment about wrist-pin due to wrist-pin friction
a	vertical distance from top of skirt to wrist-pin axis
b	vertical distance from top of skirt to piston center of gravity
C_g	horizontal distance between piston center of mass and wrist-pin
C_p	horizontal distance of wrist-pin from vertical piston axis (pin offset)
M_f	moment about wrist-pin due to all friction forces, thrust and anti-thrust sides
l_r	vertical distance(s) between wrist-pin axis and rings

These relationships are used to solve for the piston position and tilt as a function of time (or crank angle). Some inputs must be calculated iteratively, as they depend on the hydrodynamic lubrication of the piston, including side forces and piston/liner friction forces.

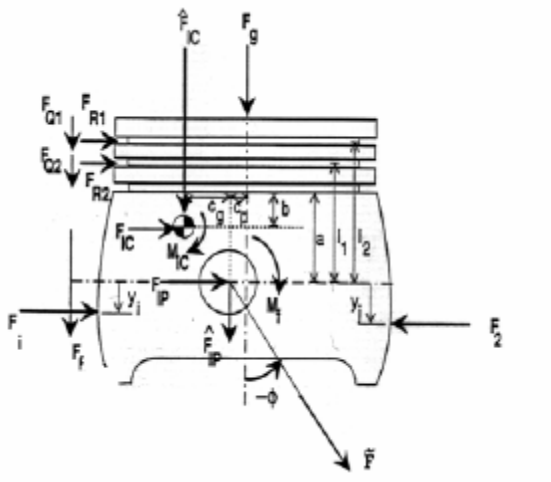

Figure 2-6: Forces and moments acting on the piston

Figure 2-7 shows the piston geometry, and definition of e_t and e_b, the eccentricities of the piston at the top and bottom of the skirt, respectively. These two terms and their time derivatives are used to define the piston tilt and displacement in the piston equations of motion:

$$\begin{matrix} m_{PP}(1 - \frac{a}{L}) & m_{Pis}(1 - \frac{b}{L}) & m_{PP}\frac{a}{L} & m_{Pis}\frac{b}{L} & \ddot{e}_t & F_\sigma & F_s\delta_s - F_f\tan\phi \\ \frac{I_{Pis}}{L} & m_{Pis}(a - b)(1 - \frac{b}{L}) & m_{Pis}(a - b)\frac{b}{L} & \frac{I_{Pis}}{L} & \ddot{e}_b & M_s & F_s y_s \delta_s - M_f \end{matrix} \quad (2.21)$$

where m_{PP} is the wrist pin mass, m_{Pis} is the piston mass, L is the skirt height, F_σ and M_s are defined in Appendix A, and all other terms are defined above in Table 2-1.

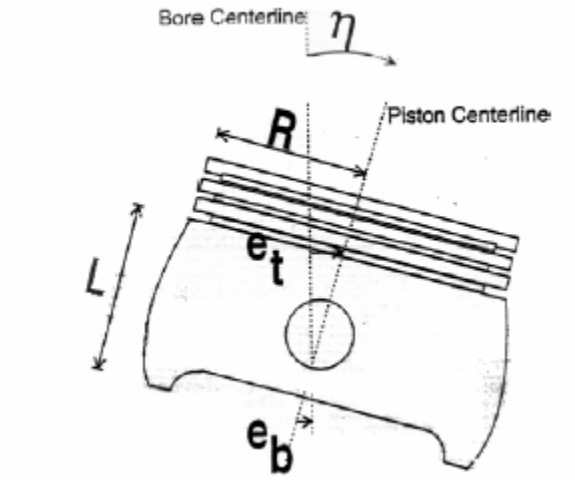

Figure 2-7: Piston geometry, showing definition of eccentricities

2.6.2. Reynolds Equation: Skirt Hydrodynamic Lubrication

The piston skirt experiences both hydrodynamic and boundary lubrication. In the hydrodynamic regime, the relationship between lubricant wetting and hydrodynamic pressure is defined by the two-dimensional Reynolds equation (see Appendix A.1 for derivation):

$$\frac{\partial}{\partial x}\left(\frac{h^3}{\mu}\frac{\partial p}{\partial x}\right)+\frac{\partial}{\partial z}\left(\frac{h^3}{\mu}\frac{\partial p}{\partial z}\right)=6U\frac{\partial h}{\partial x}+12\frac{\partial h}{\partial t} \qquad (2.22)$$

Flow factors are used in conjunction with the Reynolds equation, to account for piston roughness and waviness. The skirt/liner separation, h, consists of four components: the factory machined (cold) skirt profile, thermal distortion, deformation due to cylinder pressure force and deformation due to pressures on the skirt. Deformation at the waviness peaks is given by:

$$\begin{array}{ll} \delta & h \\ \delta & 0 \end{array} \quad \frac{h}{otherwise} \qquad (2.23)$$

where δ is the deformation, and Ω is the amplitude of the surface waviness.

These lubrication and deformation equations must be solved iteratively with the equations of motion to define the piston motion and friction conditions.

2.6.3. Boundary Conditions

Several boundary conditions are required to solve the piston/lubricant/liner system. At the edges of the wetted area, the oil pressure is assumed to be equal to the ambient gas pressure (external gas pressures are assumed to be known). Then:

$$p(wetted \quad edge) \quad P_{amb} \qquad (2.24)$$

where P_{amb} is the ambient gas pressure around the lubricant.

Also, if the skirt is symmetric, it is assumed that the pressure distribution is across a symmetry line is symmetric. For such a skirt, about thrust or anti-thrust lines:

$$\left.\frac{p}{x}\right|_{x\ 0} \quad 0 \qquad (2.25)$$

There may be a significant amount of oil that does not contact the skirt, but must be accounted for in the analysis because of its effect on neighboring wetted areas. This oil is

assumed to be at ambient pressure. Then, in the case of oil on the liner that does not contact the skirt, (is between peaks of the waviness, for example):

$$p \quad P_{amb} \tag{2.26}$$

The wetted area of the piston is determined by geometry and conservation of mass for the lubricant. When the piston transitions from one side of the liner to the other, a given thickness of oil is present on the liner (the thickness is specified in the model, so that the effects of oil availability can be easily assessed). The extent of the wetting is then controlled by the amount of available oil and volume it occupies when squeezed between the piston and liner. The wetting condition must be solved iteratively along with the piston dynamics and deformation.

2.6.4. Iteration and Solving

The piston tilt and displacement, as well as the deformed profile of the skirt must be known in order to solve for hydrodynamic and boundary friction forces, but these forces, in turn, must be known to calculate the piston dynamics. Using the boundary conditions described in section 2.6.3, the pressure distribution and skirt profile are solved iteratively, using a finite-difference method in space and time, along with a relaxation scheme. The piston is assumed to be partially flooded, with wetting conditions defined by the boundary conditions given.

The numerical approach is to first determine piston-skirt side forces, using the hydrodynamic relationships, as functions of e_t, e_b and their time derivatives, and crank angle. These are then used to solve the piston dynamics equations in the time domain. The iteration is repeated until convergence is reached.

Like the ring-pack model, the piston model also takes surface roughnesses into account using averaged flow-factor techniques. The flow modeling equations used in the simulation are different than those shown above, which do not include flow factors for simplicity. Instead, averaged flow relationships are used, which account for surface texturing as explained further in section 5.2.2.

2.7. Effect of Dynamic Phenomena for the Piston

The secondary motion of the piston is of primary importance in determining friction losses in the system. The transition from one side of the liner to other, resulting in piston slap, affects friction both the magnitude of the slapping force and the timing of the transition. The slap and subsequent travel along the thrust side of the liner, after TDC-combustion, is the source of the majority of cycle friction in many cases. Also, the piston tilt and thermal deformation can affect friction, as can the thermal deformation of the liner.

2.8. Effect of Lubricant Properties on Piston Friction

Lubricant viscosity directly affects piston/liner friction generation. An increase in lubricant viscosity tends to increase hydrodynamic friction, while it may decrease

boundary friction if the increase in film thickness causes a decrease in asperity contact. An ideal lubricant balances these effects to produce the lowest friction – for a given piston profile.

Lubricant viscosity interacts with other piston design parameters, so that a given lubricant may be ideal for one case, but not for others. There is a strong interaction between viscosity and piston profile. Sharper profiles tend to experience more asperity contact, requiring high viscosity lubricants to reduce friction. Conversely, shallow profiles experience very little asperity contact, and are ideally matched with low-viscosity lubricants. A more detailed discussion and analysis of this effect is given in section 6.3.5.

3. The Waukesha VGF 18GL Natural Gas Engine

The engine under study is the Waukesha VGF 18GL natural gas engine. It is a large, spark-ignited stationary engine that is used mainly for power generation. Because of its major application, the engine is typically run at a constant speed over long periods of time – issues of start up and shut down and changes of engine speed during operation are relatively unimportant. For this reason, a single operating condition was chosen for study, that is representative of typical Waukesha engine operating conditions. The condition studied, along with some engine specifications, is given in Table 3-1.

Table 3-1: Specifications for Waukesha engine

Engine configuration	6 Cylinders, inline
Total displacement	18 Liters
Bore, stroke	152mm, 165mm
Operating speed	1800 rpm
Load condition	1360 kPa BMEP
Lubricant grade	SAE 40W
Top ring type	Barrel
Second ring type	Napier
Oil control ring type	Twin land

3.1. Sources of Friction in Waukesha Engine Power Cylinder

As shown in Figure 3-1, approximately 50% of the firing Waukesha engine's mechanical losses are predicted to occur in the power cylinder, through rubbing of pistons, rings and rods. This region represents the largest contribution to frictional losses in the engine, and is thus the focus of the current investigation. Because friction from the rods is very small, the main focus has been on piston and piston-ring losses, each of which contribute approximately equally (25% each) to the engine mechanical losses[18].

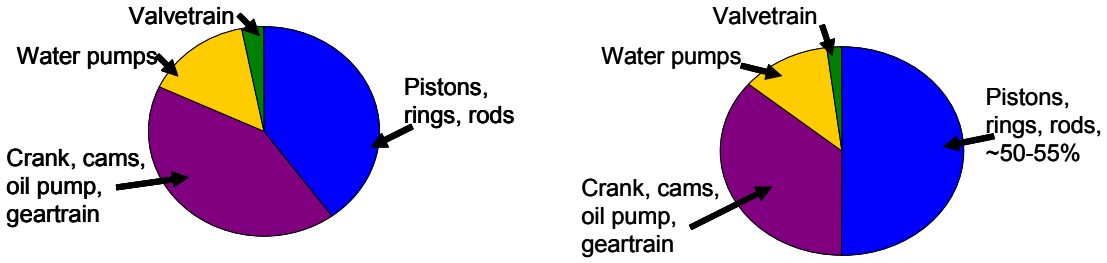

a) Motoring Tear-Down Test: Waukesha F18GL Engine 1800 RPM (2002)

b) Projected firing losses

Figure 3-1: Sources of friction in Waukesha engine

3.2. Sources of Friction in the Ring-Pack

For current mechanical and surface roughness parameters, frictional losses in the Waukesha engine ring-pack are dominated by the oil control and top rings, as shown in Figure 3-2. The OCR is the largest contributor to friction because of its high ring tension. It is required to conform very well to the cylinder liner, while maintaining enough stiffness to resist warping and breakage, so a high tension is necessary. This results in a high ring-liner load throughout the cycle, leading to high friction.

The top ring contribution to friction is also significant, because of the large friction forces associated with boundary friction near the top dead center (TDC) of the combustion stroke. In this region, two factors combine to create high friction: first, the oil supply to the top ring at TDC is very limited, because the oil control ring doesn't reach this high on the liner; second, combustion chamber gas pressure, following compression and combustion, is very high (see **Error! Reference source not found.**). The combination of high ring load and poor lubrication results in very high asperity contact pressures, and thus high friction (and also high wear). Even though piston speed is very low here, the total frictional power loss from this region is still significant.

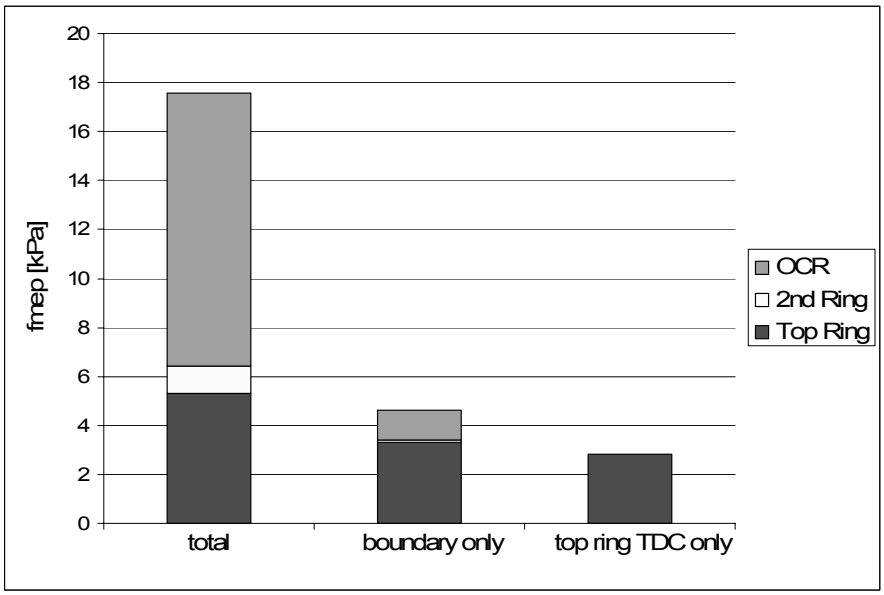

Figure 3-2: Ring contributions to ring-pack friction

Frictional losses from the second ring are relatively small, and, as a result, most friction reduction strategies focus on the top and oil control rings.

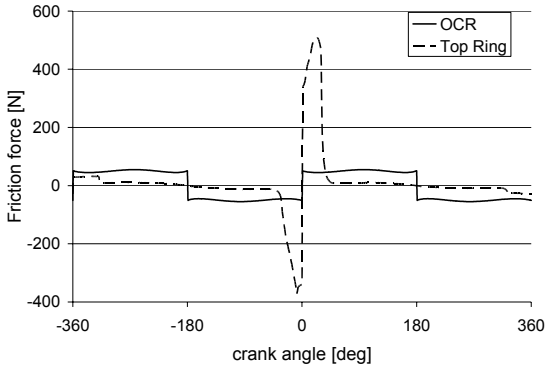

a) Top ring and OCR friction

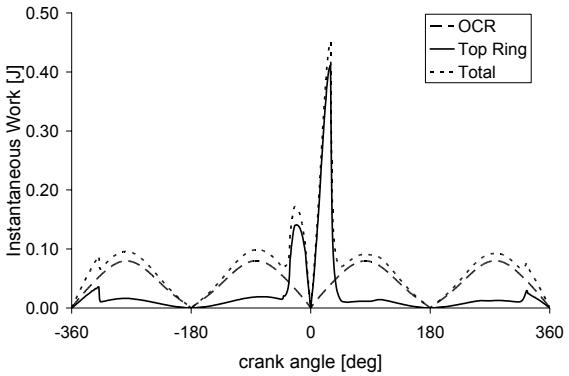

b)Top ring and OCR friction work losses

Figure 3-3: Top ring and OCR contributions to ring-pack friction losses

4. Friction Reduction Strategies – Effects of Lubricant Viscosity on Ring-pack Friction

This study focuses on the effects of lubricant viscosity, and its variation during the engine cycle, on ring/liner friction. A brief study of boundary friction coefficient is also included, as it can have a large effect on friction, and can be controlled to some extent by lubricant additives. The objective is to determine an optimized viscosity, including variations during the engine cycle, for the given engine design and operating conditions.

Both idealized and more realistic cases are considered. First, ideal cases where the lubricant viscosity at each crank angle can be independently controlled are studied, to illustrate potential benefits in a well-controlled scenario. Then, a parametric study of more practical cases is presented, based on realistic lubricant dependencies on temperature and shear rate. Also, different ring tension and roughness parameters are studied to find any interaction between these factors and lubricant effects.

While friction reduction is the focus of the current effort, other factors such as wear must also be addressed. A simple study of the effects of lubricant viscosity on wear is presented, with a slight benefit observed when viscosity variation during the engine cycle can be controlled.

It should be noted that, for most of the analyses below, the focus is on the oil control ring only, and not the entire ring pack. Figure 3-2 shows that the OCR is the largest contributor to ring-pack friction in the Waukesha engine. The top ring also contributes significantly to the total friction, but, as shown in Figure 3-3, most of this contribution comes from boundary friction in the dry region. The high friction in the dry region is due, in part, to very poor lubrication, so that controlling the lubricant viscosity should have little to no effect on friction generated here. Model results indicated that viscosity may have some influence on dry region width, and thus friction, but these results are preliminary, and are discussed briefly in section 4.4.

4.1. Effects of Lubricant Viscosity on Hydrodynamic and Boundary Losses

Two lubrication regimes contribute to friction losses for each ring: hydrodynamic losses result from shear stress within the lubricating oil, and boundary losses from rubbing between the two contacting solid surfaces. The relative contribution of each mode to total friction for a given ring depends on how well the ring-liner load can be supported by the oil film. At high enough speed and viscosity, the oil film can fully support the ring load, resulting in pure hydrodynamic lubrication. For lower speeds and/or low viscosities, a thinner film is generated and may be thin enough to allow some asperity contact to occur, resulting in mixed lubrication. At very low speeds or viscosities (or very low oil availability, as in the case of TDC combustion for the top ring) the oil film can break down, and the ring load is entirely supported by asperity contact.

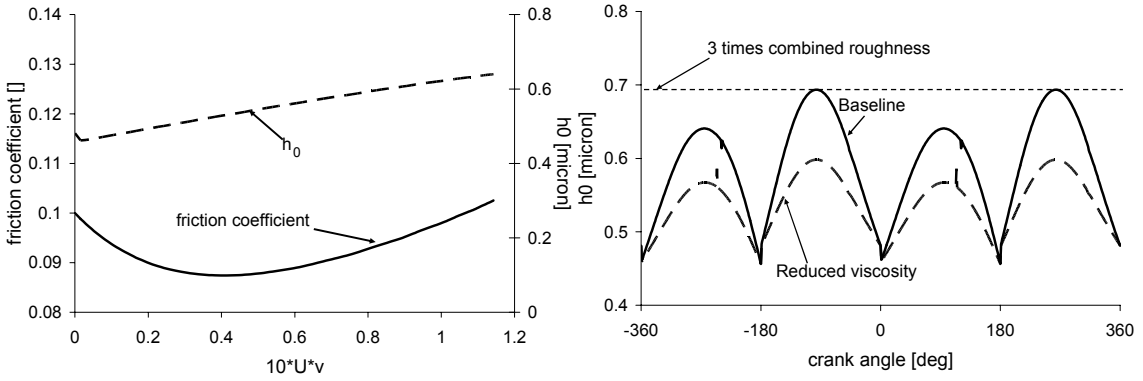

a)friction coefficient and h0 dependence on bearing # **b)minimum film thickness, for an engine cycle**

Figure 4-1: Effects of speed and viscosity on ring-liner separation (minimum film thickness) and friction, lower land OCR

The lubrication regimes of the ring during the engine cycle can be related to the ring speed, U, and lubricant viscosity, ν, for a given load. Figure 4-1a shows how the ring/liner friction coefficient varies with a bearing number N=10*U*ν for baseline engine parameters (the factor 10 was chosen so that the bearing number ranges approximately between 0 and 1). In Figure 4-1a, the oil film thickness and friction coefficient for the OCR are plotted. As the bearing number approaches 0, film thickness decreases and hydrodynamic support is lost. Asperity contact supports the load, and the coefficient of friction increases to the boundary friction coefficient, f_b = 0.1 in this case. For high bearing number, friction increases as shear stress – proportional to U and ν - increases. In the mid-range, friction coefficient drops as the balance between boundary and hydrodynamic lubrication changes.

Figure 4-1b shows the film thickness between the lower land of the OCR and the liner for an engine cycle, in the Waukesha engine studied (-360^o is the beginning of the intake stroke), for two lubricant viscosity cases. Results for the upper land are the same – only one is shown for illustrative purposes. Viscosity variation during the engine cycle for the baseline and reduced-viscosity cases are shown in Figure 4-3. Film thickness is small near dead-centers, because U=0 and hydrodynamic support is lost (film thickness does not go to 0 because of the ring and liner roughness – there is still some oil trapped in

the valleys when peaks are contacting.) Near mid-strokes piston speed is high, and film thickness is also large. The line "3 times combined roughness" indicates the film thickness that is three times the combined roughness of the ring and liner, at which there is a 5% chance of metal to metal contact. Comparing to Figure 4-1a, the film thicknesses shown in Figure 4-1b indicate that hydrodynamic lubrication dominates near mid-strokes (although there is a very small amount of asperity contact), while boundary contact supports most of the ring load near dead centers. In the reduced viscosity example, film thicknesses are lower, because the less viscous oil is less able to support the ring load.

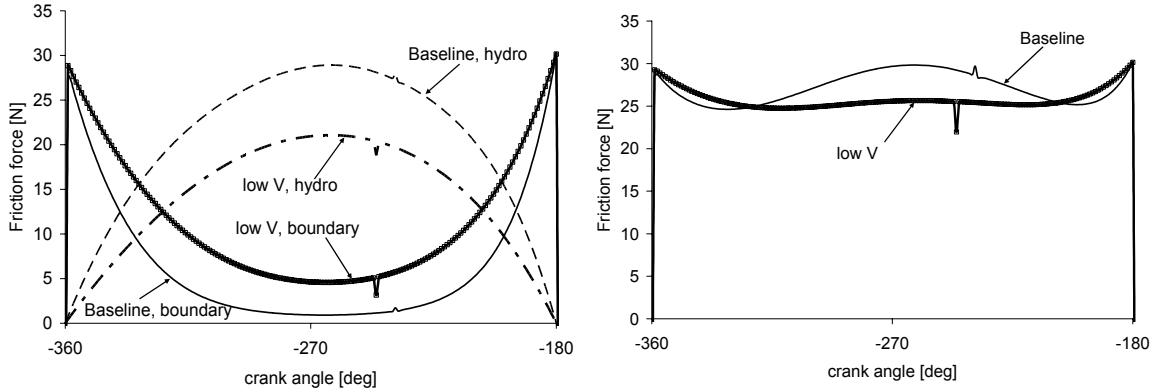

a)Ring/liner friction force, hydrodynamic and boundary

b)Ring/liner friction, total

Figure 4-2: Effect of viscosity on hydrodynamic and boundary friction, intake stroke, lower land OCR

This distribution of friction regimes is also shown in an analysis of ring/liner friction force. Figure 4-2a shows friction force, per crank angle, for a single (intake) stroke in the Waukesha engine, for the lower land only. In general, results for only the lower land are shown, except when noted, for simplicity in showing trends. The upper land shows the same trends in all cases. In the ring-pack simulation program used, asperity contact is assumed to occur only for film thicknesses less than four times the combined roughness of the surfaces. For larger film thicknesses, the chance of boundary contact (less than 2%) is assumed to be small enough to be negligible. In all other cases, the boundary contact pressure is calculated according to the model given by Greenwood and Tripp [16]

In the figure, boundary friction is high near dead-centers, where oil film thickness is small, while hydrodynamic friction is high near mid-stroke where piston speed and film thickness are large. For the lower viscosity lubricant, the hydrodynamic friction is reduced, while boundary friction is increased, corresponding to the reduction in oil film thickness shown in Figure 4-1b. Figure 4-3 shows the viscosities of the two cases compared. The variation in viscosity with crank angle is due to the dependence of viscosity on temperature, which is high near TDC and decreases to a minimum value at BDC. Viscosity values for two strokes are shown, to indicate the full range of viscosity variation during an engine cycle.

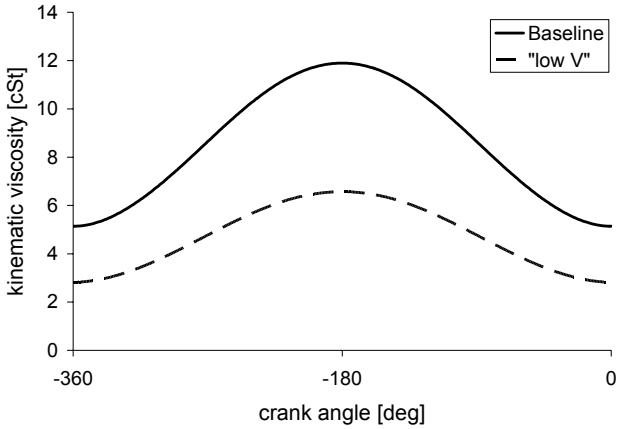

Figure 4-3: Viscosity change during the engine cycle, Baseline and low-viscosity cases. Intake and compression strokes shown

The power lost to ring/liner friction is proportional to the ring/liner friction force and the piston speed at which that force is generated. Although the friction force near dead-centers is of a similar magnitude to the friction force near mid-stroke, mid-stroke power losses are much higher because of the dependence on piston speed. Changes in mid-stroke friction force, then, have a greater effect on total cycle friction than changes in end-stroke friction force. Figure 4-4, which shows the friction work loss per crank angle associated with the friction forces shown in Figure 4-2, illustrates this, as do further examples given in sections 4.2 and 4.3.

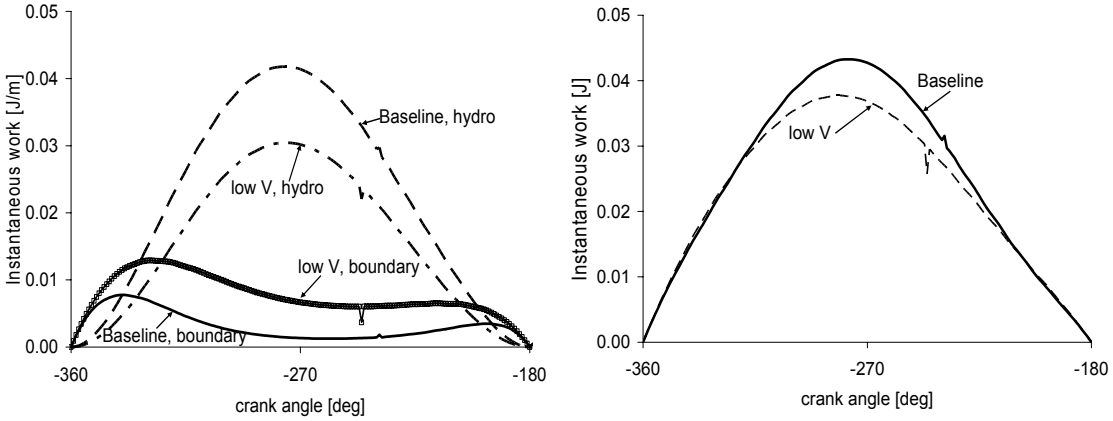

a)Ring/liner friction power loss, hydro and boundary **b)Total ring/liner friction power loss, for 2 viscosity cases**

Figure 4-4: Effect of viscosity on boundary and hydrodynamic friction work, per crank angle, intake stroke, lower land of OCR

Figure 4-4a shows the boundary and hydrodynamic work losses. For the baseline case, most of the frictional energy losses are due to hydrodynamic lubrication near mid-stroke. For the lower viscosity case, there is an increase in boundary losses at mid-stroke because of the increase in asperity contact there, with a corresponding decrease in hydrodynamic losses. The balance between these two changes determines the extent of the change in overall friction, which is shown in Figure 4-4b. In this figure, it is clear that the mid-stroke effects of changing viscosity almost entirely determine the change in overall friction, for this example, with only minimal contribution from the dead-center region.

The hydrodynamic/boundary friction trade-off occurs not only during the engine cycle, but for the ring pack as a whole. Figure 4-5 illustrates the trade-off between hydrodynamic and boundary lubrication for total cycle friction for the entire Waukesha engine ring-pack. The figure shows the same trends presented above – friction tends to decrease with viscosity as long as the oil is viscous enough to support hydrodynamic lubrication. When viscosity gets too low, friction begins to increase, as boundary friction becomes large. An ideal viscosity is found at the balance of these trends, where a minimum friction loss is found. The goal of this study is to define this ideal viscosity, taking into account viscosity variation during the engine cycle, for the Waukesha engine.

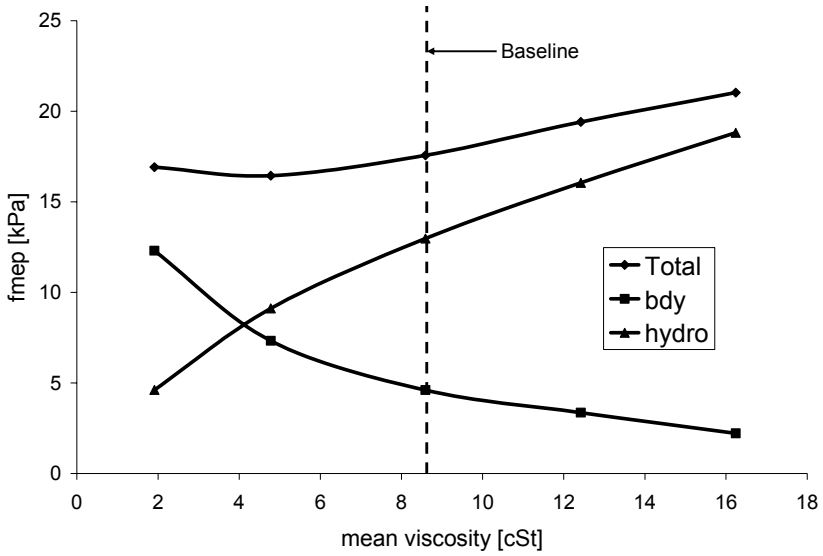

Figure 4-5: Trade-off between hydrodynamic and boundary friction for the baseline ring-pack. Oil is a straight-weight oil (no shear thinning). Fmep is the friction mean effective pressure, a measure of total friction power loss over the engine cycle.

4.2. Viscosity Variation During the Engine Cycle – Idealized Cases

Ring/liner friction is closely related to lubricant viscosity - if viscosity variation during the engine cycle can be controlled, friction reduction may be possible. Several idealized cases were investigated analytically to assess this possibility. The main conclusion of these analyses is that viscosity in the mid-stroke region, where ring speed is high, is the most important parameter to control. Controlling viscosity near dead-centers was the focus of the investigation, and was shown to provide only a small possible friction reduction benefit. A greater advantage of controlling dead-center viscosity may lie in wear reduction, which is discussed in section 4.6.

Two categories of idealized cases were considered: (a) in which viscosity is held constant throughout the cycle, and (b) in which viscosity is increased or held high near dead-centers, to reduce dead-center asperity contact. Initially, the mid-stroke viscosity in each of these cases is kept the same as the baseline case, so that the effect of the viscosity variation can be assessed independently of overall mean viscosity effects. The mid-stroke viscosity was chosen as a reasonable "mean" viscosity both because it is close to the actual mean for the baseline case, and because the mid-stroke region is the source of most of the ring frictional losses. The effect of reducing overall viscosity in both cases

(a) and (b) was also evaluated. Viscosity variation during an engine cycle for the example cases discussed, as well as the baseline case, is shown in Figure 4-6.

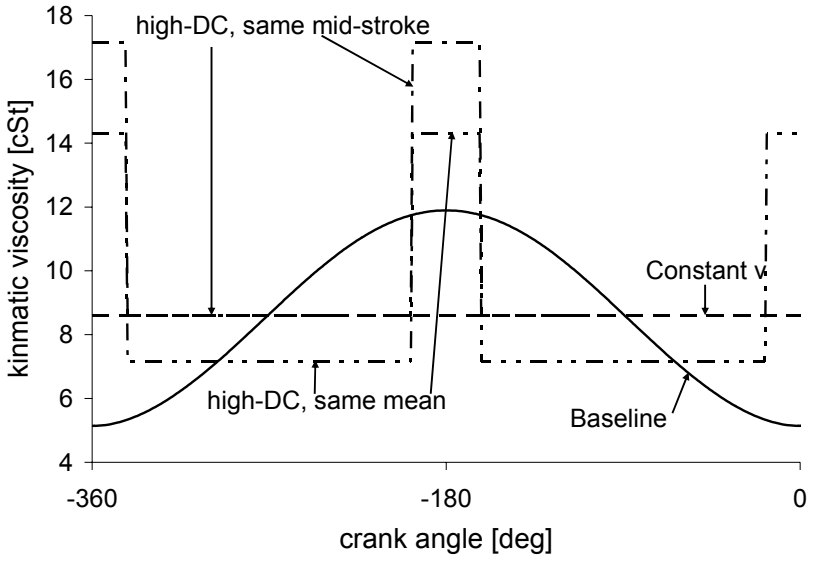

Figure 4-6: Viscosity variation during an engine cycle for three representative cases

4.2.1. Case (a) – Viscosity held constant throughout the stroke

Only a small change in friction was observed between the baseline and constant viscosity case (see Table 4-1) where the friction losses were ~1% higher than the baseline. This is because, for the baseline case, the mean viscosity occurs near mid-stroke, so that any viscosity effects that occur before mid-stroke tend to cancel out those that occur after. Figure 4-7 shows this effect, where the friction forces and frictional power losses for these two cases are plotted. In the beginning of the stroke, the viscosity of the baseline lubricant is lower than that in the constant viscosity case, so that baseline hydrodynamic friction is lower, and boundary friction is higher, than for the constant viscosity case. The opposite occurs in the second part of the stroke, so that the overall result is the shift observed, and the overall change in friction is relatively small.

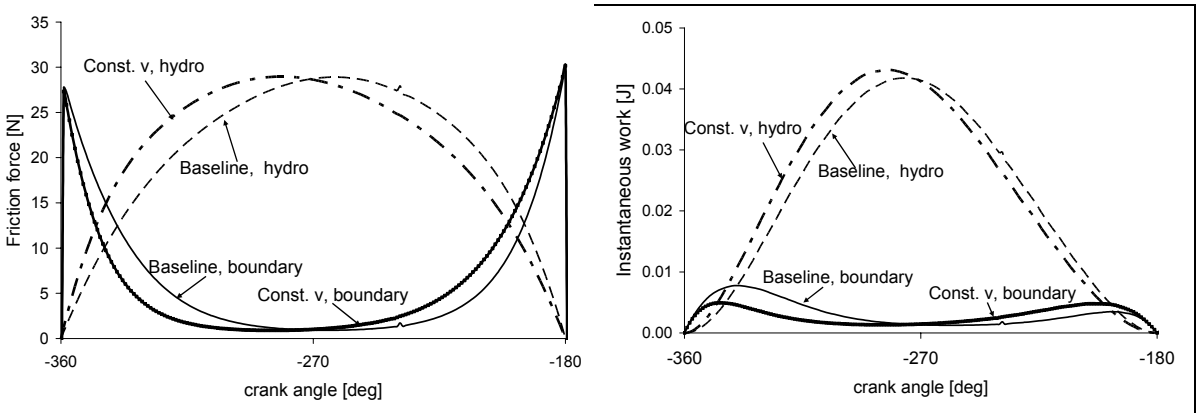

a) Friction force, per crank angle **b) Friction work loss, per crank angle**

Figure 4-7: Constant viscosity case compared to baseline viscosity case, lower land OCR

This is further illustrated in Figure 4-8, which shows the same friction work as a function of piston speed during the intake stroke (other strokes show the same trends), where the arrows indicate the direction of increasing crank angle. This figure shows clearly the effects of the changing viscosity – plotting the friction force vs. piston speed for a stroke removes the effect of the speed, so that viscosity effects are seen more clearly. Figure 4-8a shows that friction for the baseline case is lower than average in the first part of the stroke (where viscosity is lower) and higher in the second. Over the entire stroke, the friction in these two periods averages to a value that is close to that for the constant viscosity case. For the constant viscosity case, there is almost no difference between friction in the first and second parts of the stroke.

Figure 4-8b shows the effect of changing viscosity when the viscosity is held constant during the stroke (the study of mean viscosity effects is further discussed below). The lower viscosity case clearly has lower frictional losses, with the majority of the friction reduction occurring near mid-stroke, due to decreased hydrodynamic friction. This figure shows that the effects of viscosity are largest near mid-stroke, and are small near dead-centers, for this viscosity range. This phenomenon contributes to the relatively small friction benefit predicted for the second idealized case considered, which is summarized below.

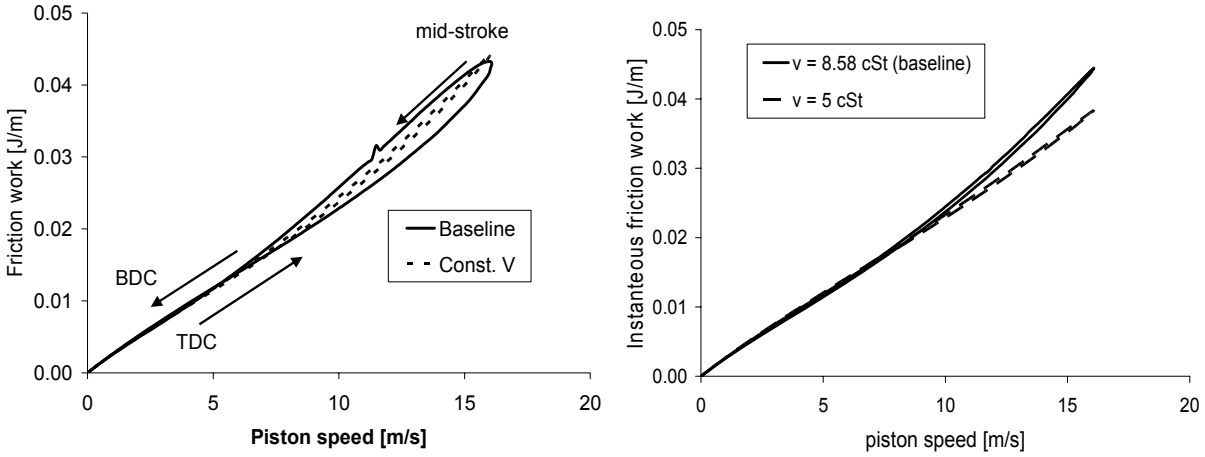

a) Instantaneous friction work, as a function of piston speed

b) Effect of mean friction reduction, constant viscosity case

Figure 4-8: Effect of viscosity temperature dependence, comparing baseline and constant viscosity cases, intake stroke, lower land, OCR

4.2.2. Case (b) – Viscosity held high at dead-centers – "High-DC" cases

Several different viscosity profiles were investigated in which viscosity near dead-centers was held high and viscosity near mid-stroke was held constant or reduced. In one group, a mean viscosity that was the same as the baseline case was maintained, and the width of the high-viscosity peak was varied (number of crank angles for which viscosity was held high). In a second group, the mid-stroke and dead-center viscosities were held constant, with the mid-stroke viscosity matching the baseline case, while the width of the high-viscosity peak was varied. In both groups the end-stroke viscosity was maintained at twice the mid-stroke viscosity. These viscosity variation cases are referred to as "high-

DC", for the high viscosity found near dead-centers, and some examples are shown in Figure 4-9. Example results from both groups are presented below.

When the mid-stroke viscosity is kept the same as the baseline case, there is only a small difference in friction between the baseline and high-DC cases – and almost no difference in frictional losses between the high-DC and constant viscosity cases. Two examples are shown, one in which the transition from high to low viscosity occurs near the crank angle at which boundary and hydrodynamic friction are equal (about 18^{o} ATDC), and one in which the transition occurs earlier (closer to dead-center) than this, at 12^{o} ATDC (see Figure 4-11a). Figure 4-10 shows both high-DC cases compared to the constant viscosity case, which shows the effects of the viscosity variation more clearly than comparison with the baseline. Both high-DC viscosity strategies cause boundary friction to decrease near dead-centers, with a corresponding increase in hydrodynamic friction due to the increased viscosity compared to the constant-viscosity case.

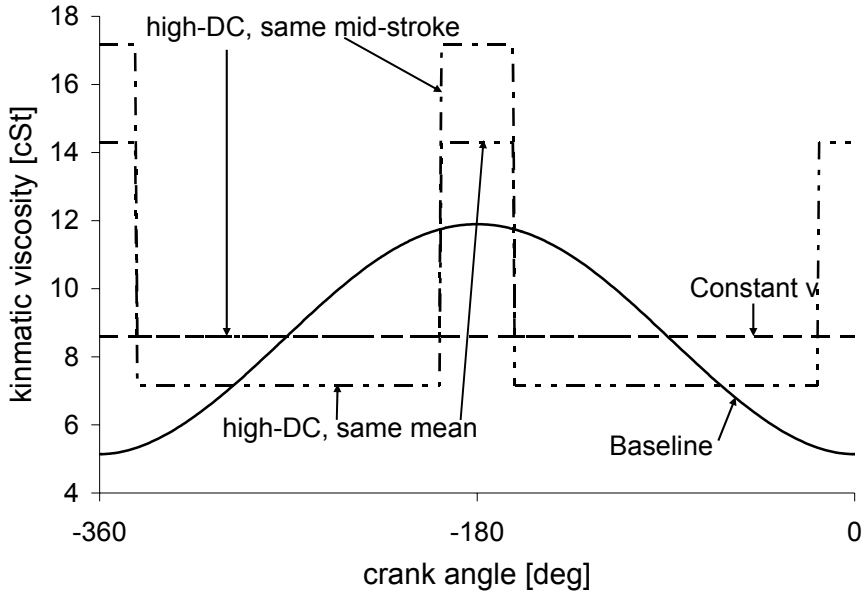

Figure 4-9: Example high-DC cases, viscosity variation during the engine cycle

Figure 4-11b shows the net result of these changes. For the 18^{o} case, there is a net reduction in friction close to dead-centers, but a net increase as the piston speed increases and hydrodynamic friction becomes important, at around 12 ^{o} ATDC, (at the beginning of the stroke only). The result is zero net change in fmep compared to the constant-viscosity case – the reduction in boundary friction and increase in hydrodynamic cancel each other. For the12 ^{o} case, there is the same net decrease in friction near the end-strokes, and the transition is timed well so that there is only a small subsequent increase in hydrodynamic friction. The result is a net decrease in fmep, compared to the constant viscosity case. However, because the net reduction in friction is so small (note that the scale on the friction axis in Figure 4-11b is magnified) and the contribution to friction power loss near dead-centers is small, this reduction is negligible. Results for both cases are summarized in Table 4-1.

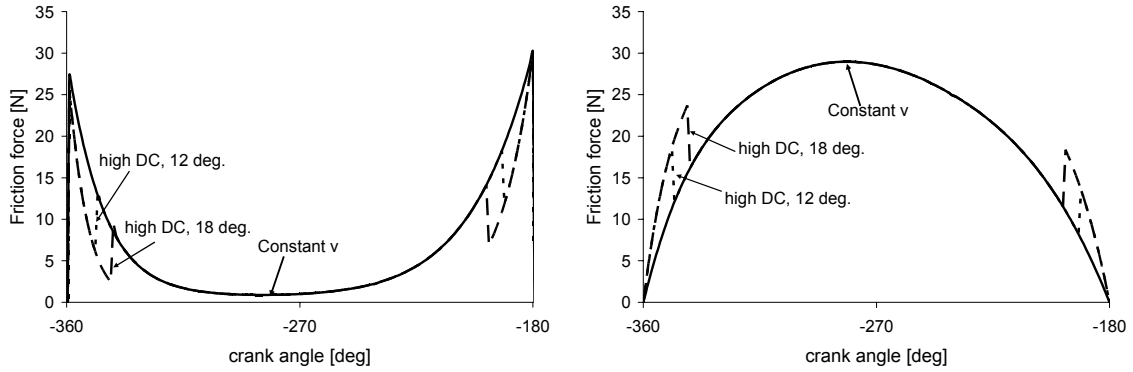

a) Boundary friction, constant viscosity and two high-DC cases, intake stroke

b) Hydrodynamic friction, constant viscosity and two high-DC cases, intake stroke

Figure 4-10: Effect of high-DC viscosity variation on hydrodynamic and boundary friction

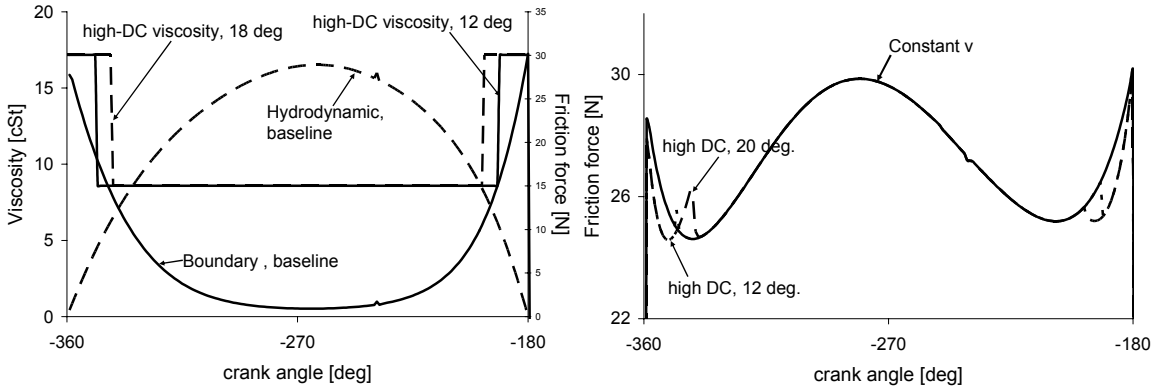

a)The transition crank angles for high-DC cases were based on the hydrodynamic/boundary transition

b) Total friction force for constant viscosity and two high-DC cases, intake stroke

Figure 4-11: Effect of high-DC viscosity on total ring/liner friction

A case in which mean, rather than dead center, viscosity was held the same as the baseline case was also considered. In the example shown in Figure 4-12, the high/low viscosity transition occurred at 18^{o} ATDC. An overall reduction in friction of ~4% from the baseline was observed for this case, but the reduction was due entirely to a decrease in mid-stroke hydrodynamic friction, and did not stem from effects in the dead-center region. The same friction reduction could have been obtained with a constant-viscosity strategy, with the constant viscosity the same as occurs the mid-stroke region of this high-DC case.

Figure 4-12 shows a comparison of the hydrodynamic, boundary, and overall friction forces for this high-DC and constant-viscosity cases. The high-DC case shows lower hydrodynamic friction near mid-stroke, as well as lower boundary friction near dead-centers, compared to the constant viscosity case, as expected based on the viscosity distribution. The high-DC case also shows higher boundary friction near mid-stroke and higher hydrodynamic friction near dead-centers, however, because there is a trade-off between the two lubrication regimes when viscosity changes. The boundary friction reduction near dead-centers is entirely offset by the increase in asperity contact near mid-stroke (see Table 4-1), while the reduction in mid-stroke hydrodynamic friction produces

a net decrease in hydrodynamic losses. The net result, as shown in Figure 4-12b, is an overall friction reduction of about 4%.

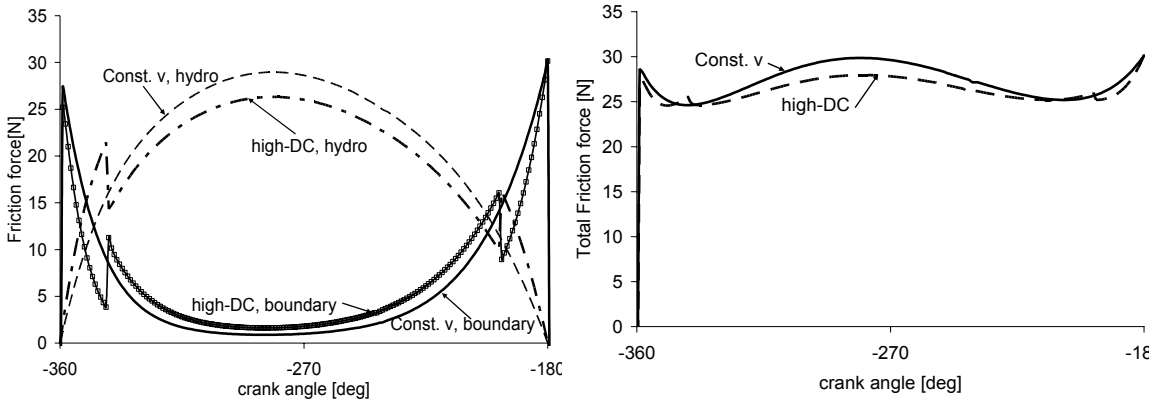

a) Hydrodynamic and boundary friction forces **b) Total friction force**

Figure 4-12: Comparison of friction force in high-DC and constant viscosity cases, lower land, OCR

These examples show that, for the cases studied, controlling viscosity near dead-centers has almost no effect on total cycle friction. One reason for this is that any reduction in boundary friction near dead-centers is always at least partially offset by a corresponding increase in hydrodynamic friction. If the high/low transition is not well-placed, the increase in hydrodynamic friction may become large and result in a net increase in friction, rather than the desired decrease. If another method of reducing boundary friction – for example, with surface modifiers – can be used, and this increase in hydrodynamic friction can be avoided, a larger friction reduction benefit is possible, both at dead-centers and throughout the stroke.

Another factor leading to lack of benefit in controlling end-stroke viscosity is that the contribution to overall friction from dead-centers is only a small fraction of the total cycle losses. Although friction forces may be high, the slow piston speeds in this region keep friction power losses low. Dead-center boundary friction (where the "dead-center region" is taken as +/-18 crank-angle degrees around each ring-reversal) accounts for only a few percent of the total ring friction, as shown in Figure 4-13. Then, any friction reduction associated with reducing boundary friction here cannot exceed this relatively small amount.

Table 4-1: Effects of different viscosity variation cases on friction, constant mid-stroke viscosity

	Fmep, [kPa]	Fmep, bdy [kPa]	Fmep, hydro [kPa]	Fmep change, from baseline
Baseline	11.14	1.19	9.95	--
Constant viscosity	11.25	1.02	10.23	+1%
High–DC, same mid-stroke, 18 deg	11.25	0.88	10.34	+1%
High-DC, same mid-stroke, 12 deg	11.25	0.97	10.28	+1%
High-DC, same mean, 18 deg	10.72	1.32	9.4	-4%

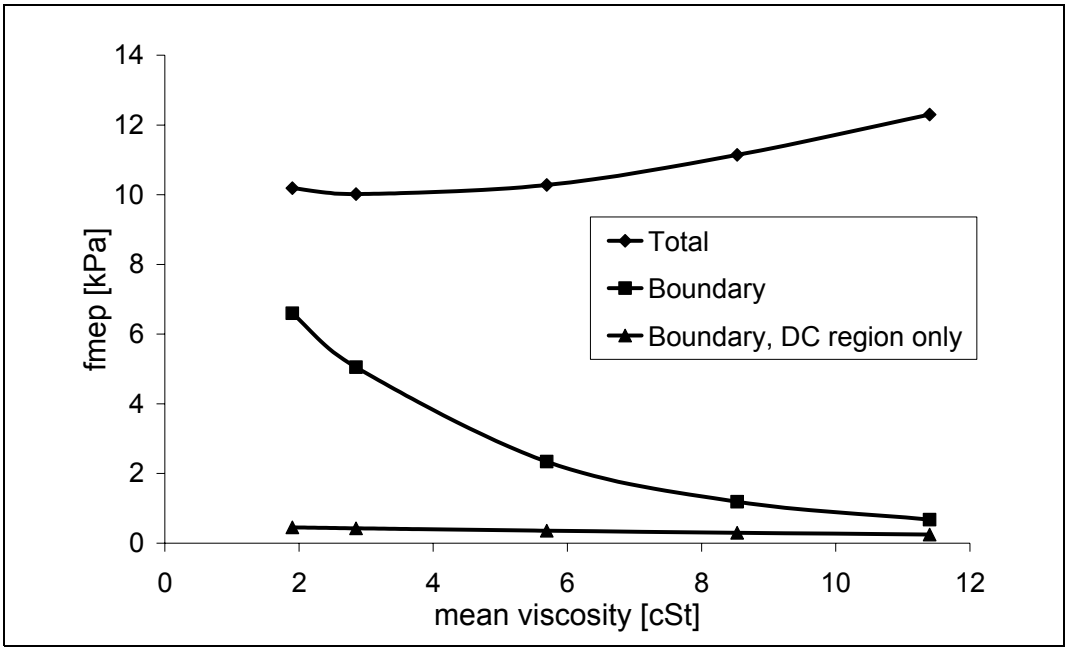

Figure 4-13: Friction forces and friction power loss, baseline viscosity

4.2.3. Changing Mean Viscosity

Friction depends on both viscosity variation during the cycle and the overall mean cycle viscosity. The three viscosity variation cases (baseline, constant viscosity, and high-DC) considered above were evaluated for different mean viscosities. For the high-DC case, the dead-center viscosity was held constant, and the mid-stroke viscosity reduced. As was indicated in Figure 4-5, overall ring friction changes with viscosity, and a minimum fmep is found at a balance between hydrodynamic and boundary friction during the ring cycle. This study showed that the minimum friction loss obtainable is approximately the same for each viscosity condition.

Figure 4-14 shows the change in total cycle friction losses for the OCR for the baseline viscosity profile, with the corresponding boundary and hydrodynamic components. As the figure shows, there is the potential for an ~10% reduction in ring

friction from the current baseline. This reduction results from a decrease in hydrodynamic friction in the mid-stroke region.

In Figure 4-15, the results for the three cases are compared, and plotted against mid-stroke viscosity. There is almost no difference between the three viscosity strategies for the range of viscosities studied, with the high-DC case showing a small (less than 1%) reduction in minimum friction. As in the case described in section 4.2.2, the high-DC case does provide a consistently lower boundary friction loss than the baseline case, but this is offset by a matching increase in hydrodynamic friction (see Figure 4-16). Again, it is shown that the major effect of viscosity on friction is in the mid-stroke region, and controlling dead-center viscosity has a relatively small effect.

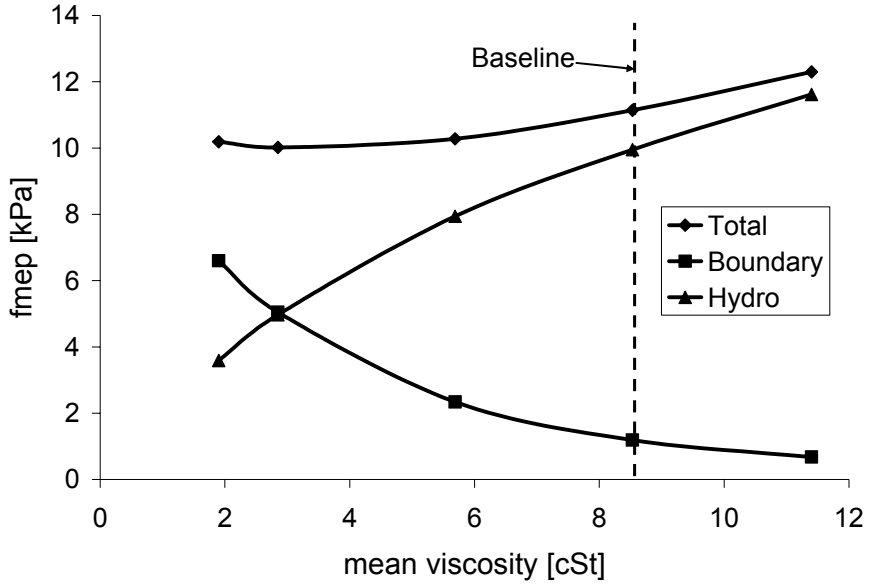

Figure 4-14: Hydrodynamic vs. boundary friction trade-off for the OCR, baseline viscosity variation

It should be noted that, although there is only a small friction benefit in controlling dead-center viscosity, there may be a wear benefit. High boundary friction is an indicator of wear. Although reducing the high friction near dead-centers may not substantially reduce frictional losses, reduction of asperity contact in this region should cause a wear reduction. A simple analysis of this possibility was performed, and is discussed briefly in section 4.6.

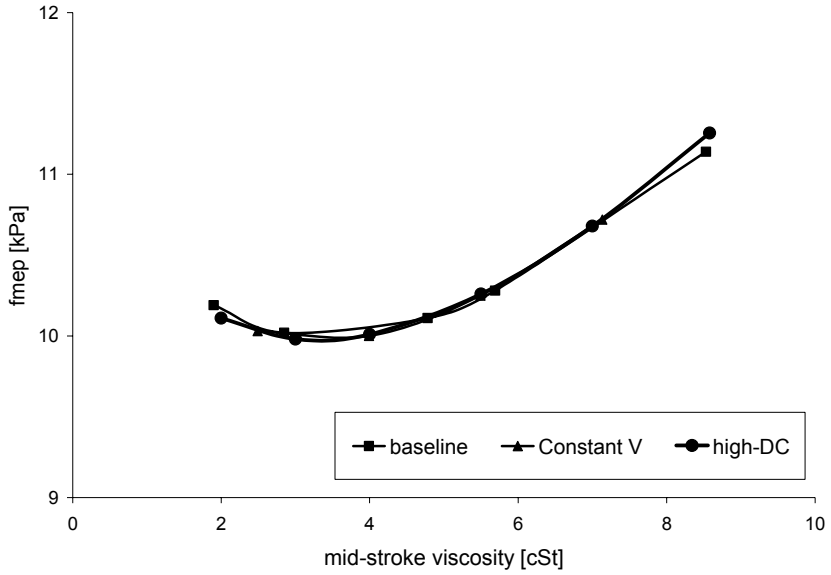

Figure 4-15: Reduction in total cycle friction with mean viscosity, three viscosity variation cases, OCR.

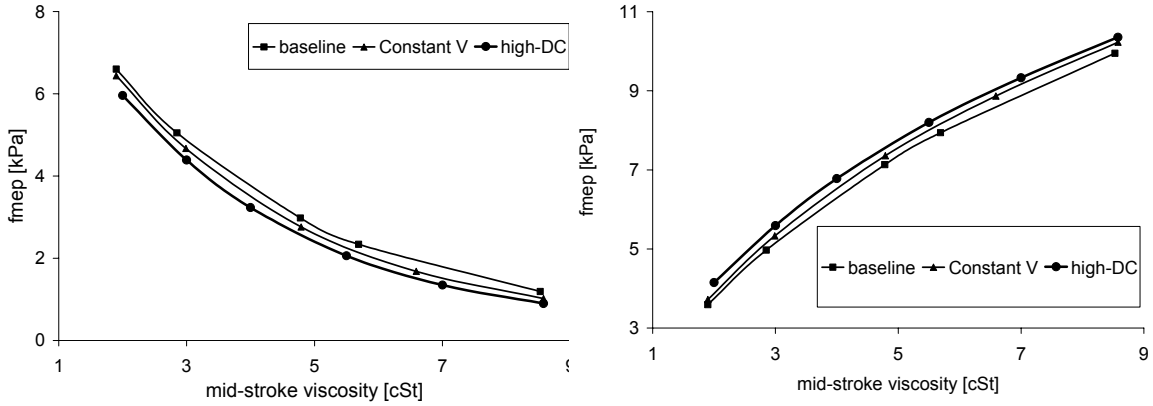

a)Fmep from boundary friction **b)Fmep from hydrodynamic friction**

Figure 4-16: Hydrodynamic and boundary contribution to total fmep, three viscosity cases

4.3. Viscosity Variation During the Engine Cycle – Real Engine Conditions

Although it is useful to study idealized conditions to evaluate viscosity control strategies and best-case scenarios, in the engine the realistic temperature and shear-rate dependence of the lubricant viscosity must be taken into account. The effects of both temperature and shear rate parameters were studied, and results are summarized below. In the case of temperature dependence, the effects of the "steepness" of the variation – the strength of the viscosity temperature dependence – were considered. In the case of shear rate dependence, the high/low shear transition region was studied, and parameter values assigned to mimic an idealized case discussed above – high viscosity near dead centers and low near mid-stroke.

4.3.1. Lubricant viscosity parameters

The dependence of lubricant viscosity on temperature and shear rate were modeled by commonly used relationships: the Vogel equation for temperature dependence, and the Cross equation for shear rate dependence. These equations and the parameters used in them are described below.

4.3.1.1. Temperature Dependence

Because the oil film is very thin, the temperature across the film (in the radial direction) is assumed to be constant. Then, for each axial lubricant element, the viscosity is assumed to be constant across the film thickness and dependent on the oil temperature, as described by the Vogel equation:

$$\nu \quad z \; e^{\frac{T_1}{T_2 \; T}} \tag{4.1}$$

where ν is the kinematic viscosity of the lubricant, z is an oil "thickness" parameter, T_1 is an overall temperature-viscosity dependence parameter, T_2 is a lower bound parameter that is related to the glass transition temperature of the lubricant, and T is the lubricant temperature. Increasing T_1 increases the change in viscosity for a given temperature change, while increasing T_2 has the opposite effect. For a small T_1 or large T_2, the viscosity can become virtually independent of temperature.

To evaluate the effect of the strength of the viscosity-temperature relationship, lubricants with several values of T_1 were compared (while z was changed accordingly to keep mid-stroke viscosity constant). Figure 4-17 shows viscosity as a function of temperature for a few of the T_1 values studied. The liner temperatures at TDC for the top ring and BDC for the OCR are shown. A square-root distribution is assumed for the liner, bounded between these two temperatures.

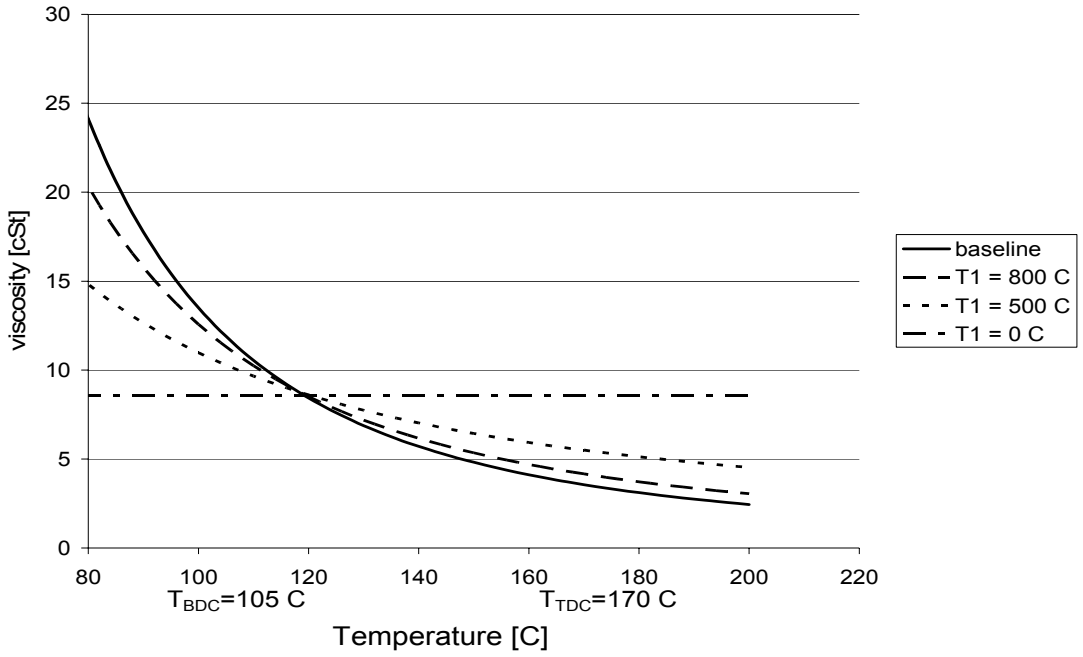

Figure 4-17: Examples of viscosity variation with temperature.

4.3.1.2. Shear-Rate Dependence

The large temperature variations in the internal combustion engine cause large variations in viscosity, as shown in Figure 4-17. Viscosity index improvers (VII's), are added to many engine lubricants to decrease this dependence of viscosity on temperature. A side effect of such additives is to cause shear thinning in the lubricant – the viscosity becomes dependent on the oil shear rate, where high shear rates cause the oil viscosity to be reduced.

The Cross relationship was used to model the dependence of viscosity on shear rate:

$$\nu = \nu_0 \frac{1 + \left(\frac{\nu_\infty}{\nu_0}\frac{\gamma}{\beta}\right)^m}{1 + \left(\frac{\gamma}{\beta}\right)^m} \tag{4.2}$$

where ν_0 is the low shear viscosity (obtained from the Vogel equation, above), ν_∞/ν_0 is the ratio of high shear viscosity to low shear viscosity, γ is the lubricant shear rate, m is a parameter governing the width of the low shear-high shear transition region, and

$$\beta = 10^{c_1 + c_2 T} \tag{4.3}$$

is the critical shear rate, which controls the shear rate at which the low shear/high shear transition occurs (c_1 and c_2 are parameters controlling β). Figure 4-18 shows several typical viscosity-shear rate relationships that were used for the current study, with parameters given in Table 4-2 (in section 4.3.3).

For very low and very high shear, viscosity is approximately constant. A transition region, whose width is determined by the parameter m and whose location is determined by β, the critical shear rate, separates the high and low shear regions. In the case of piston rings, the lubricant between ring and liner generally experiences a higher shear rate than the critical shear rate for almost the entire cycle, with the exception of a few crank angles near dead centers. Then, the lubricant is essentially dependent only on temperature. The value of the critical shear rate was adjusted in this study, to assess the effects of having the transition occur during the ring stroke.

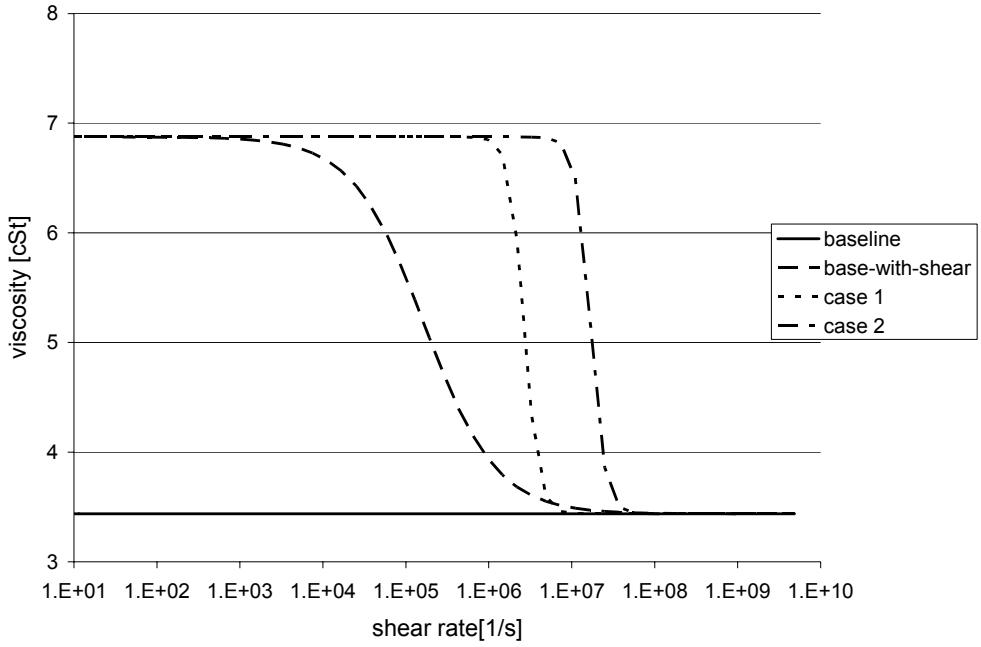

Figure 4-18: Viscosity variation with shear rate, for cases studied

4.3.2. Temperature Dependence - OCR

The parameter T_1 was varied in order to vary the degree to which viscosity changes with changing temperature, while z was also changed proportionally, in order to maintain a constant average viscosity for the cycle. For all of the cases studied, the mean viscosity occurred near mid-stroke, so maintaining a constant mid-stroke viscosity was equivalent to maintaining a constant mean, with the amount of viscosity variation between TDC and BDC varying between cases. A range from a high temperature dependence to no dependence ($T_1 \sim 0$) was considered. Figure 4-19 shows the lubricant temperature change for an engine cycle, and the corresponding cycle lubricant viscosities for each case.

For each case considered, the viscosity variation is close to symmetric about mid-stroke – that is, it is low on one side (either the beginning or end of the stroke), passes

through mid-stroke at close to the mean viscosity, then is high on the other, as shown in Figure 4-19b. This is the same phenomenon that was described in the ideal, constant-viscosity case studied in section 4.2.1. As in that case, the resulting change in friction is small, because the friction changes due to changing viscosity during each half of the stroke largely cancel each other out.

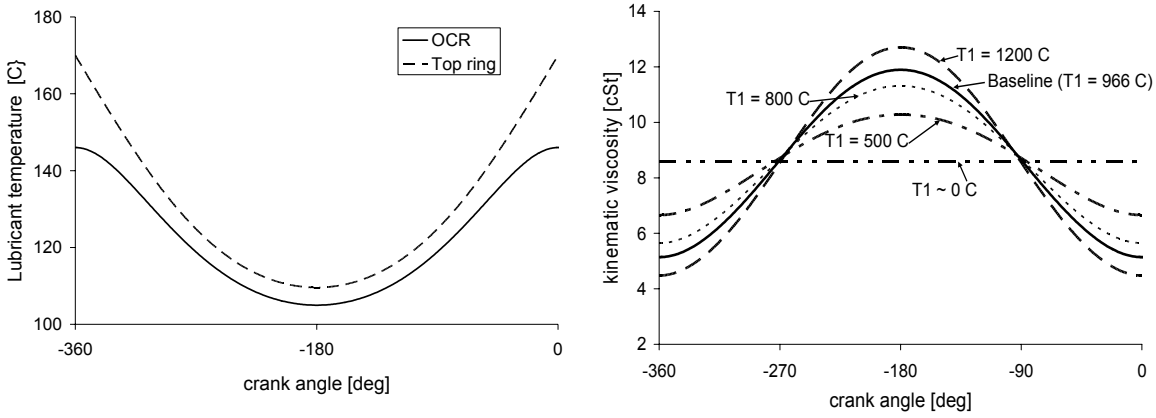

a) Temperature variation of oil film in the engine

b) Variation of viscosity for an engine cycle, 2 strokes

Figure 4-19: Variation of viscosity during an engine cycle for test cases considered

Simulations were run considering the different temperature-dependence cases at different mid-stroke viscosity values. An example of a group of profiles with different mean viscosities, with temperature dependency T_1 = 800° C, is shown in Figure 4-20. Figure 4-20 shows the results of the study – almost no difference in fmep values is seen between the cases. Cases with low T_1 (relatively "flat" profile) showed slightly higher friction at high viscosities, due to a slight increase in hydrodynamic friction, but for the most part all of the cases gave the same friction for the viscosity range studied. This is again due to the effect illustrated in Figure 4-8, section 4.2.1, which indicates that friction generation over a cycle remains approximately constant, for the types of viscosity variations studied here, as long as the variation is symmetric about mid-stroke.

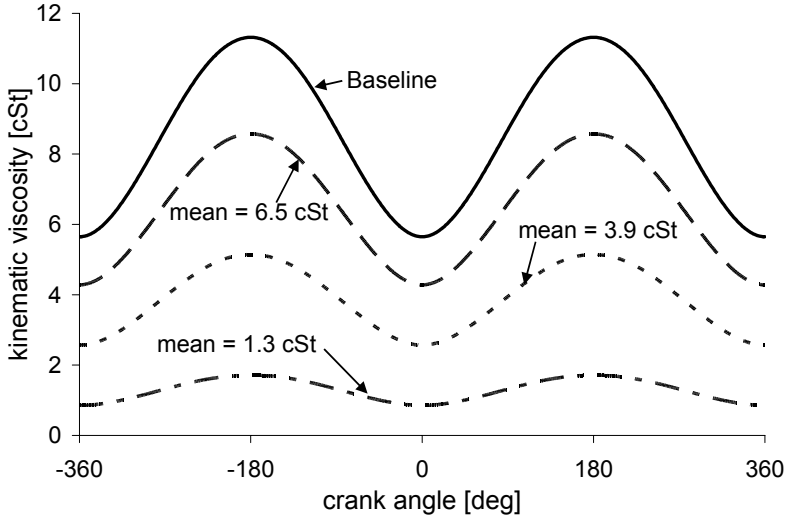

Figure 4-20: Viscosity variation during the engine cycle for changing mean viscosity, T_1 = 800C

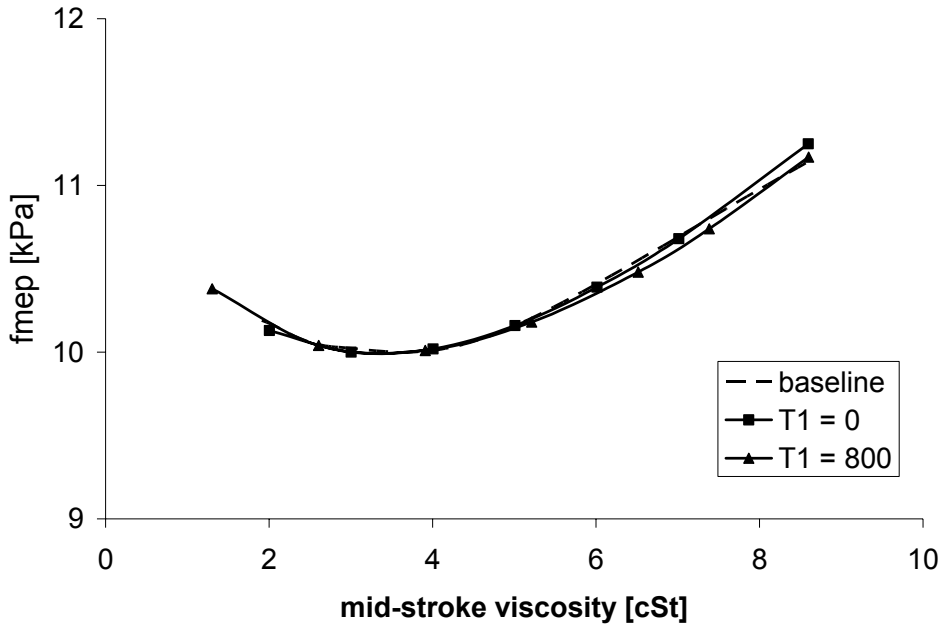

Figure 4-21: Dependence of fmep on mean/mid-stroke viscosity, different temperature dependence cases

4.3.3. Shear Rate Dependence – OCR

In addition to being dependent on temperature, the viscosities of many lubricants are also dependent on the shear rates experienced by the oil. In this study, the critical shear rate and transition region were controlled to study the effects of viscosity transitions taking place during the stroke. This is a method by which to approximate the idealized cases described above, where viscosity can be held high near dead-centers and low near mid-strokes (although the temperature dependence is still present). As is shown below, the results of this study are similar to those of the idealized case – friction benefits are relatively small – but the reduction in minimum friction that is achieved is slightly larger than in the idealized case, of ~1% below the baseline value.

Many sets of Cross equation parameters were studied, and several examples are presented. The parameters for these examples are given in Table 4-2, and variation in viscosity during an engine cycle corresponding to the cases presented is shown in Figure 4-22b. As is shown in the figure, the effect of controlling the Cross equation parameters in this manner is to keep viscosity high near dead-centers and lower near mid-strokes, where the temperature dependency of the viscosity (which was kept at the baseline value) also contributes to the variation. The two cases 1 and 2 demonstrate the effects of changing the width of the high-viscosity region.

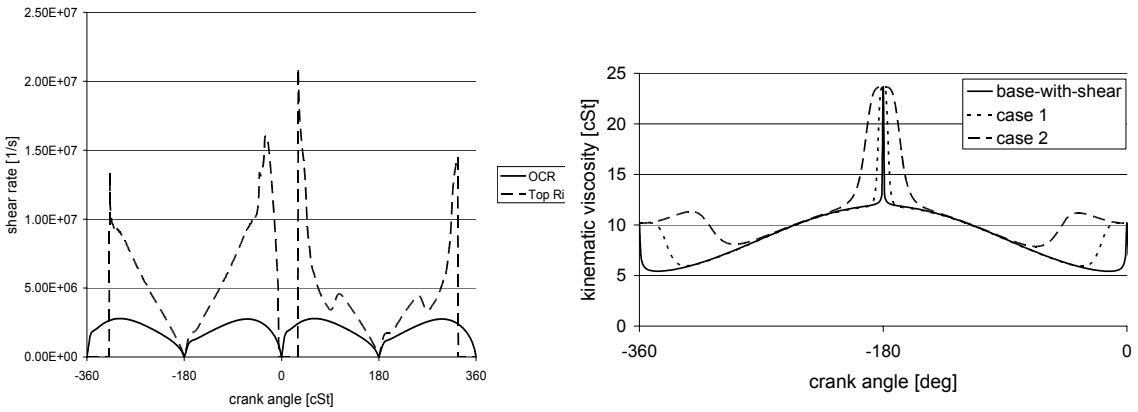

a) shear rate variation during an engine cycle **b) viscosity change during 2 strokes, studied cases**

Figure 4-22: Shear rate variation and viscosity (shear-rate dependent) variation during an engine cycle

Table 4-2: Cross equation parameters for three cases studied

Case	m	$v_{high\text{-}shear}/v_{low\text{-}shear}$	c_1	c_2	ν_∞/ν_0
baseline with shear*	1	.5	2.3	.0225	0.5
case 1	5	.5	3.8	.0225	0.5
case 2	5	.5	4.3	.0225	0.5

*** 1 This case uses all baseline Cross equation parameters except ν_∞/ν_0=0.5, which adds shear dependence to the baseline case, which is a straight-weight oil.**

As in the idealized case, keeping viscosity high near dead centers causes a decrease in boundary friction there, with a corresponding increase in hydrodynamic friction, as is shown in Figure 4-23. When the mid-stroke viscosity is matched with the baseline case, the case 1 viscosity distribution shows a slight reduction in friction, while case 2 shows a slight increase. This is related to the hydrodynamic/boundary friction balance in the engine cycle. In baseline conditions, the high/low viscosity transition for case 2 occurs relatively late in the stroke, in a region where hydrodynamic lubrication accounts for a large fraction of the total ring/liner friction. Then, the effect of the high viscosity is to increase the already high hydrodynamic friction. For case 1, the high viscosity period remains within a zone where boundary friction is dominant, so that the reduction in boundary friction is slightly higher than the increase in hydrodynamic friction.

As overall viscosity changes, the hydrodynamic/boundary friction balance in the engine cycle changes. In particular, as viscosity is decreased, hydrodynamic lubrication becomes less effective and boundary friction increases. The zone around dead-centers where boundary friction is dominant extends farther toward mid-stroke, and contributes more to total friction losses because it extends into a zone where piston speed is increased. Then, a larger high-viscosity zone, such as occurs in case 2, provides more benefit. This is shown in Figure 4-25, which shows the effect of changing mid-stroke viscosity on ring friction, for the cases considered. It also explains why no friction

benefit is observed in the idealized case at low viscosity – the width of the high-viscosity region in the idealized case is not large enough to provide much friction reduction, because it remains within the low-speed, dead-center region.

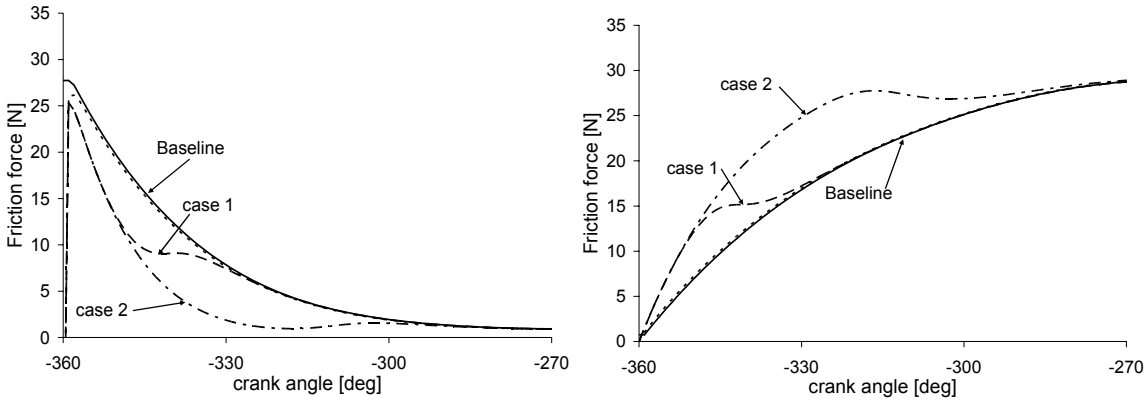

a)Boundary friction near TDC, intake, cases 1 and 2 **b)Hydrodynamic friction near TDC, intake, cases 1 and 2**

Figure 4-23: Hydrodynamic and boundary friction effects in cases 1 and 2.

It should be noted that, in Figure 4-25, the ratio of high-shear to low-shear viscosities is not kept constant as mean viscosity changes. This is because, as mean viscosity is reduced, the magnitude of the low-shear viscosity (the high viscosity at dead-centers) decreases, as shown in Figure 4-24a. To counter this decrease and keep dead-center viscosity approximately constant, the high:low viscosity ratio was changed with mean viscosity - example of this are shown in Figure 4-24b.

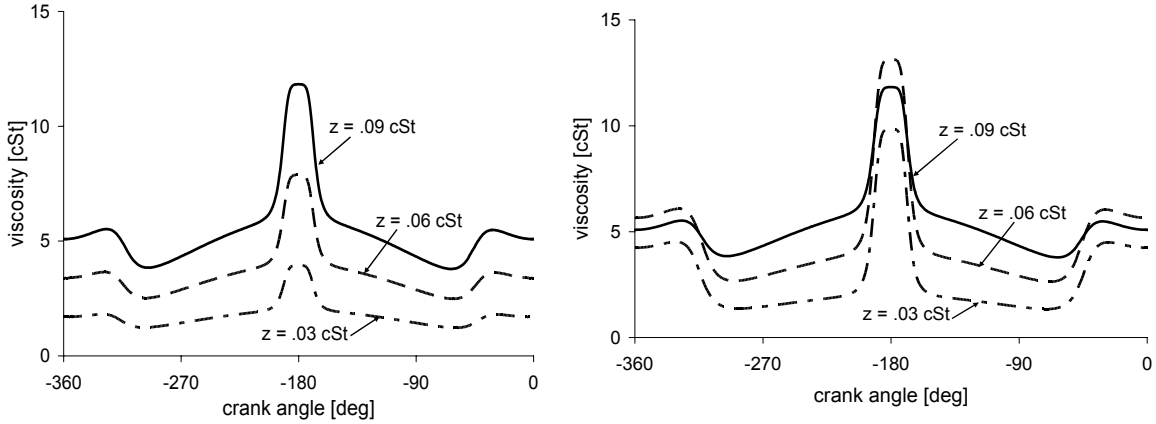

a) High/low shear viscosity ratio kept constant **b)High/low shear viscosity ratio set to maximize friction reduction for a given z value.**

Figure 4-24: Viscosity variation during the engine cycle, case 2

Figure 4-25 shows the effects of changing mean viscosity for the cases considered, with the high/low shear viscosity ratio optimized for low friction, at a given mid-stroke viscosity. The figure shows that there is a small friction benefit of ~1% using case 2 parameters. Simply reducing mean viscosity can reduce cycle friction by about 10%, if viscosity variation is controlled in the manner described here, a reduction of ~11% may be possible, from the current baseline oil.

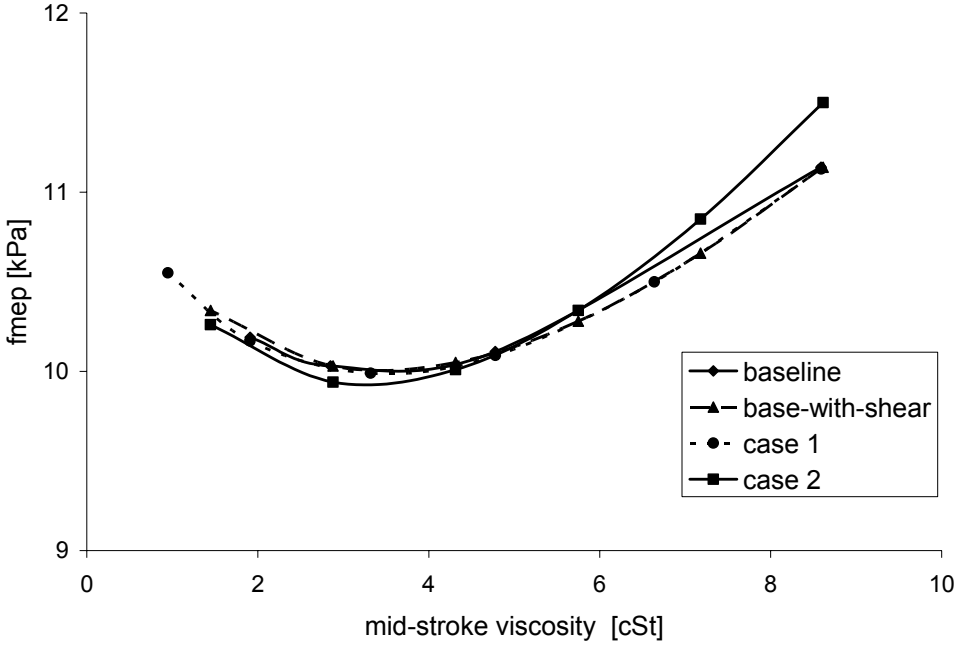

Figure 4-25: Dependence of OCR friction losses on mid-stroke viscosity, for different shear-rate dependence cases.

Because their benefits are dependent on reducing dead-center boundary friction, which is only a small contributor to overall friction, the friction reductions offered by controlling viscosity temperature and shear dependence are small. Still, some benefit may be gained, and, as discussed in section 4.6, there may also be a benefit in wear reduction in keeping dead-center viscosity high.

4.4.Top Ring - Dry Region

The top ring experiences pure hydrodynamic lubrication during most of the stroke, but is subject to a large "spike" of boundary friction near TDC combustion, as shown in Figure 4-26. This spike is caused by a combination of factors: very high post-combustion gas pressures and temperatures, slow piston speed and poor lubrication. Lubricant availability is very poor near TDC because the oil control ring does not reach this area, so the region is lubricated only by oil that is scraped up by the compression and scraper rings. Because of the very harsh conditions, this "dry region" is the site not only of high friction generation but also of high ring/liner wear and possible scuffing failure. It contributes the majority of top ring friction, and approximately 30% of total ring pack friction (see Figure 3-2).

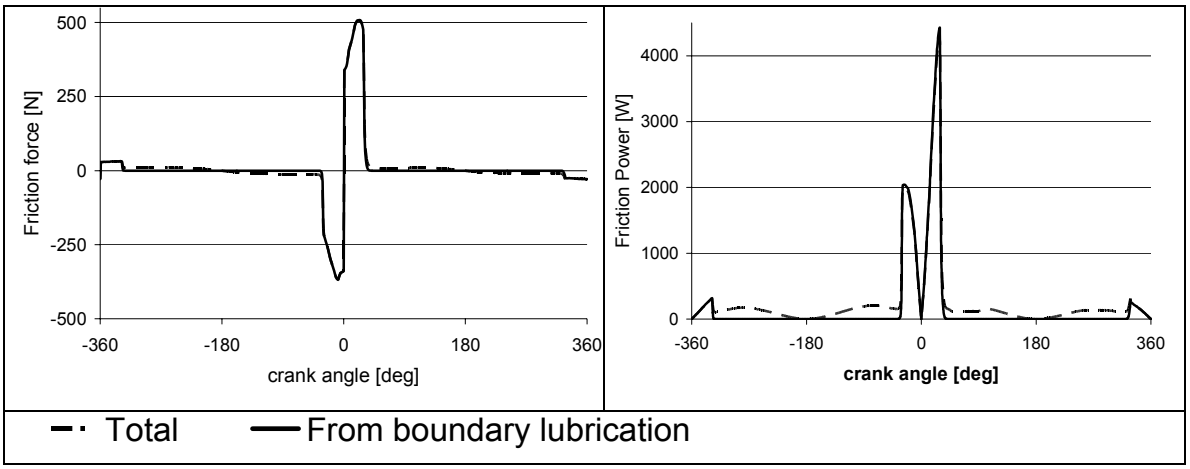

Figure 4-26: Top ring friction force (left) and friction power loss (right) for an engine cycle.

Lubricant viscosity does not have a direct affect on top ring/liner friction, because full boundary lubrication occurs there, and the frictional losses are affected only by the boundary friction coefficient. However, the lubricant viscosity may affect this region indirectly, by influencing the size of the poorly lubricated zone. As is shown in Figure 4-27a, simulations show that oil availability in the dry region is greater for thinner lubricants. The result is less asperity contact and a smaller "spike" of high ring/liner force, as shown in Figure 4-27b.

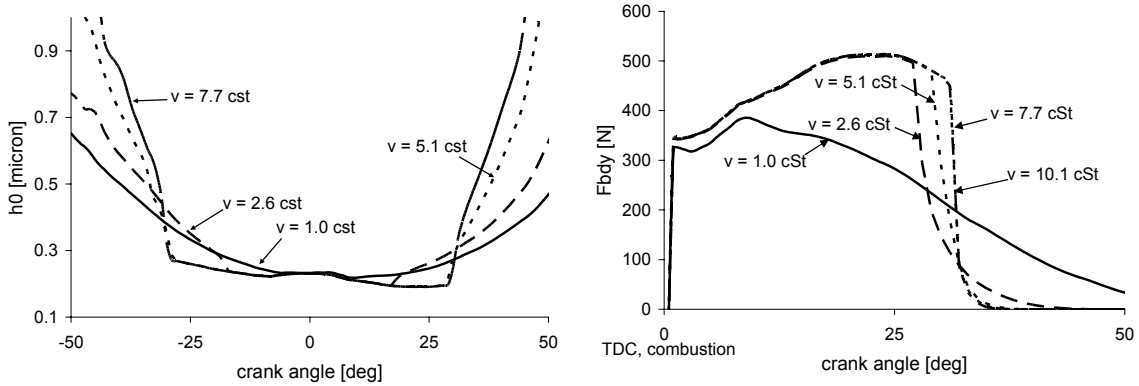

a)Minimum film thickness, h0, near TDC combustion **b)Boundary friction near TDC combustion (0 deg)**

Figure 4-27: Dry region width increases with lubricant viscosity, for the top ring

Figure 4-27a shows the change in dry-region width with oil viscosity, for an idealized case where viscosity is constant throughout the cycle. As the figure shows, the dry region (the relatively flat region, between the sharp drop and subsequent sharp rise in film thickness) increases in width as viscosity increases, approaching a maximum. For very low viscosity (ν = 1 cSt) there is almost no dry width. For viscosities greater than ν~5 cSt, there is very little change in dry region width – a maximum dry width and maximum boundary friction have been reached. Between these values, the size of the un-wetted region increases with lubricant viscosity. This corresponds to the boundary friction force shown in Figure 4-27b. For the lowest viscosity case, the "spike" barely appears and is replaced by a region of gradually decreasing boundary friction. As

viscosity increases, the width of the boundary friction "spike" increases with the viscosity until it reaches a maximum.

These results indicate that thinner oils are upscraped into the dry zone more easily than thicker oils, although the details of the mechanism are not well-understood. It is not clear that this is a real effect – simulations may show this effect because of underlying assumptions or simplifications that have not been considered. Also, other studies [5] have shown the opposite trend – an increase in dry-region wetting with higher viscosity. More research is required to determine the extent of viscosity effects on dry region width. Some possible lubricant effects are illustrated in Figure 4-28.

Figure 4-28 illustrates some effects of lubricant viscosity on oil upscraping by the top ring. The extent of the upscraping depends on lubricant availability on the liner before the dry region and the ring/liner clearance, as well as other factors such as the ring load. For thinner lubricants, the distance between ring and liner is smaller, because low viscosity oils create thinner hydrodynamic films in response to ring load (this is illustrated in Figure 4-28b, where h_0 can be used as an indicator of ring/liner clearance). This encourages upscraping. However, there is also less available lubricant for thinner oils, for the same reason – the smaller clearance causes more oil to be scraped down the liner on down-strokes. The balance between these two factors plays a part in determining how much oil is scraped up the liner. Many factors also contribute to oil transport, including oil travel along the piston lands and pumping by the rings.

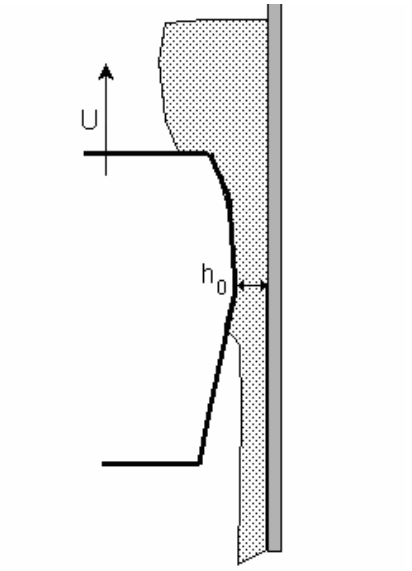

a) upscraping by top ring

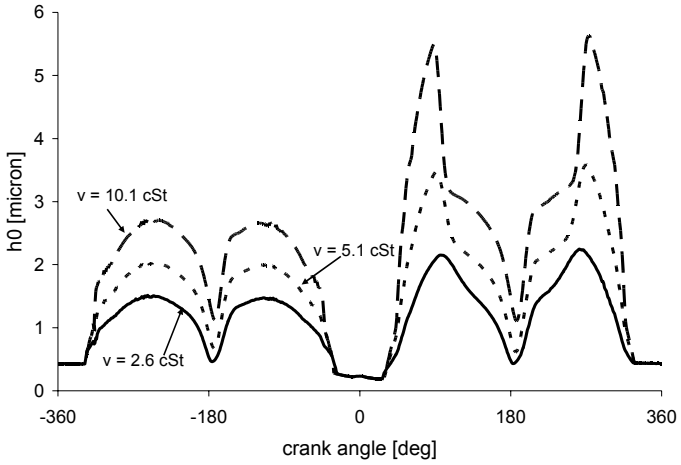

b) ring-liner separation increases with lubricant viscosity (units are cSt)

Figure 4-28: Lubricant upscraping mechanism

The total cycle friction losses for the top ring depend on both transport of oil into the dry region and the ability of the oil to support hydrodynamic lubrication in the rest of the stroke. In Figure 4-29, a minimum fmep, corresponding to a minimum boundary friction, is found at a low viscosity. This viscosity balances between allowing more oil to be transported into the dry region, reducing friction there, but making asperity contact more likely during the rest of the stroke. This is illustrated in Figure 4-27b – for the

lowest viscosity of 1cSt, the height of the dry region "spike" is decreased, but its width is increased. The very low viscosity oil was transported into the dry region, but then was too thin to support hydrodynamic lubrication for the entire stroke outside of the dry region. At higher viscosities, boundary friction remains approximately constant with viscosity, consistent with Figure 4-27 (dry region width stays constant), while hydrodynamic friction increases with viscosity, leading to an overall increase in friction.

Comparing Figure 4-29 to Figure 4-14, for the oil control ring, the minimum frictional losses for the two rings occur at approximately the same viscosity. Then, an additional benefit in reduction of top ring friction may occur if viscosity is reduced to this value. A reduction in top ring friction of ~ 30% is possible, which corresponds to a ring-pack friction reduction of ~ 9%. However, increasing oil upscraping may increase oil consumption, which must also be considered in the total engine design. Also, it is not clear whether this is a real benefit, or only appears due to model assumptions or simplifications. More research is required to assess this possibility.

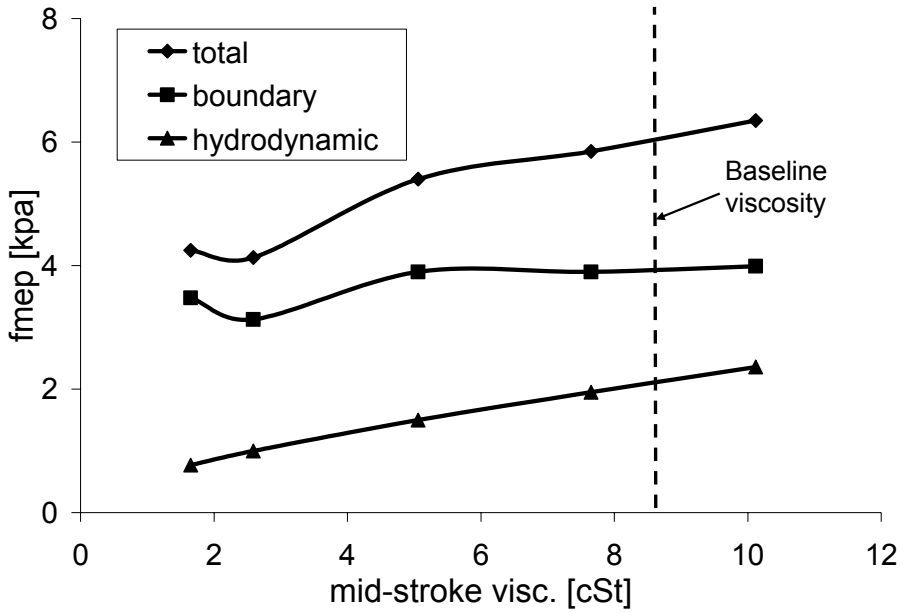

Figure 4-29: Dependence of top ring friction on lubricant viscosity, baseline viscosity case

4.5. Other lubricant properties: Boundary friction coefficient

If ring/liner boundary friction coefficient can be decreased - for example, with surface-modifying lubricant additives - a large friction benefit is possible. Decreasing boundary friction coefficient, f_b, reduces ring/liner friction both directly, by reducing friction due to asperity contact, and indirectly, by allowing lubricant viscosity to be reduced and thus reducing hydrodynamic friction as well. The latter effect occurs because changing f_b alters the balance between hydrodynamic and boundary friction for the ring and liner - a low friction coefficient allows viscosity to be reduced without incurring a large friction penalty because of the increased asperity contact. The lower f_b

becomes, the lower the viscosity can become before the corresponding increase in asperity contact - and thus boundary friction - out-balances the reduction in hydrodynamic friction that resulted from the viscosity reduction. This is illustrated in Figure 4-30, which shows the dependence of total ring-pack fmep on boundary friction coefficient for different lubricant viscosities (baseline viscosity-temperature dependence).

As is shown in the figure, at a given viscosity, reducing f_b causes a reduction in total friction - this results from the direct reduction of boundary friction with decreasing friction coefficient that is shown in Figure 4-30b. Also, the viscosity at which the minimum frictional loss occurs decreases with f_b, as does the minimum friction - this is a result of the effect of f_b on the hydrodynamic/boundary friction balance. Reducing boundary friction coefficient has a dual effect on ring/liner friction - it both reduces boundary friction and allows a lower viscosity lubricant to be used, thus reducing hydrodynamic friction – and thus can have a substantial, beneficial effect on overall ring-pack friction.

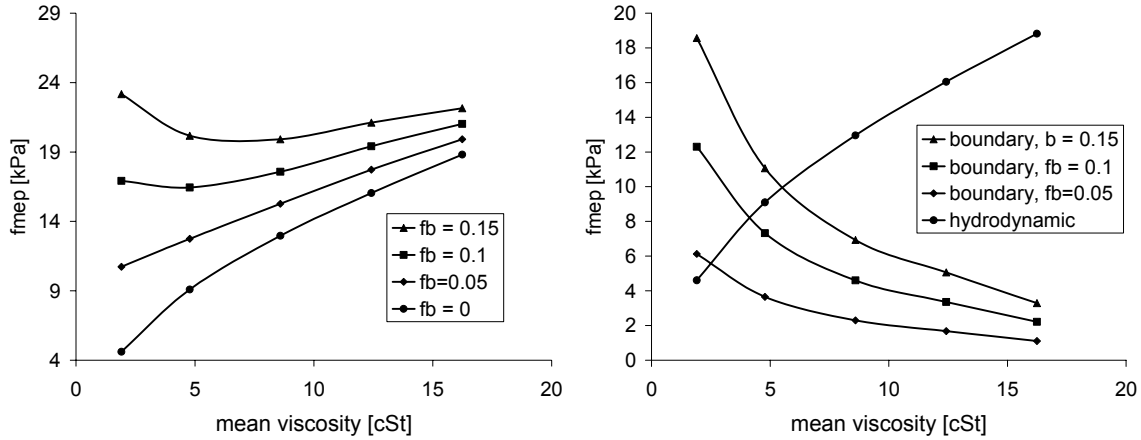

a)Total ring pack friction losses **b) Boundary and hydrodynamic ring-pack losses**

Figure 4-30: Effect of boundary friction coefficient on total ring-pack friction

4.6. Other Considerations: Wear

In addition to frictional losses, wear of the rings and liner must also be taken into account when designing an optimized lubricant. Ring/liner wear leads to leakage of combustion gases out of the engine cylinder ("blow-by") and a corresponding reduction in efficiency and increase in engine emissions. Limiting this degradation of engine performance, and avoiding the need to service and replace parts, requires that ring/liner wear be controlled.

The actual wear of the ring and liner is a complicated and not well-understood phenomenon, and actual wear predictions have not been made in this study. Instead, a factor is calculated, which takes into account two main contributors to wear: asperity contact pressure and sliding distance. The wear factor presented is a mean factor for an engine stroke, and is calculated as the integral of the contact pressure multiplied by the piston speed, integrated over the stroke distance.

The wear factor increases as mean lubricant viscosity is reduced, as is shown in Figure 4-31a, because the amount of asperity contact occurring increases. Figure 4-31b shows that the wear increases strongly even as frictional losses remain low – the minimum fmep is found at a viscosity corresponding to a high wear rate. Then, choosing an ideal lubricant viscosity represents a balance between friction and wear considerations – the desire for low friction must be balanced against a need for low wear.

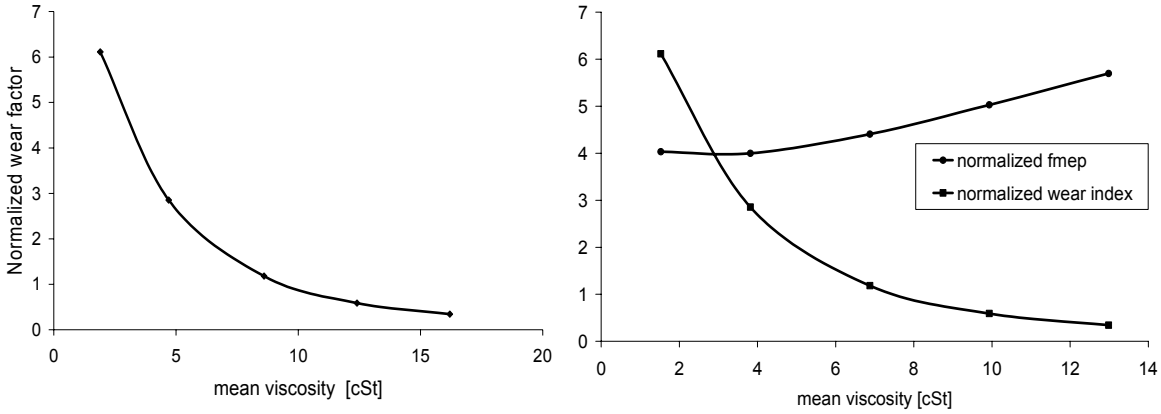

a) Wear increases as viscosity decreases

b) Minimum friction occurs at a large wear factor

Figure 4-31: Effect of lubricant viscosity on friction and wear parameter

It is possible to decrease wear slightly by controlling the viscosity change during the engine cycle, as is shown in Figure 4-32, where the baseline case is compared to a constant-viscosity case and the controlled shear-dependence "case 2", described in section 4.3.3. Maintaining high viscosity near dead-centers can reduce asperity contact in the end-stroke regions, decreasing wear. Figure 4-32a shows that, for a given ring friction loss, the viscosity-shear rate relationship "case 2" shows the lowest wear rate (or, similarly, for a given wear rate case 2 gives the lowest friction). This is because this case maintains the highest dead-center viscosity, and so allows the least asperity contact to occur during the stroke, as shown in Figure 4-32b. In Figure 4-32b, instantaneous wear parameter is shown for the three viscosity cases at the same fmep, which is the baseline fmep = 11.14 kPa.

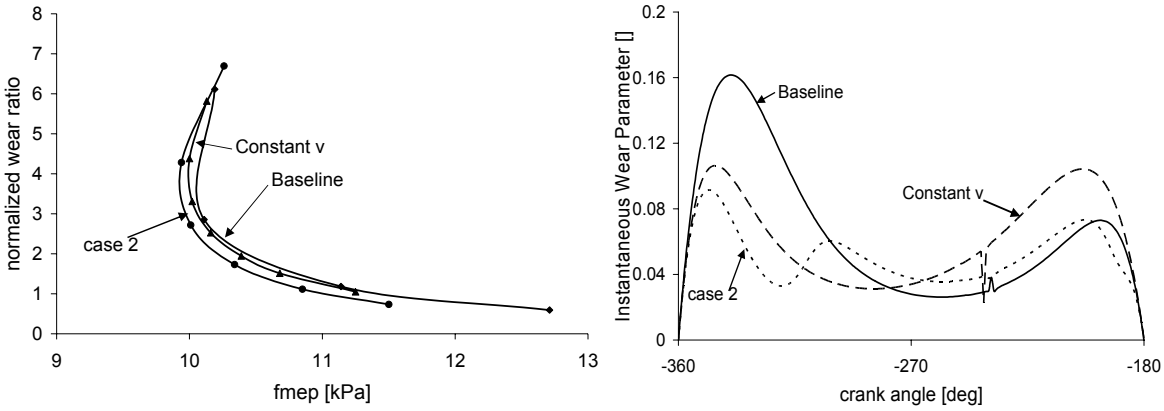

a) Overall cycle wear parameter vs. overall cycle friction losses **b) Instantaneous wear parameter, intake stroke**

Figure 4-32: Changing temperature and shear properties of the lubricant can reduce wear at a given fmep.

4.7. Ring Properties: Ring Tension and Surface Roughness

The ring lubrication studies presented above all used the same ring and liner parameters, including ring tension, surface roughness, etc., which are the parameters of the current, baseline set-up of the Waukesha engine and are given in Table 4-3. For a different set of engine parameters viscosity effects may be different - the interaction between the lubricant, engine properties and engine running conditions may change as parameters are varied. To illustrate some of these cross-coupling effects a study of the interaction of two important ring parameters - tension and surface roughness - with lubricant changes is presented. In these studies, the realistic temperature and shear-rate dependencies of the lubricant viscosity are used, as described in section 4.3. Table 4-3 summarizes the range of ring factors considered, including lubricant properties.

Table 4-3: Ranges of ring parameters considered

Parameter	Range	Baseline value	Unit
Ring tension	81-40	81	N
Ring surface roughness, R_q	0.05 – 0.2	0.1	micron
Boundary friction coefficient, ring/liner	0.05 – 0.15	0.1	-
T_1, Vogel equation (controls T dependence)	0 - 1200	965.76	^oC
c_1, Cross equation (controls critical shear rate)	2.3 – 4.3	2.3	-
μ/μ_0, Cross equation (controls high/low viscosity ratio)	1-.1	1	-

4.7.1. Ring Tension

The ring tension is one factor that controls the balance between hydrodynamic and boundary lubrication between the ring and liner. For a given viscosity (and sliding speed), as ring tension is reduced asperity contact decreases. Regions of the ring stroke that experience mixed lubrication at high ring tension may experience pure hydrodynamic lubrication at lower tension (see Figure 4-33a). Also, the ring tension can affect the lubricant viscosity, if it is dependent on shear-rate, as shown in Figure 4-33b. A lubricant that is optimized to balance hydrodynamic and boundary contributions to ring friction must take these effects into account.

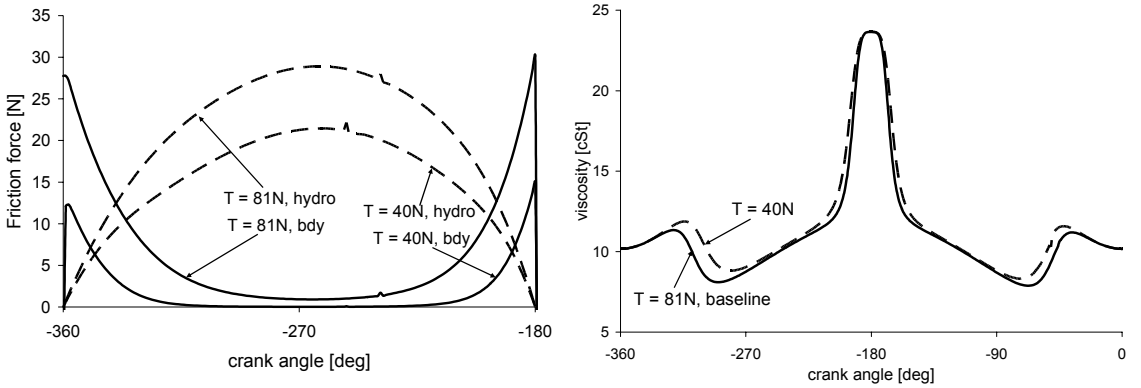

a) Lower ring tension leads to reduced asperity contact and a larger hydrodynamic region

b) Shear rate in the oil depends on ring tension, so lubricant viscosity does as well

Figure 4-33: The lubrication regime of the ring depends on ring tension

The interaction between ring tension and lubricant viscosity is illustrated using the example of the "case 2" viscosity distribution, which is described in section 4.3.2. For this case, the shear-dependence of the viscosity is controlled to produce high viscosity near dead-centers and low viscosity near mid-stroke. The high/low viscosity transition point is matched to the transition between the high boundary friction near dead-centers and high hydrodynamic friction near mid-stroke, for the baseline ring tension of T=81N. When the ring tension is reduced, the case 2 transition point is no longer well-matched to the lubrication regime of the ring.

Figure 4-33a shows that for a ring tension of 40N only a small amount of asperity contact occurs, very close to dead-centers. For the case 2 viscosity distribution, viscosity is still held high outside of this region, because it was intended to apply to a higher tension ring that experienced more asperity contact. In addition to this, as is shown in Figure 4-33b, the high/low viscosity transition occurs even later for the reduced tension ring, because shear rates in the oil are lower. The result of these effects is an increase in friction, compared to the baseline case, because of increased hydrodynamic friction. This is shown in Figure 4-34. For high mid-stroke viscosities (viscosities that are high enough to maintain hydrodynamic lubrication at mid-stroke), the case 2 viscosity distribution gives higher friction than the baseline. As ring tension is decreased, the increase in friction due to the case 2 distribution increases.

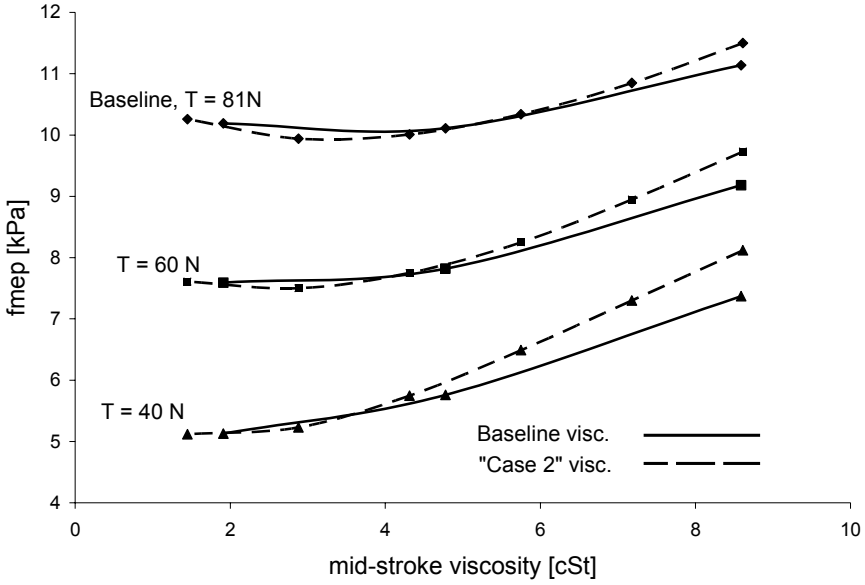

Figure 4-34: Interaction of ring tension and viscosity effects, comparing baseline and "case 2" viscosity distributions

Figure 4-34 also indicates that as ring tension is reduced the benefits of using the case 2 strategy at low viscosities are reduced. For T = 40N, the baseline and case2 fmep value are almost the same, for mid-stroke viscosity less than 4cSt. This is because the friction benefit of the case 2 viscosity distribution lies in reducing dead-center boundary friction, and, as ring tension is reduced, boundary friction also decreases. For low ring tensions there is very little benefit to reducing dead-center boundary friction, because the high-boundary region is small and occurs only where piston speeds are low.

4.7.2. Surface Roughness

Ring friction has a more complicated dependence on surface roughness than on ring tension. Friction may increase or decrease with surface roughness, because roughness (described here by the standard deviation of the surface mean height) affects both asperity contact and hydrodynamic lubrication. For a rougher surface asperities are larger, and so asperity contact occurs at a larger film thickness. Then boundary friction tends to increase with roughness, as shown in Figure 4-35a. However, hydrodynamic friction tends to decrease with roughness, as shown in Figure 4-35b, because of the effect of the surface texture on oil flow and hydrodynamic pressure generation. In general friction tends to increase with ring roughness, but in the region near the baseline roughness of the Waukesha engine, R = 0.1μ, the opposing hydrodynamic and boundary effects make the influence of the roughness less clear. In Figure 4-36 and Figure 4-37, it should be noted that ring friction is lowest for the mid-range roughness R = 0.1μ, and both the less rough and the more rough cases exhibit higher friction.

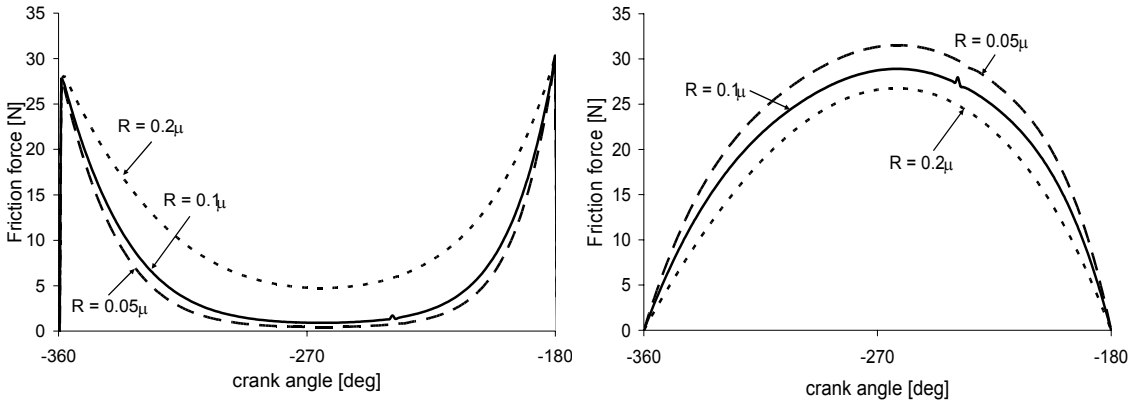

a) Boundary friction **b)Hydrodynamic friction**

Figure 4-35: Effect of ring surface roughness on friction, intake stroke

The constant viscosity and "case 2" viscosity cases are compared to the baseline case, for different roughnesses, in Figure 4-36 and Figure 4-37. Both figures show that for the roughest case, R=0.2μ, viscosity effects are the weakest. This may be because the large asperities prevent a substantial reduction in boundary friction from occurring, negating any benefits from the constant viscosity and "case 2" cases. For the two lower roughness cases, the results are similar. A small reduction in minimum friction is observed for both the constant viscosity and case 2 distributions, while friction is slightly larger at higher viscosities. It appears that a large roughness can negate the benefits of controlling viscosity variation during the cycle (for the cases considered), but for baseline and lower roughness, there is little lubricant/roughness interaction.

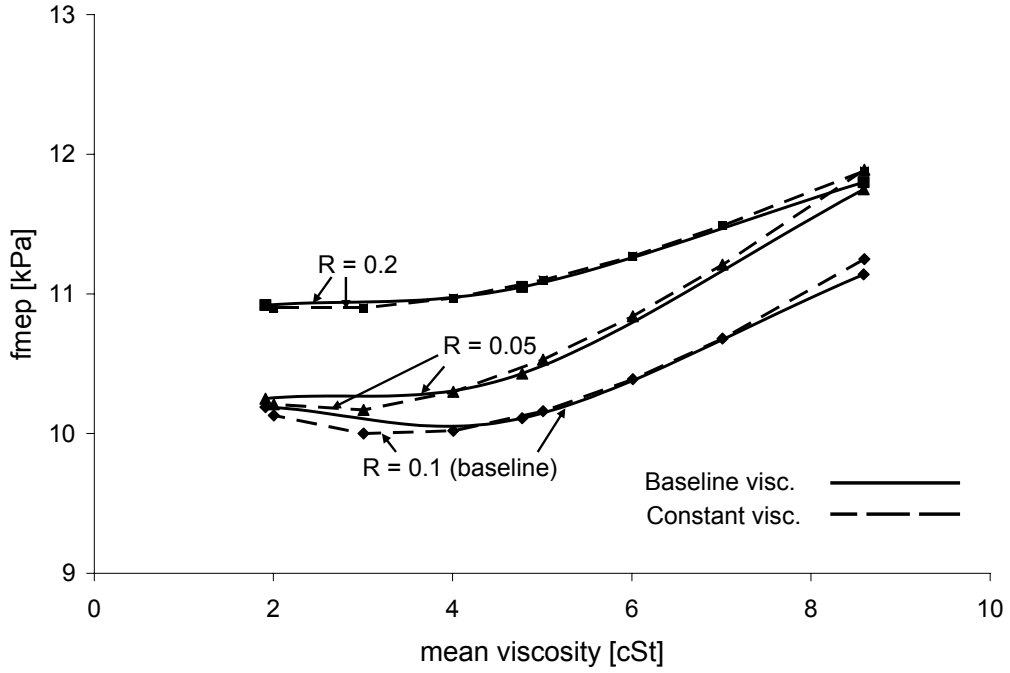

Figure 4-36: Interaction of ring roughness and viscosity effects, baseline and constant viscosity

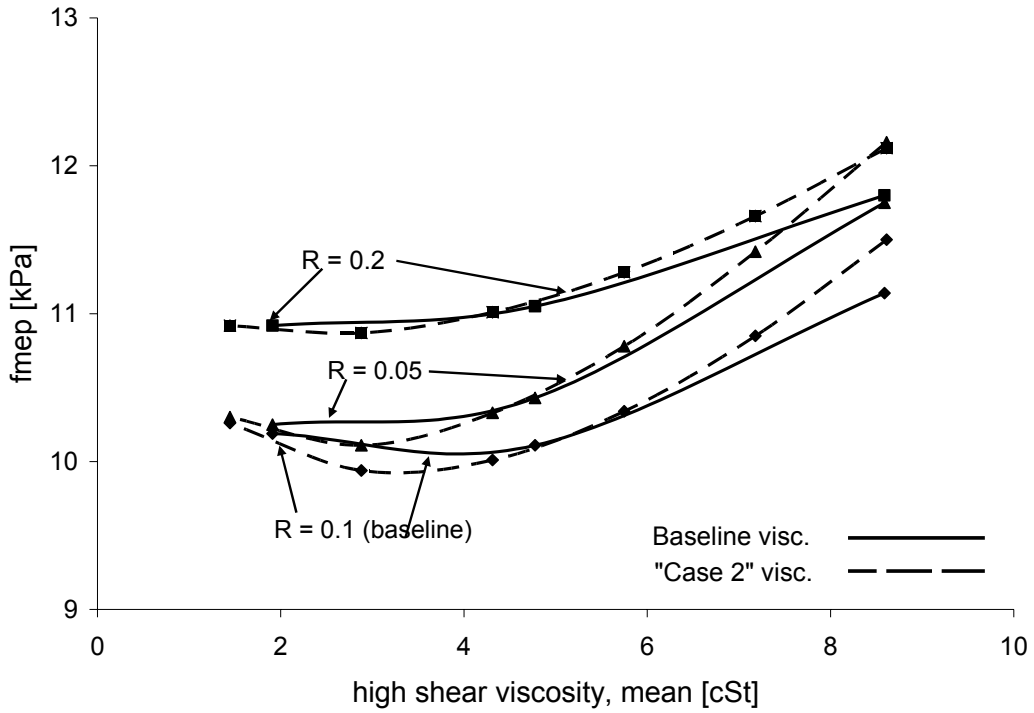

Figure 4-37: Interaction of ring roughness and viscosity effects, baseline and "case 2"

4.8. Conclusions and Friction Reduction Strategies

The piston rings experience hydrodynamic, boundary, and mixed lubrication modes during engine operation, where the amount of friction loss due to each mode depends on engine design and running parameters. For given parameters, the lubricant viscosity plays a main role in determining the lubrication mode, as well as the frictional losses during the engine cycle. In this study, the role of lubricant viscosity in controlling ring/liner lubrication mode, and thus ring/liner friction, was considered. The viscosity can be used to optimize the lubrication regime, leading to reductions in friction and wear.

Oil viscosity affects friction directly in the hydrodynamic regime, where hydrodynamic friction increases with viscosity. It also influences boundary friction indirectly by controlling oil film thickness, and thus the amount of asperity contact that occurs. Reducing viscosity can reduce hydrodynamic friction but also causes a decrease in oil film thickness that makes asperity contact more likely. A thicker oil may reduce boundary friction but increase hydrodynamic losses. At the optimum viscosity (the viscosity at which minimum friction losses are incurred) there is a balance between hydrodynamic and boundary friction losses.

As piston speed, ring loading, and other parameters change during the engine cycle, the optimum oil viscosity also changes. Near mid-stroke, high speeds support hydrodynamic lubrication, making a low viscosity lubricant desirable to reduce hydrodynamic losses. Near dead-centers, low speeds cause hydrodynamic support to decrease. Then, a high viscosity oil is desirable, to maintain thicker oil films and reduce asperity contact. If viscosity variation during the cycle can be controlled so that the viscosity is optimum at all times, ring-pack friction reduction is possible. Several

idealized and realistic cases were studied to quantify the friction benefit obtainable by controlling viscosity variation during an engine cycle.

Idealized cases with low mid-stroke viscosity and high dead-center viscosity were considered, as were several realistic cases with typical temperature and shear-rate dependencies. It was found that friction reduction is possible when viscosity variation during the cycle is controlled, but it is small compared to the reduction that can be obtained simply by reducing mid-stroke viscosity. Two mechanisms lead to the small size of the friction benefit: the contribution to total cycle ring friction from the dead-center area is small, because of low piston speeds there; and any reduction in asperity contact is accompanied by an increase in hydrodynamic friction, which cancels out some of the benefit. Oil viscosity near mid-stroke, where most of the ring/liner friction is generated, is the dominant viscosity that controls the overall friction losses for the ring.

A friction reduction of ~10% is predicted for the OCR, from the baseline case, when viscosity is in the mid-stroke region reduced. An additional reduction of 1-2% is possible when dead-center viscosity is held high to reduce boundary friction. For the Waukesha engine, the oil control ring accounts for ~65% of the total ring-pack losses. Then, an OCR friction reduction of 11% leads to a total ring-pack friction reduction of ~7%.

The top ring contributes most of the remainder of the ring-pack friction, but experiences most of its losses (~70%) as boundary friction in the poorly-lubricated TDC region of the stroke. Then, viscosity does not have a large direct affect on top ring friction. However, simulations show an indirect effect, where oil transport into the dry region may increase as viscosity decreases. This leads to a decrease in friction of up to 30%, leading to a ring-pack friction reduction of ~9%. However, the mechanism for this reduction is not clear, and further research is required.

Ring/liner wear was also briefly considered, in a simple analysis of a wear coefficient related to boundary contact force and ring/liner sliding distance. Wear was found to increase strongly with decreasing viscosity, even as friction remains low. In the interest of keeping wear low, then, it may be necessary to accept a higher-than-minimum level of ring friction. Controlling viscosity variation was shown to have some potential benefit in reducing wear, because of the reduction in asperity contact forces near dead-centers, with a wear coefficient reduction of ~42% for the minimum-friction case.

For the Waukesha engine, an OCR friction reduction of ~11% was shown to be possible, translating to a total ring-pack reduction of ~7%. A further reduction in friction from the top ring may be possible, resulting in a total ring-pack friction reduction of ~18%, but the top ring benefit is not well-understood This benefit must be balanced with consideration of wear increases that may occur. If surface modification additives can reduce the boundary friction coefficient for ring-liner contact, even greater friction reductions are possible.

Lubricant properties providing minimum friction for the Waukesha ring-pack are summarized in Table 4-4. The parameters proposed are those for case 2, at the minimum-friction viscosity.

Table 4-4: Cross and Vogel equation parameters for friction reduction

Parameter	Current Value (Unworn)	Proposed	Friction Reduction
z (viscosity "thickness")	.09	.06	7%
c_1 (controls critical shear rate)	2.3	4.3	
m (width of transition region)	1 (more gradual transition)	5 (sharper transition)	

5. Friction Reduction Strategies – Surface Texture Effects on Ring-pack Friction

In this section, several aspects of surface texture that affect ring/liner friction are analyzed. The surface texture affects friction in two ways: by controlling asperity contact pressure and by influencing lubricant flow, which influences the generation of hydrodynamic pressure. The heights and shapes of surface asperities determine the surface separation at which contact occurs, as well as the rate of increase in contact pressure as the surfaces move closer together. The asperity geometry also influences lubricant flow, where textures that tend to impede flow result in greater hydrodynamic pressure generation.

The stochastic surface properties roughness and skewness are considered. Also, the effect of the liner honing cross-hatch angle is studied.

5.1. Surface Characterization

There are two main methods of characterizing rough surfaces, stochastic and deterministic. For a deterministic characterization, measurements of the actual rough surface to be studied are made, and a numerical representation of the actual surface is used as a basis for calculations. In the stochastic case, measurements of representative surfaces are used to define a number of statistical parameters, which are then used in further calculation. This method is appropriate for parametric studies, and in cases where detailed surface information is not available. The deterministic approach is preferred when a detailed analysis of three-dimensional surface characteristics is required.

This study used the stochastic approach to assess the effects of different statistical parameters, and to find if certain asperity distributions or geometries could reduce ring-liner friction.

5.1.1. Stochastic Surface Texture Characterization

A stochastic surface description consists of a few discrete statistical parameters that define a probability distribution function for the height of a surface. The parameters describe the distribution of asperity heights and shapes, with an assumption that the distribution is random and uniform over the surface considered. Different sets of parameters can be used to describe a given surface. This study uses three parameters: σ, the standard deviation or "RMS roughness" of the surface, Sk, the skewness, and Ku, the kurtosis.

σ, the roughness, is the standard deviation of surface distance from the mean. A large σ indicates tall asperities, while a small σ describes a relatively smooth surface. Skewness, Sk, is a measure of the asymmetry of the surface about the mean line. A high skewness indicates tall, thin peaks above the mean line, while a low (negative) skewness describes a plateau surface that is relatively flat with deep, thin valleys (see Figure 5-1). Kurtosis is a measure of the "peakedness" of the distribution. A distribution with higher kurtosis has more asperity peaks with near-average height, as well as thicker "tails" – more peaks very far from average (see Figure 5-2). That is, in a high-kurtosis case, more of the variance results from infrequent but extreme variations from average, and less from frequent but small variations from average, a high-kurtosis surface is relatively flat with a few very high peaks or very low valleys. For a normal (Gaussian) distribution, the skewness is zero and the kurtosis is three. These three parameters are defined as:

$$\sigma \quad \sqrt{\quad y^2(z)\phi(z)dz} \tag{5.1}$$

$$Sk \quad \frac{1}{\sigma^3} \quad y^3(z)\phi(z)dz \tag{5.2}$$

$$Ku \quad \frac{1}{\sigma^4} \quad y^4(z)\phi(z)dz \tag{5.3}$$

where y(z) is the distance from the mean and ϕ(z) is the probability distribution function, normalized to unity.

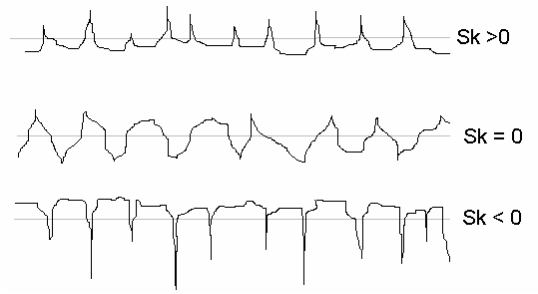

Figure 5-1: Illustration of surface skewness

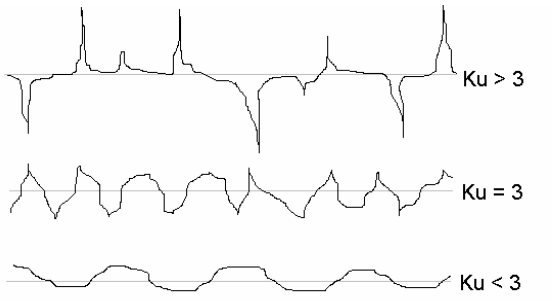

Figure 5-2: Illustration of surface kurtosis

In this study, the effects of both roughness and skewness were considered. Kurtosis was considered to be less applicable to the ring pack/liner case, since different ring and liner materials can currently be finished to produce differing roughnesses and skewnesses, but producing a specific kurtosis is not within the realm of current manufacturing procedures.

5.1.2. Deterministic Surface Texture Characterization

When a more accurate analysis is required, a deterministic description of surface geometry may be used. Two-dimensional surface measurements are made with a profilometer, which measures the movement of a small stylus that is swept over the surface. The profilometer accuracy is limited by the size of the stylus tip, which must be smaller than the smallest radii that are to be measured. Three-dimensional measurements can be obtained by taking several profilometer traces, or using white light interferometry (WLI). WLI uses measurements of light reflected from the surface to produce a 3-D texture map. Contaminants on the surface and sharp grooves, that do not receive or reflect light as assumed by the measuring instrument, can harm the accuracy of this method.[19]

5.2. Analytical Methods

Surface texture affects both asperity contact and oil flow between the ring and liner, thus influencing both boundary and hydrodynamic lubrication. The asperity contact model used for the analysis was based on the Greenwood and Tripp[16] model, while the oil flow analysis used the average Reynolds equation and flow factor analysis of Patir and Cheng[20]. Both of these methods are adapted for the stochastic surface representation used.

5.2.1. Asperity Contact Model

Greenwood and Tripp's asperity contact model uses the distribution of asperity peaks (not the distribution of surface heights) to consider the probability that contact will occur, and calculate the contact pressure. Initial contact is assumed to occur when the mean separation of the surfaces is less than four standard deviations of the combined asperity distribution of the two surfaces. Once contact has occurred, nominal asperity contact pressure between two rough surfaces is given as:

$$P_c \left(\frac{d}{\sigma}\right) = K' E' \int_{\frac{d}{\sigma}}^{z} \left(\frac{d}{\sigma}\right)^{2.5} \phi(z)\,dz \tag{5.4}$$

where

$$K' = \frac{8\sqrt{2\pi}}{15} \eta\beta\sigma^2 \sqrt{\frac{\sigma}{\beta}} \tag{5.5}$$

where P_c is the contact pressure, d is the mean separation of the two surfaces, η is the asperity density per unit area, β is the asperity peak radius of curvature, $\phi(z)$ is the probability distribution of asperity peak heights, and z is the offset between the asperity height mean and the surface height mean. E' is the composite Young's modulus of the

two surfaces, and σ is the composite standard deviation of asperity heights for the two surfaces, given by:

$$E' \quad \frac{2}{\frac{1 \quad \nu_1^2}{E_1} \quad \frac{1 \quad \nu_2^2}{E_2}} \tag{5.6}$$

$$\sigma \quad \sqrt{\sigma_1^2 \quad \sigma_2^2} \tag{5.7}$$

where E_1 and E_2 are the Young's moduli of the two surfaces, ν_1 and ν_2 are the Poisson ratios of the surfaces, and σ_1 and σ_2 are the standard deviations of the asperity heights for the two.

The effect of oil film and oxide layers on the ring and liner surfaces may play an important role in asperity contact, but has not been considered here. Also, it is assumed that contact deformation is elastic, although in reality plastic deformation may occur, especially during the break-in period.[21] However, it has been shown by Greenwood and Tripp that asperity pressure calculated for plastic deformation is similar to that for elastic deformation.

5.2.2. Lubricant Flow Model

The ring pack model accounts for effects of surface roughness with an average, one-dimensional Reynolds equation developed by Patir and Cheng[20]:

$$\frac{\partial}{\partial x} \quad \phi_p \frac{h^3}{\mu} \frac{dp}{dx} \qquad 6U \frac{\partial}{\partial x} \quad h \quad \phi_g \quad \sigma \quad \phi_s \quad 12 \frac{h}{t} \tag{5.8}$$

where h is the nominal oil film thickness, p is the pressure in the oil film, U is the piston sliding speed, σ is the composite standard deviation of roughness for the two surfaces (from Eq. 4.7), and ϕ_n are flow factors. Then the volumetric flow rate (per unit width) in the cross-flow direction is given as:

$$q_x \qquad \phi_p \frac{h^3}{12\mu} \frac{dp}{dx} \quad \frac{U}{2} \quad h \quad \phi_g \quad \sigma \quad \phi_s \tag{5.9}$$

This averaged equation is a modified form of the Reynolds equation for smooth surfaces, with flow factors added to account for the surface roughness. The pressure flow factor, ϕ_p, accounts for the influence of surface texture on flow driven by the pressure difference across the oil film (Poiseuille flow). The shear flow factor, ϕ_s, accounts for the influence of surface texture on flow driven by the relative movement of ring and liner (Couette flow). The geometric flow factor, ϕ_g, accounts for the difference between the nominal oil film thickness, h, and the mean oil film thickness (which is the correct film thickness to use in the shear flow term), so that the same thickness parameter is used throughout the calculations.

Patir and Cheng also developed stress factors to modify calculation of the shear stress in the lubricant:

$$\tau_x \quad \frac{\mu U}{h}\phi_{fg} \quad \varphi_{fs} \quad \phi_{fp}\frac{h}{2}\frac{dp}{dx} \tag{5.10}$$

where ϕ_{fg} is the geometric stress factor, ϕ_{fs} is the shear stress factor, and ϕ_{fp} is the pressure stress factor. These factors correspond to the flow factors – the pressure stress factor accounts for shear stresses caused by the pressure drop across the oil, the shear stress factor accounts for shear stresses caused by relative movement between the ring and liner, and the geometric stress factor represents the difference between the nominal and mean film thickness.

Patir and Cheng's flow factor analysis is based on an assumed Gaussian distribution of surface roughness. To account for this assumption, and for the relatively simplified stochastic description of surface roughness that is used, a truncated Gaussian texture is derived for use in the flow factor analysis. As has been done in the literature, it was proposed that the very deep valleys in a negatively skewed surface play a negligible role in lubricant flow, and are ignored. A bearing curve truncation method was used to derive an equivalent Gaussian roughness representing the core and peak regions of a negatively-skewed surface. As a surface becomes more negatively skewed, its equivalent roughness decreases, because a greater population of the surface lies within the valley region. This truncated roughness was used with Patir and Cheng's analysis to study ring-liner friction and lubricant flow.

5.2.3. Flow Factor Calculation

The flow factors were calculated using a program developed by Yong Li at MIT, to determine the highly viscous flow solution between a smooth plate and a rough surface. The case of two rough surfaces was modeled as one smooth surface and one surface with the composite characteristics of the two rough surfaces under study. It was assumed that the liner surface texture dominates the ring texture, so that studying one rough and one smooth surface was not far from the realistic case. Figure 5-3 illustrates the set up of the program.

The program uses finite element analysis to calculate lubricant flow between two 3-dimensional surfaces, for different input conditions. Comparing the program results with the smooth case where the pressure across the sample is set to zero and only relative surface movement is present yields the shear flow and stress factors, while setting the relative surface speeds to zero and applying a pressure drop yields the pressure flow and stress factors.

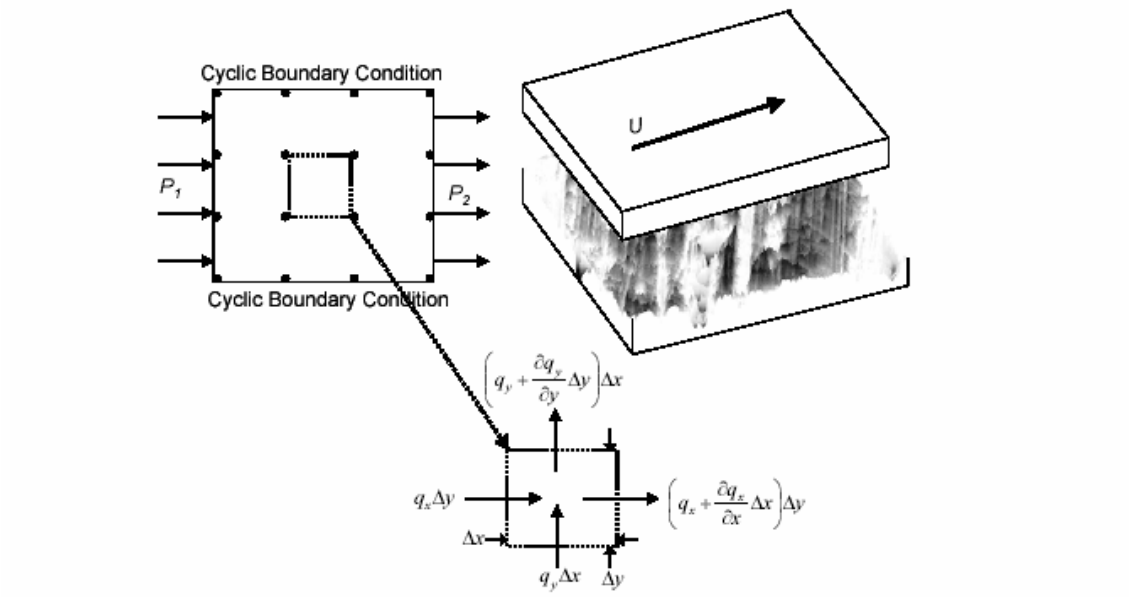

Figure 5-3: Flow factor program set up

In Figure 5-3, q_x and q_y are the unit flow rates in the x and y directions, respectively, and Δx and Δy are the element dimensions. The cyclic boundary condition requires that all fluid flow leaving the element, perpendicular to the main flow direction, from one side of the element return through the other side. For the case of the piston and ring, this is equivalent to requiring conservation of mass for lubricant flowing tangentially between the ring and liner, which is a more realistic assumption than the no-tangential-flow assumption used in other analyses.

The surface used for calculation is a 3-dimensional patch chosen by the user. The patch size is chosen so that it is large compared to surface texture features. For this analysis, the patch surface was generated by the Volvo Surface Generator, using the statistical parameters under study.

5.2.4. Experimental Verification of Surface Model

The model described above was verified experimentally for two cases: a slide honed cylinder liner and a plateau honed cylinder liner. Due to the difficulty of evaluating ring friction in a full engine test rig, verification testing was done using a reciprocating bench tester. The testing was performed at MAHLE, a component manufacturer.

The set up for the reciprocating tester is shown in Figure 5-4. The testing apparatus was a Microtribometer UMT-2 (Universal Micro-Tribometer)from CETR, the Center for Tribology, Inc. The bench tester operated at much lower temperatures and speeds than an actual engine, but since the reciprocating motion was maintained, a range of lubrication conditions from hydrodynamic to boundary was still experienced by the test ring.

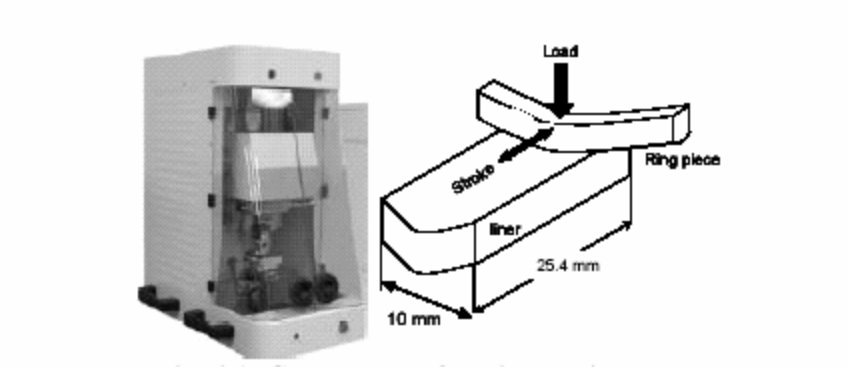

Figure 5-4: CETR UMT-2 reciprocating tester

Good correlation was found between the model and experimental results, as shown in Figure 5-5. The data was sampled at too low a rate to obtain a good measurement of instantaneous friction, so that only the cycle average friction coefficient was used for the comparison. Several different surface measurements, from different sections of the experimental liner, were analyzed, with the error bars in Figure 5-5 representing the differences in cycle friction obtained.

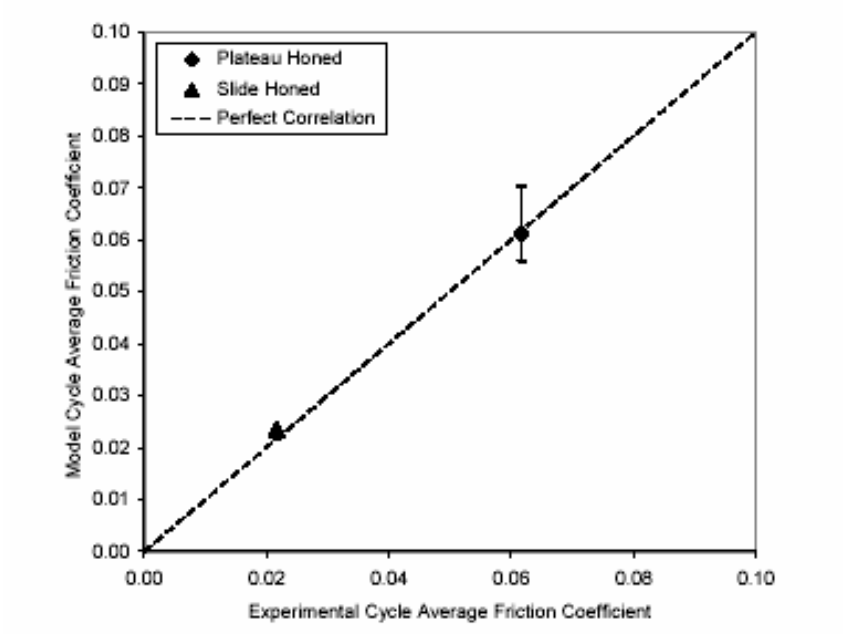

Figure 5-5: Comparison of predicted and measured cycle average friction coefficient

5.3. Effect of Surface Characteristics on Friction

5.3.1. Stress and Flow Factors

The changes in the stress and flow factors with varying surface characteristics correlate to changes in the lubricant flow and friction between the two surfaces under study. Increases in stress factors lead to increases in shear stress, which cause friction to increase. Changes in the flow factors have a more complicated interpretation. In general, when resistance to oil flow is higher, more hydrodynamic pressure is generated. This can

lead to high hydrodynamic friction, but it may also reduce friction if the increased hydrodynamic pressure prevents asperity contact from taking place.

5.3.2. Roughness

Surface roughness affects friction in two ways: by controlling the oil film thickness at which boundary contact occurs, and by influencing the flow of lubricant between the surfaces, thus affecting hydrodynamic pressure generation. As shown in Figure 5-6, boundary friction increases with roughness and then reaches a plateau. Once the roughness is large enough that boundary contact occurs throughout the cycle, and almost all of the load is supported by metal-metal contact (not hydrodynamic pressure from the oil) changing the surface roughness has little effect. Hydrodynamic friction decreases as roughness increases and more of the load is taken by asperity contact. Although oil film thickness is large for large roughnesses, the load supported by the oil is small, resulting in a small hydrodynamic contribution to total friction.

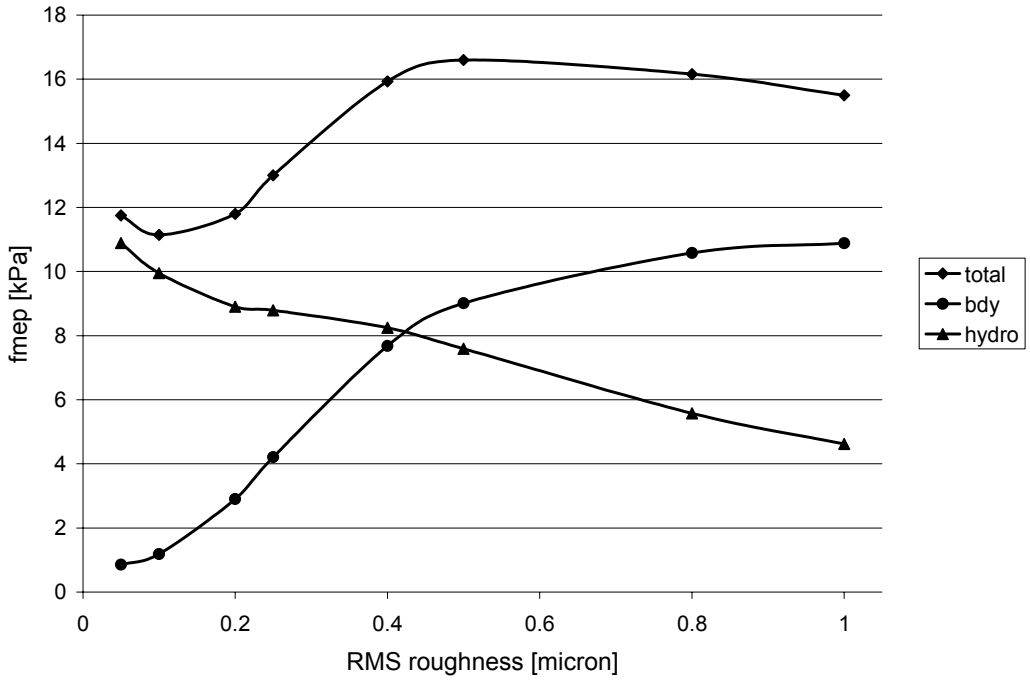

Figure 5-6: Change in cycle friction with surface roughness

Figure 5-6 shows a large range of surface roughnesses, to show the different friction regimes possible. However, in the power cylinder ring roughness is kept relatively small (compared to expected film thicknesses), at less than ~.5μ, or within the range where friction is increasing with roughness in the figure. Because of this, although friction losses do not simply decrease with roughness in all cases, when optimizing power cylinder surface treatment friction can generally be reduced by reducing roughness, as long as the surfaces are not made too smooth.

Experimentation has shown that very smooth surfaces can experience increased friction and wear, and even seizure. There may be several explanations for this

phenomenon that have not been taken into account in the model. For example, very smooth surfaces have no pockets for lubricant retention, which may help reduce friction and wear for more textured surfaces. Poorly lubricated surfaces are expected to exhibit higher friction and wear. Also, smoother surfaces tend to contact over a larger surface area than rough surfaces, because the asperities are more closely spaced (more asperities will contact per unit surface area) as shown in Figure 5-7. When two rough surfaces contact, asperity peaks may undergo plastic or elastic deformation, or even be sheared off, with relatively low total force since the initial contact area is small. For very smooth surfaces, however, a large area may come in contact at the same time, resulting in high friction.

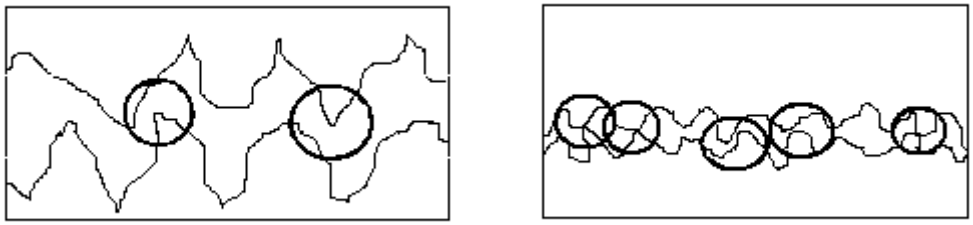

Figure 5-7: For rougher surfaces (left), fewer asperities contact than in smoother cases (right)

A third explanation depends on the materials involved – while some pairs of surfaces may have no affinity and easily slide past each other, the chemistry of others makes them more likely to bond when brought together under high temperatures and pressures. For materials such as these, the large contact area provided by the smooth surfaces, together with heat generated by friction, may cause surface-surface bonding and seizure. For these reasons – or possibly because of other explanations not yet discovered – surfaces of low roughness are recommended for low friction, but surfaces that are too smooth should not be used.

5.3.3. Skewness

Experimental investigations[22,23] have indicated that plateau honed cylinder liners, which have a negatively skewed surface finish as shown in Figure 5-8, exhibit lower friction than conventionally honed liners with close to Gaussian surface finishes (zero skewness). A detailed analysis of skewness effects, performed to investigate these findings, also indicated a reduction in friction with skewness [24,25]. The primary cause for this reduction was a reduction in boundary friction, caused by a reduction in the film thickness at which initial asperity contact occurs. This results in less boundary friction generation throughout the cycle, as is illustrated in Figure 5-9.

Figure 5-8: Typical plateau-honed finish

Figure 5-9 also indicates that, while asperity contact is initiated at a smaller film separation for more negatively skewed surfaces, once the two surfaces have contacted the

contact pressure increases more quickly for lower skewness. This was not seen to cause an increase in friction for very low skewness, most likely because the film thicknesses involved in ring-liner lubrication do not get very small, but it may have an effect on ring wear and scuffing, as described below.

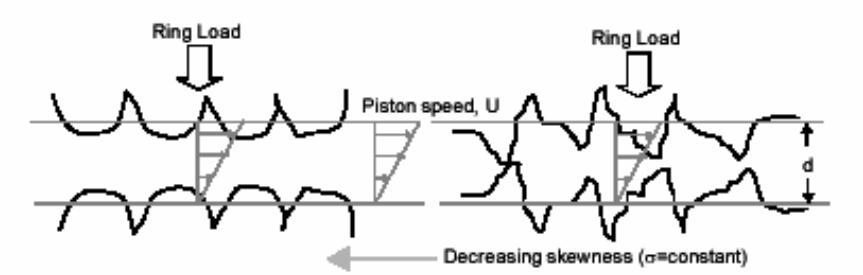

Figure 5-9: Effect of skewness on initial asperity contact

A stochastic surface model, as described in section 5.1.1, was used to model the rough cylinder liner. The piston rings were modeled as smooth, since in general the ring roughness is much smaller than the liner roughness. The effects of liner surface skewness on both oil flow resistance and asperity contact were then modeled using the flow factor technique described in section 5.2.3. Figure 5-10 and Figure 5-11 show the results of this analysis for the top and second rings.

Figure 5-10 shows the relative contributions of hydrodynamic and boundary lubrication to top and second ring friction. As expected, boundary friction decreased with decreasing skewness, indicating that less asperity contact takes place for more negatively skewed surfaces. This reduction in boundary contact results in an overall reduction in friction, as indicated in Figure 5-11.

Figure 5-11 shows greater friction reduction for the rougher ($\sigma = 0.5\mu$) surface than for a less rough case. This is because the smoother surface experiences less asperity contact at all skewness values, so reducing asperity contact further has a relatively small effect.

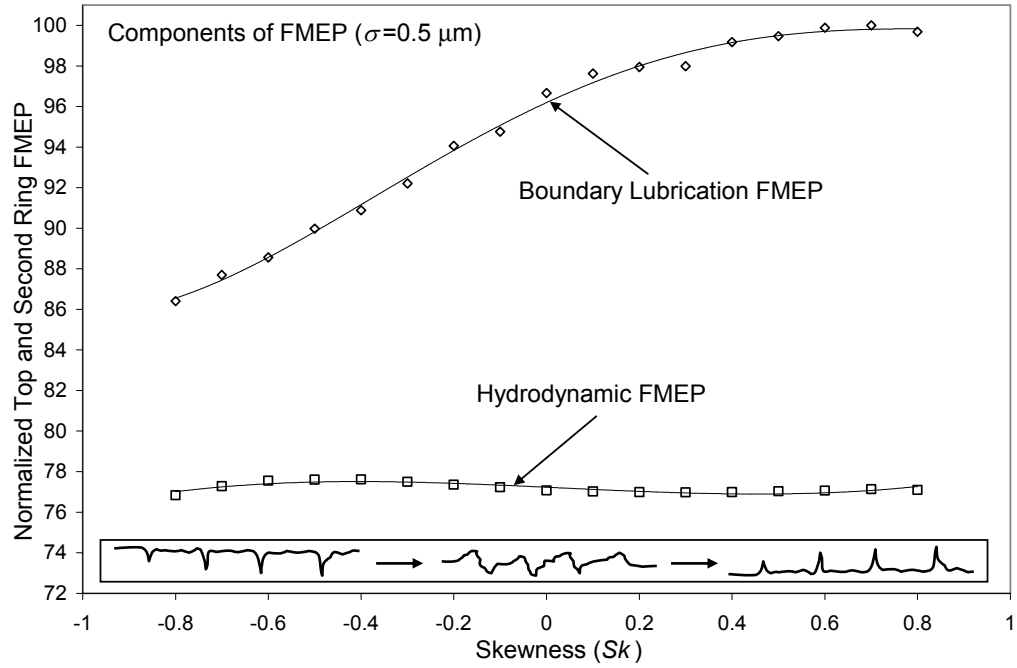

Figure 5-10: Balance of hydrodynamic and boundary friction for top and second rings vs. skewness

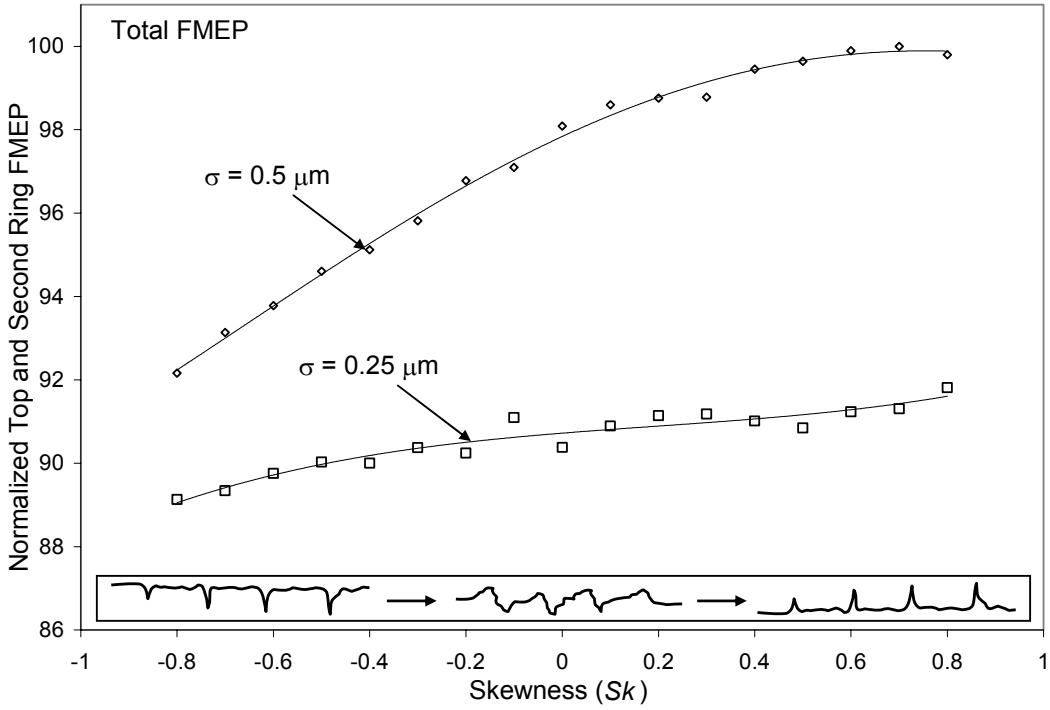

Figure 5-11: Total top and 2nd ring fmep, vs. skewness

As mentioned above, decreasing skewness causes a decrease in friction, but may also have negative consequences. Figure 5-12 shows that decreased skewness leads to an increase in the maximum real area of contact experienced during the engine cycle. Asperity contact begins at a smaller film thickness for more negatively skewed surfaces, but once contact is initiated the contact area increases more quickly than for a positively or neutrally skewed surface. This leads to a large real area of contact near dead centers, where piston speed goes to zero so no hydrodynamic pressure is generated and the entire ring load is supported by asperity contact. For very negatively skewed surfaces, then, friction losses are low but wear near dead centers may become a problem.

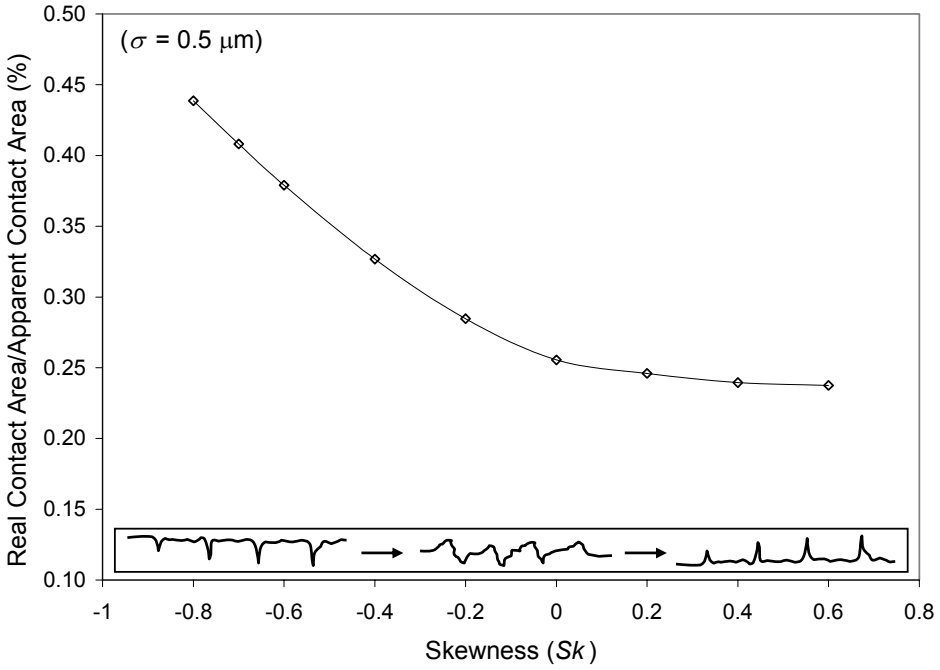

Figure 5-12: Top ring, cycle maximum real area of contact increases with decreasing skewness

5.3.4. Honing Cross-Hatch Angle

The final finish on the cylinder liner is made using a honing process. In this process, a number of abrasive sticks or stones are attached to a rotating honing head, which is then fed in and out of the cylinder as it rotates. The result is a cross-hatched pattern whose angle depends on the rotational and axial speeds of the honing head. This angle has been found to affect both friction and wear. A study was performed to better understand the manner in which the honing cross-hatch angle affects friction, and to find the optimal cross-hatch angle for the Waukesha engine.

Figure 5-13 shows some examples of the liner surface finish at different cross-hatch angles. In this study, a smaller cross-hatch angle indicates that the cross-hatch lines are more perpendicular to the direction of piston motion, while a larger angle indicates lines that are more parallel to the direction of piston motion (the axial direction). The "cross-hatch angle" is the included angle between two lines, and cross-hatch lines are assumed to be symmetric in the axial direction, as shown in the figure.

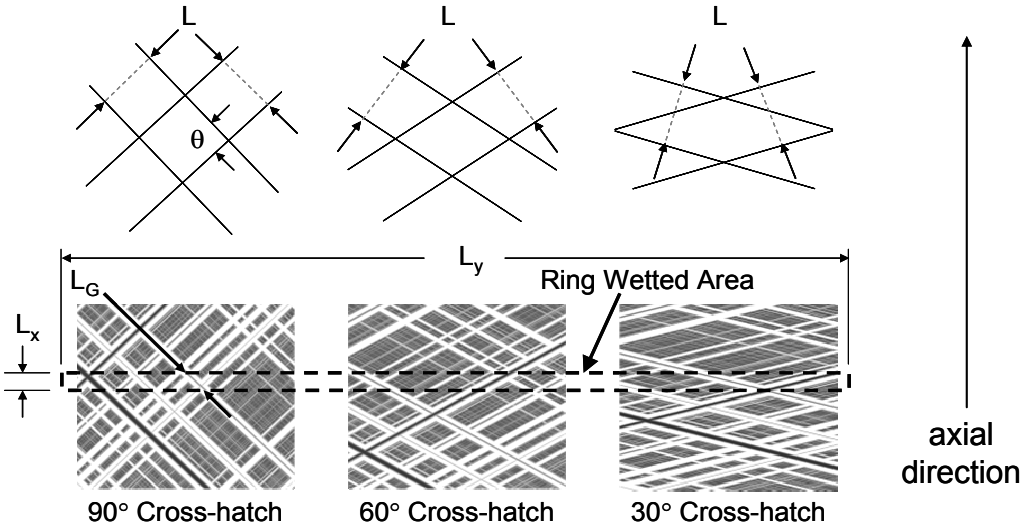

Figure 5-13: Different liner honing cross-hatch angles

Analytical results agreed with experimental observation, indicating that ring/liner friction tends to decrease with honing cross-hatch angle [24,26]. Looking at the change in lubricant flow factors, in relation to cross-hatch angle, gives an indication of the physical cause for this decrease.

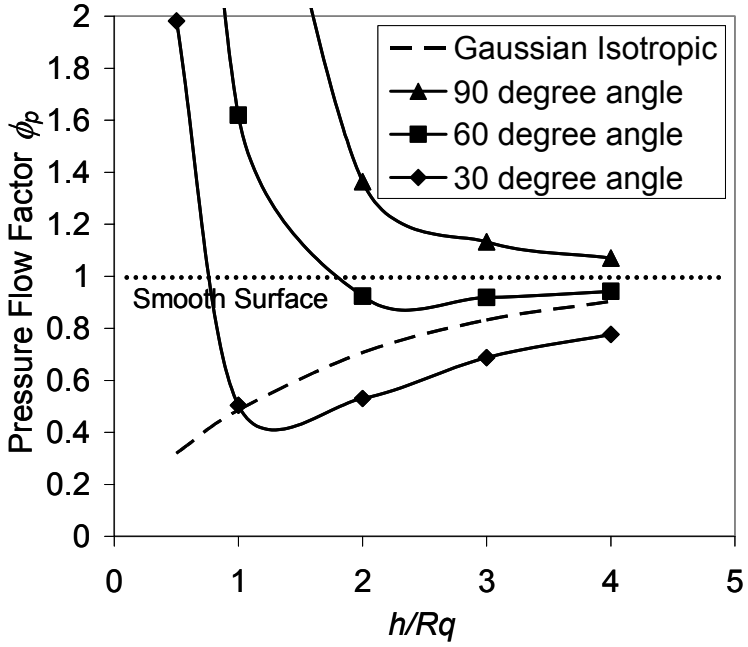

Figure 5-14: Change in pressure flow factor with honing angle. Rq is a measure of surface roughness, h is the film thickness.

The friction reduction due to decreased honing cross-hatch angle results from a decrease in asperity contact with decreasing angle. For the Waukesha engine, some boundary contact occurs throughout the stroke, as even mid-stroke oil films are thin enough that surface asperities come into contact. Reducing honing angle increases the resistance to lubricant flow, increasing hydrodynamic pressure generation. This allows more of the ring load to be supported by the oil film at a given film thickness. Less asperity contact occurs, and friction is decreased, because the ring load can be supported by a thicker film. If ring parameters or running conditions were such that no asperity contact occurred during mid-stroke at any honing angle, a decrease in honing angle might increase friction, since an increase in hydrodynamic friction could be expected. In the case of the Waukesha engine, however, friction should decrease because of the decrease in asperity contact, as indicated by both the pressure and honing flow factors.

Figure 5-14 shows that the pressure flow factor, ϕ_p, decreases with honing angle – that is, it decreases as the honing grooves become more perpendicular to the lubricant flow direction. This indicates that the more perpendicular grooves provide more resistance to lubricant flow that is driven by a pressure differential. This can be explained by the change in length of honing grooves within the ring wetted area with honing angle. As the angle is decreased, the length of a groove crossing the wetted area increases. If the honing grooves are thought of as channels for lubricant flow, this increase in groove length increases flow resistance. This, in turn, allows more hydrodynamic pressure to be generated in the film at a given film thickness, so that more load can be supported. Then, the film thickness required to support a given ring load is larger, and less asperity contact occurs. This results in a reduction in friction.

The effect of the pressure flow factor can also be understood in terms of an "equivalent viscosity". In equation 4.9, which is given again, below, the pressure flow factor and lubricant viscosity are both found to affect the first term in the lubricant flow relationship. These two factors can be combined into a single parameter, an equivalent viscosity, given in equation 4.12. The change in this equivalent viscosity with pressure flow factor has the same effect as a change in actual lubricant viscosity – when viscosity increases flow is impeded and more hydrodynamic pressure is generated, when viscosity decreases the lubricant flows more easily and oil films are thinner. Figure 5-15 shows the change in equivalent viscosity with honing angle. A smaller honing angle gives the largest equivalent viscosity, implying that more hydrodynamic pressure is generated and oil films are thicker, as expected.

$$q_x \quad \phi_p \frac{h^3}{12\mu}\frac{dp}{dx} \quad \frac{U}{2} h \ \phi_g \quad \sigma \ \phi_s \tag{5.11}$$

$$\mu^* \quad \frac{\mu}{\phi_p} \tag{5.12}$$

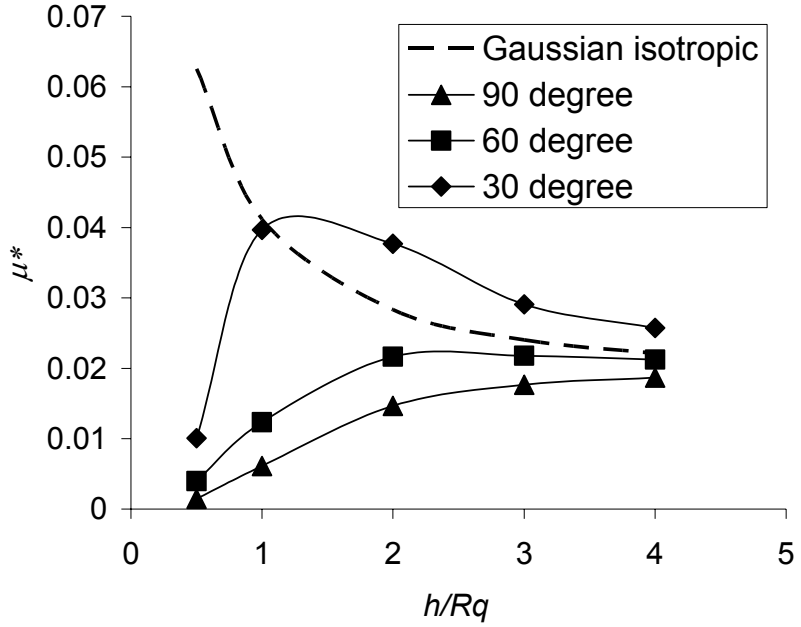

Figure 5-15: Change in equivalent viscosity with honing angle

The shear flow factor, ϕ_s, for the liner surface, increases with honing angle, as shown in Figure 5-16. An increase in the shear flow factor for a moving surface indicates that that surface is more able to carry lubricant along with it, increasing lubricant flow due to its movement. This increase in flow may be due to more fluid being carried in pores and valleys, or to hydrodynamic effects around asperities. In the present case, however, the flow factor considered is for the cylinder liner, which is *stationary* relative to the lubricant movement. The increase in flow factor still indicates that a liner finish with grooves at a lower honing angle is more able to hold the lubricant, but in this case the effect is to increase resistance to fluid flow, rather than decrease it. Thus, as in the case of the pressure flow factor, the increase in liner surface shear flow factor, with decreasing honing angle, causes an increase in generated hydrodynamic pressure and corresponding drop in friction.

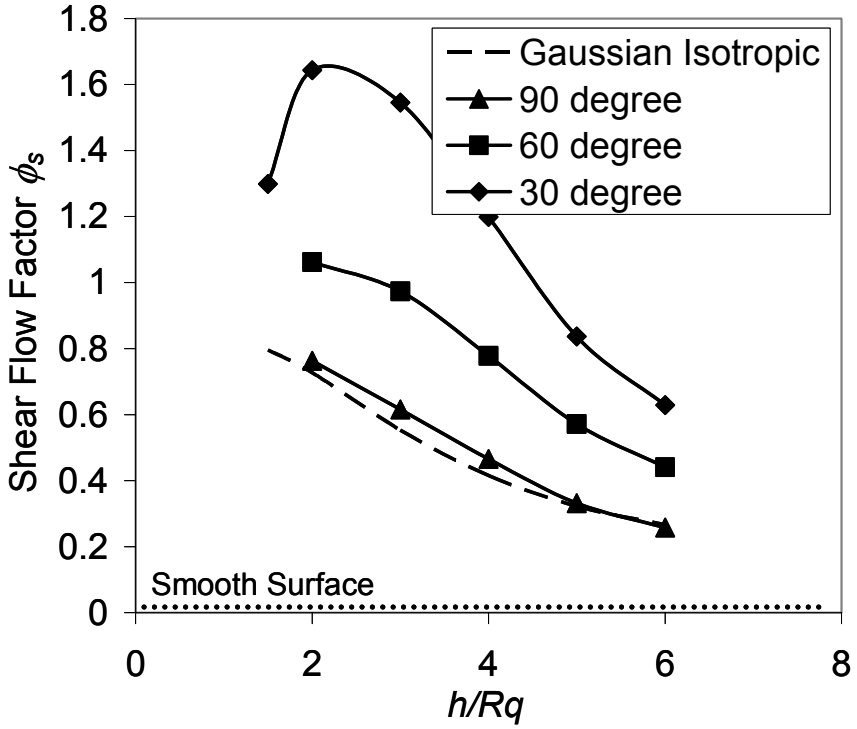

Figure 5-16: Change in shear flow factor with honing angle

Changes in the stress factors have a more straightforward interpretation: an increase in a stress factor corresponds to an increase in friction, while a decrease indicates a corresponding friction decrease. Pressure and shear stress factors are shown in Figure 5-17. Pressure stress factor, ϕ_{fp}, decreases with honing angle, indicating that shear stress due to pressure drop across the oil film decreases. The shear stress factor, ϕ_{fs}, increases slightly as honing angle decreases, but the change is small relative to the effects of both the pressure stress factor and the flow factors.

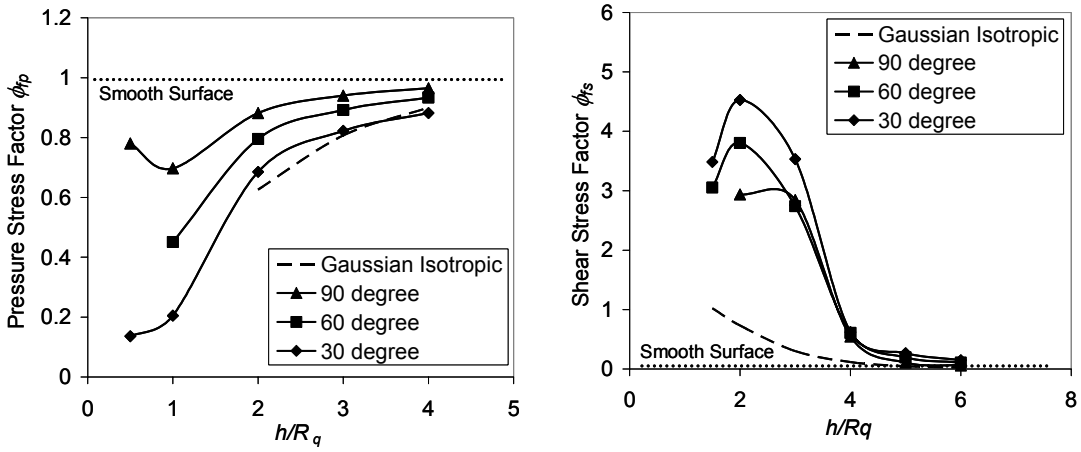

a) Pressure stress factor

b) Shear stress factor

Figure 5-17: Change in pressure and shear stress factors with honing angle

The overall picture given by the shear and stress factors indicates that friction in the Waukesha ring-pack should decrease with decreasing cross-hatch angle, and that is what was observed in the model results. Figure 5-18 shows the change in ring-pack friction mean effective pressure with cross-hatch angle. A friction reduction of approximately 8% is predicted for a change in cross-hatch angle from 90^o to 30^o. The decrease in slope as cross-hatch angle decreases is due to the diminishing returns associated with decreasing mid-stroke boundary friction. As asperity contact decreases, boundary friction becomes a smaller contributor to the overall friction, and thus reducing it becomes less important. Also, as indicated in equation 4.4, contact pressure increases at a greater-than-linear rate as film thickness decreases. Then, as film thicknesses increase with cross-hatch angle, the corresponding decrease in boundary friction is large at first, and then decreases as the surfaces move farther apart.

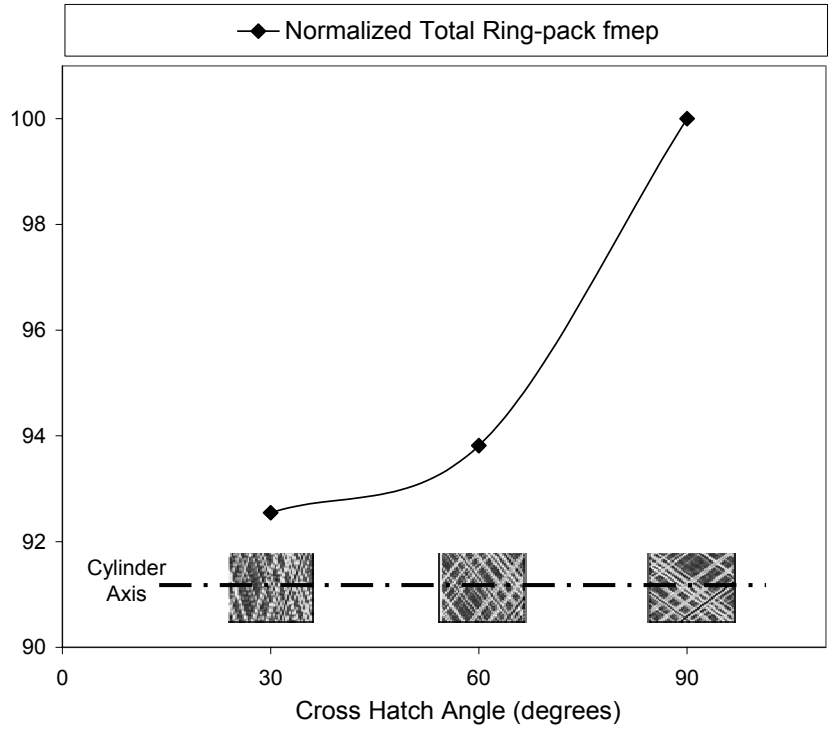

Figure 5-18: Change in ring-pack friction with honing cross-hatch angle

As in the case of surface skewness, changing the honing angle affects not only friction but other important parameters as well. Figure 5-19 shows the change in top ring/liner clearance with cross-hatch angle. The top ring minimum cycle clearance decreases as the honing angle decreases, indicating that more asperity contact takes place near dead-centers. This could lead to increased wear and scuffing in the dead-center regions of the liner, particularly near TDC. Conversely, the average top ring clearance increases slightly when honing angle decreases, indicating that oil films are generally thicker throughout the stroke, except near top and bottom dead-centers. If a correspondingly increased amount of oil is left on the liner during down-strokes, this may indicate an increase in oil consumption.

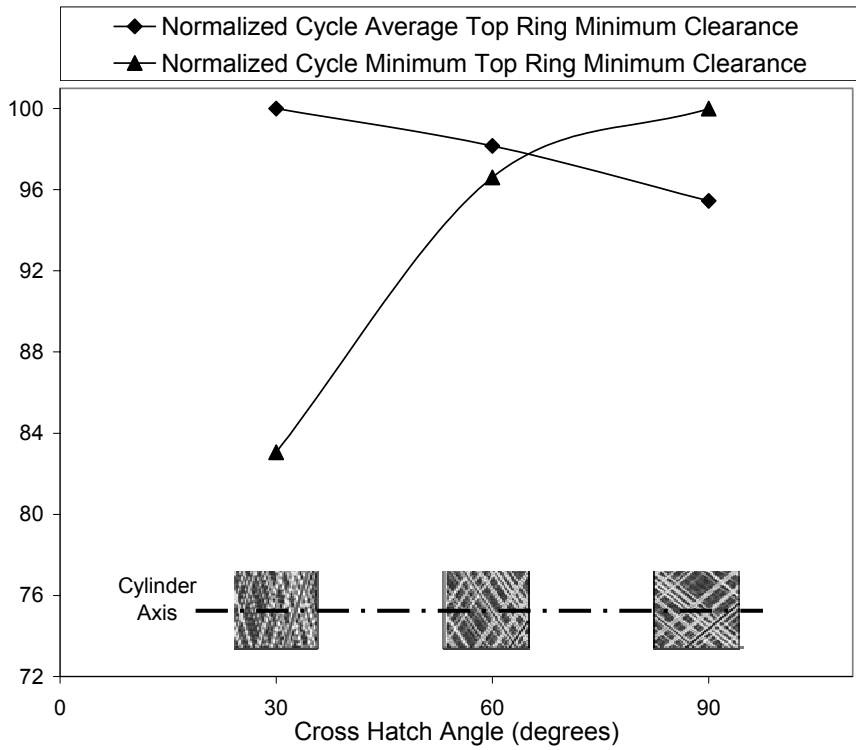

Figure 5-19: Change in ring clearances with honing cross-hatch angle

5.4. Conclusions and Friction Reduction Strategies

Waukesha engine ring-pack friction reduction is predicted for decreased surface skewness and decreased honing cross-hatch angle. In both cases, the friction reduction is due to an increase in hydrodynamic pressure generation in the oil film, which allows a higher ring load to be supported at a given film thickness. In the Waukesha engine boundary contact occurs throughout the stroke, so that thicker films result in a decrease in asperity contact, and, thus, in boundary friction, throughout the stroke. The Waukesha engine ring-pack is already well-optimized, but a further reduction in friction of about 5% is believed possible, with parameter changes indicated in Table 5-1.

Table 5-1: Recommended surface finish parameters

Parameter	Current Value (Unworn)	Proposed	Friction Reduction
Skewness	-2.28	-3.15	5%
Honing angle	45^o +/- 5^o	25^o	

While reducing skewness and honing angle can reduce friction, there may also be drawbacks to these strategies. In both cases an increase in wear or scuffing near dead-centers may occur, in particular near TDC for the top ring. Also, decreasing honing angle may lead to a small increase in oil consumption. The mechanisms behind these issues, and the extent to which they occur, have not been investigated in detail - further investigation is required.

5.5. Preliminary Literature Study – Possible Friction Benefits of Surface Dimpling/Texturing

Analyses of surface texturing completed thus far have concentrated on existing surface finishes, so that existing ring and liner surfacing processes can be optimized for low friction. New, novel finishes may also be developed, however, that are not currently in use, and it is desirable to also understand and optimize the effects of these new developments. Future surface finish analyses will concentrate on new technologies, to model and assess these techniques as they are developed.

A preliminary literature review has been performed on surface micro-dimpling, a technique that has been gaining attention in recent years as the laser surface texturing (LST) technique has shown promise of making surface dimpling relatively simple and inexpensive. Surface dimpling has been shown to reduce friction in some cases, including simulated ring-liner conditions. The dimpling is believed to reduce friction in the same manner as the textures analyzed above – when a mixed friction regime is present, the dimples can act to increase hydrodynamic pressure, thus reducing boundary friction. Also, the dimples may act as containment for wear particles, or as reservoirs for lubricant in poorly-lubricated areas such as the "dry region" for the top ring. A brief summary of the literature review is included below.

Surface texturing has been recognized as a method for enhancing the tribological properties of surfaces for many years. Early studies recognized the potential of microasperities to provide hydrodynamic lift during film lubrication [27,28,29] while later research indicated that small-scale texturing could also provide lubricant reservoirs and trap wear particles[30] in poorly lubricated cases. All of these effects may decrease friction and wear between two sliding surfaces, but some experimental results also show a negative effect from surface texturing. In some cases texturing is not optimized for a given case, in others there is no optimal case – any kind of texturing may be worse than a smooth surface. Research and analysis presented to date demonstrates both the potential to improve tribological properties via surface texturing, and the need to understand the effects of materials, lubricants, and running conditions before a surface texture is applied.

Recent and past studies have explored the effects of controlled surface texturing, and of different microasperity parameters on friction, wear, and other issues. A limited number of analytical models have been proposed, mostly considering hydrodynamic effects of microtexturing, while the majority of studies have been largely experimental. The results of several studies are summarized below, grouped according to the apparent benefit of the texturing.

5.5.1. Hydrodynamic Effects

Like large scale converging-diverging surfaces, micro-scale asperities can experience an asymmetric pressure distribution that results in hydrodynamic lift. In cases of mixed lubrication, this added lift can alter the balance between hydrodynamic and boundary lubrication, reducing the amount of asperity contact that takes place, and thus reducing both friction and wear. Several studies have considered the effects of

distributed surface patterns of microshapes. The amount of friction reduction that occurs in these cases has been found to be largely independent of asperity shape, and highly dependent on depth:diameter ratio, with some dependence on area density.

Kovalchenko and others looked closely at the lubrication regime effect in a series of experiments using a pin-on-disk test rig with unidirectional sliding, with a textured disk.[31] This study produced Stribeck curves for various lubricants and load conditions, and different dimpled area densities (the depth:diameter ratio for the dimples was maintained at an "ideal" value in all cases). In general, dimpling expanded the range of parameters under which hydrodynamic lubrication took place, leading to a longer span of low friction, hydrodynamic lubrication to occur before increases in friction due to asperity contact occurred.

Stephens and Siripuram[32] studied the effects of different cross-section shapes, for both positive and negative asperities. Circular, square, diamond, hexagonal and triangular cross-sections were considered (right prism 3-D shape), over a range of area densities. A Reynolds equation based analysis indicated that minimum friction coefficient was largely independent of asperity shape, but that the area fraction at which friction coefficient was minimized had some dependence on shape, with positive asperities providing lower friction at a small (~20%) area fraction and negative asperities showing a minimum in friction coefficient at large (~80%) area fraction. No experimental evidence is yet available to validate this theoretical study.

Etsion, with others, has completed several experimental studies and developed a theoretical model with the aim of defining optimal dimple parameters for fields of evenly spaced pores created with the LST technique. A model based on mechanical seals indicated that adding micropores can increase load capacity and reduce friction. This model indicated that the depth:area ratio of a dimple can be optimized for seal performance, with diameter:depth ratio around 0.05, found to be optimal. This model showed close agreement with experimental results obtained using a simple sliding test rig, while an in-place test in a water pump indicated that seal wear was substantially reduced when micropores were added to one sealing surface[33].

Ronen, along with Etsion and others also developed a simple model for a piston ring-liner system, modeling the ring and liner as two flat, nominally parallel surfaces, with dimples introduced on the ring surface. This analysis indicated that a reduction in friction of ~30% is possible with optimal surface texturing. [34] The analysis found that the optimum pore depth:diameter ratio was 0.1-0.18, over the range of parameters considered, and that the variation of friction within an area ratio span of 5%-20% was small.

Experimental results showed good correlation between this analysis and a test rig using the same simplified, flat "ring" and "liner" geometry as the analysis. A test using production ring and liner sections also was also performed. Both cases showed a reduction in overall friction of ~30% for dimpled "rings", vs. untextured samples, with the flat-surfaces tester showing up to 40% reduction in some cases. [35]

5.5.2. Reduction of boundary and unlubricated friction

Surface texturing has been shown to reduce friction in both boundary and unlubricated sliding cases. Here, surface pores may retain lubricant, for re-supply to the sliding surfaces, and also retain wear particles, reducing friction and wear resulting from surface plowing. When plowing is not the main friction/wear mechanism, however, adding surface dimples can increase friction. Since surface-surface contact occurs, the material properties of the two surfaces become important, in addition to load and other external conditions. Surface interactions, including surface affinities and chemical reactions, greatly increase the complexity of texture optimization, and of the decision to add texture at all.

Several researchers considering fretting wear and failure observed some benefit from micro-grooved surfaces. Varenberg, et al.[36], observed that the friction and wear benefit from microgrooves depends on both materials and loading conditions. Ball-on-flat and flat-on-flat tests showed that friction could be reduced and load capacity increased in some cases. For bronze-on-steel cases microgrooves reduced friction at all load conditions, which is expected because bronze and steel have only a week adhesive interaction – the dominant friction mode should be plowing, which is reduced when wear particles are removed from the interface. For steel-on-steel cases, friction was reduced at low loads, but increased for higher loads. This may indicate a change in friction regime with loading – plowing may be dominant at lower loading, while adhesion mechanisms dominate at high loads.

Varenberg's observations also confirmed that fewer wear particles are trapped between the sliding surfaces when microgrooves are present. Electrical resistance between flat, untextured surfaces remained constant with load, and decreased when microgrooves were added to one surface. The reduction in resistance indicates that the surfaces are closer together – no longer separated by a layer of wear particles – in the textured case.

Ryk [35] observed a negative effect when using dimples in poorly lubricated conditions. The same experimental set up used to observe dimple effects for well-lubricated conditions (described above) was used with varying lubricant feed rate. As lubricant availability decreased friction increased in all cases, with several dimpled cases showing higher friction than the smooth surface case. One possible cause for this phenomenon is that the presence of dimples reduced the availability of lubricant between the sliding surfaces, since much of the available lubricant was trapped in the pores. This hypothesis is supported by the observation that deeper pores exhibited higher friction in the lubricant-starved regime.

A few analytical studies have been made of the problem of poorly lubricated, textured surfaces. Zhao and others[37] considered the use of micropores as lubricant reservoirs for a highly-loaded, poorly lubricated case. Finite element analysis was used to show that a single surface micro-pocket shows a reduction in volume with loading (from a cylinder), and, thus, if the pockets are filled with lubricant, the squeezed lubricant

will be enabled to support some of the applied load, reducing surface-surface loading. Lubricant-filled pockets were compared to empty pockets, and shown to reduce pressure spikes and high sub-surface stresses associated with the empty pockets.

5.5.3. Summary

The effect of microtexturing on sliding surface interaction is very complex, depending on the lubrication regime, loading and other external conditions, surface materials, and other factors. Several analytical and experimental studies have shown that surface texturing can provide benefits – some very substantial, as the reduction in friction by 30% or more for a piston-ring-like case demonstrated by Etsion – while others have shown no effect or even a negative effect to adding surface micro-texture. Analytical models developed thus far are relatively simple and are mostly limited to analysis of hydrodynamic effects, but show reasonably good agreement with experimental data.

In applications where a substantial amount of mixed lubrication takes place, friction and wear can most likely be reduced with the application of micro-dimpling, where the exact geometry of the ideal pores is determined by the specifics of the application. In boundary and dry sliding cases, the potential for friction reduction or lifetime extension via microtexturing is highly dependent on the surfaces and loads involved. Attention must be paid to the type of friction and wear that dominate the process (plowing, adhesion, oxidation, etc.) and to any chemical reactions that may be taking place. These mechanisms have the potential to reduce friction and wear, increase load capacity, and increase lifetime in numerous applications, but extensive research still needs to be performed to further define and explain the mechanisms, and means by which to optimize the use, of surface microtexturing.

6. Friction Reduction Strategies - Piston Design

The piston skirt is approximately equal to the ring-pack in the amount of friction it contributes to the engine mechanical losses, and, like the ring-pack, its friction can be reduced if asperity contact is reduced. Several piston parameters were studied, including design parameters such as the skirt profile and waviness, and other factors including lubricant viscosity and skirt-liner clearance, with the goal of reducing friction. The most important parameters identified thus far are oil film thickness and skirt waviness, which can both be manipulated to reduce friction by reducing skirt/liner asperity contact.

6.1. Analytical Methods

A previously developed and experimentally validated model of piston secondary motion, developed by Wong et al., was modified and used in this study [17], and is described in detail in section 2.2. The modifications to the model consisted of including the influence of temperature on lubricant viscosity.[38] When the piston moves up and down in the cylinder, it experiences substantial changes in temperature, which affect the local viscosity of the oil on the piston-skirt/liner interface. While the original model did

not include this effect, and assumed a constant viscosity, a Vogel equation relationship was subsequently added in order to obtain a more accurate model of oil viscosity. For simplicity, only straight-weight oils (SAE-20, SAE-30, SAE-40, and SAE-50) were included in the analysis (shear rate dependence was not considered).

6.2. Piston Lubrication

The piston experiences both hydrodynamic and boundary lubrication, with the dominant lubrication regime changing during the engine cycle. Figure 6-1 shows the cumulative fmep (a measure of friction power loss) from hydrodynamic and boundary sources, major and minor thrust sides. While the hydrodynamic frictional losses from the two sides are approximately equal and occur throughout the stroke, boundary contact is only observed on the major thrust side, during the expansion stroke. This results from the high gas pressures present after combustion, as well as the piston "slap" as it moves from the minor to the major thrust side. The boundary friction generated in this region of the stroke contributes a significant amount – in many cases, the majority – of total piston skirt losses [39].

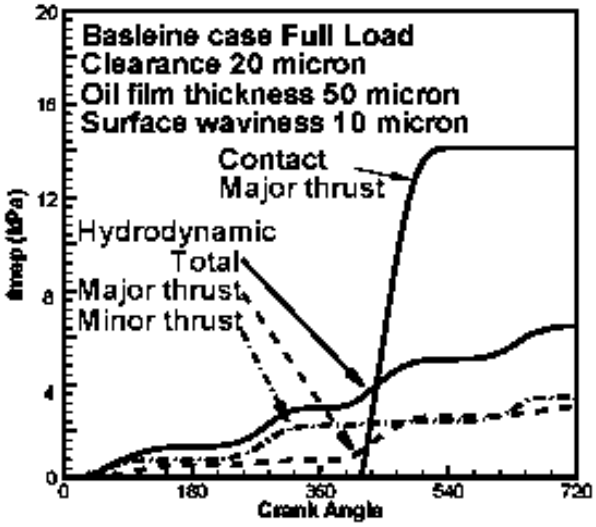

Figure 6-1: Cumulative hydrodynamic and boundary friction contributions to piston friction

6.3. Effect of Piston Parameters on Friction

6.3.1. Skirt-Liner Clearance

As the piston travels up and down in the cylinder, it also rotates and moves transversally in a secondary motion, due to changing gas pressures and inertias. Instead of traveling along the axis of the cylinder, the piston presses against on side of the liner as it moves towards the combustion chamber, then moves to the other side as it travels down. When the piston transitions from one side to the other a "slap" occurs, when the

piston hits the liner and oscillates briefly before remaining pressed against it. The impact velocity of this slap affects the amount of noise produced by the engine as well as the piston frictional losses.

The skirt/liner clearance directly affects the impact speed of the piston slap. Figure 6-2 shows how the skirt impact velocity changes with cold clearance. A larger clearance allows the piston to accelerate over a larger distance, resulting in a faster impact speed at the slap. Large impact velocities lead to large impact forces, which lead in turn to large contact friction losses. Then, skirt/liner friction should be reduced as clearance is reduced. This was found to be the case for larger oil thicknesses, but for thinner oil films, as shown in Figure 6-3, a minimum point observed, where friction begins to increase again when clearance is decreased.

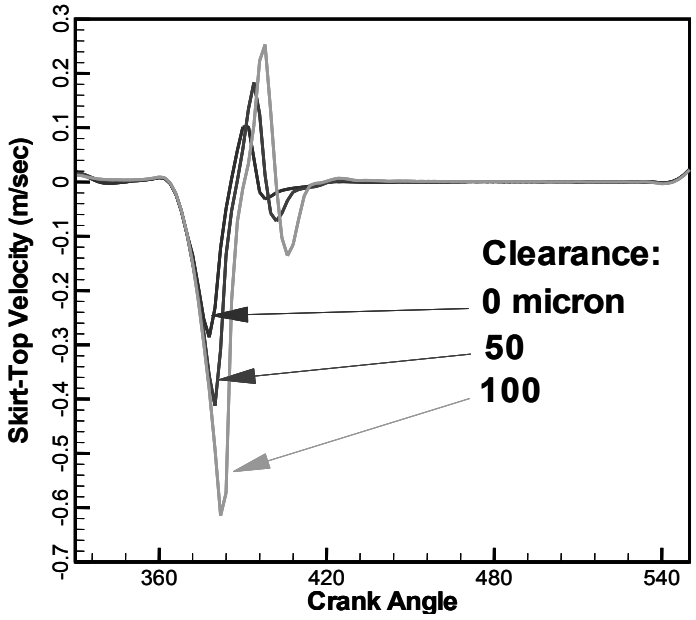

Figure 6-2: Skirt impact velocity increases as cold clearance increases

This minimum point results from asperity contact occurring at tight clearances, which increases friction, by bringing the skirt and liner surfaces closer together for low oil film thicknesses. In Figure 6-3, for large clearances the slapping velocity dominates and friction decreases as clearance decreases, while for very small clearances asperity contact becomes important and friction begins to rise while clearance is decreased. The figure also shows almost no change in hydrodynamic friction with clearance, showing that the cause for the friction change is largely due to changes in asperity contact.

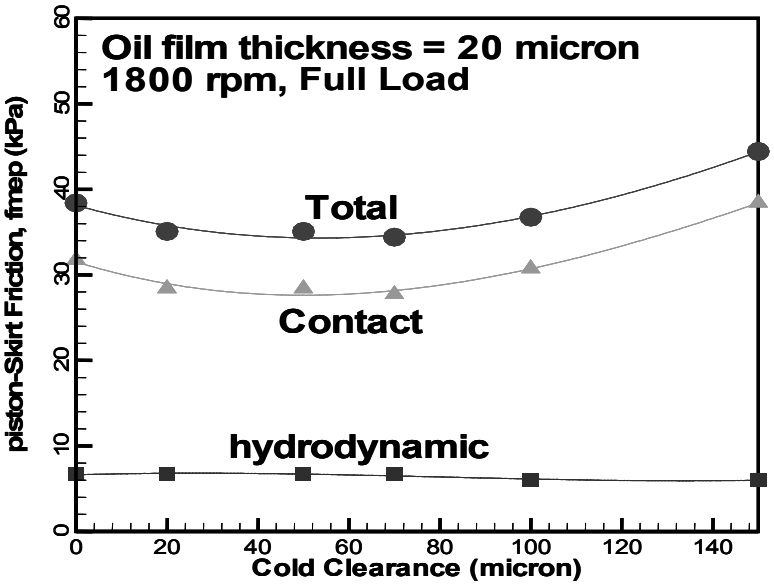

Figure 6-3: Effect of skirt/liner clearance on friction

6.3.2. Oil Supply/Oil Film Thickness

The mechanisms of oil distribution between the piston and liner are not fully understood. For the purposes of a parametric study, a simplified model was used that allowed oil availability to be set as a model input. It is assumed that, prior to piston impact, an oil layer of a given thickness is available on the liner. The wetting locations are determined by the boundary condition that the oil film pressure is equal to the gas pressure around the skirt at the wetted edges, as well as piston and liner geometry. This served to specify the oil supply to the skirt and the oil film thickness between skirt and liner.

The oil film thickness has a much greater impact on boundary friction than hydrodynamic. Figure 6-4 shows a rapid increase in boundary friction as film thickness is decreased, due to an increase in the amount of boundary contact that occurs as the piston and liner surfaces are brought closer together. (The minimum point shown in the figure stems from the fitting technique used to fit the simulation data points, and probably does not have any physical basis). Only a small change in hydrodynamic friction is observed throughout the range of film thicknesses considered.

Comparing Figure 6-4 to Figure 6-3 also shows that the oil film thickness has a much larger effect on piston friction than skirt/liner clearance. The main effect of the clearance is to control friction at the “slap” period of the piston transition, while the film thickness affects skirt/liner contact throughout the cycle.

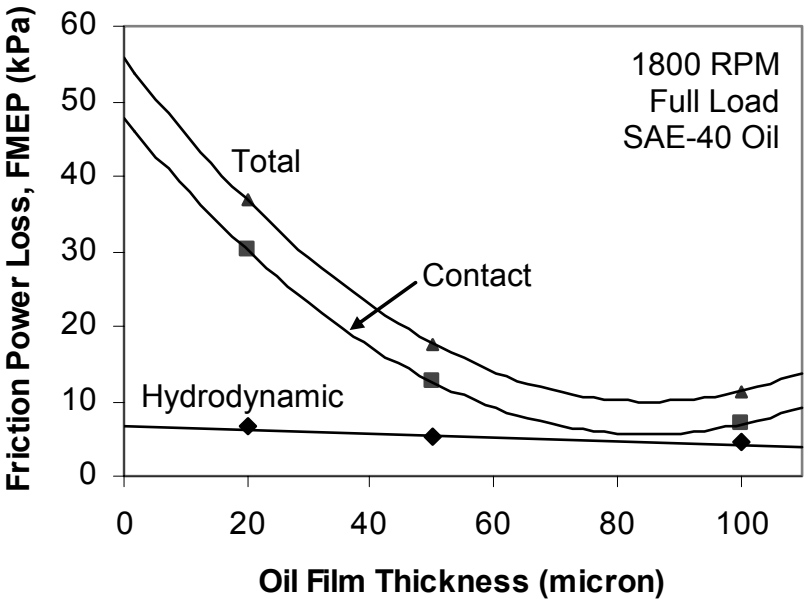

Figure 6-4: Effect of oil film thickness on skirt/liner friction

While its effect on friction is clear, the lubricant film thickness may also effect other engine parameters. For example, a thicker oil film can serve to cushion engine slap, reducing engine noise and vibration as well as friction. However, if the film is too thick, oil consumption may become a problem.

6.3.3. Surface Finish/Waviness

The piston skirt is typically machined so that it is covered by circumferential grooves, with depths on the order of 10μ, as well as smaller scale "roughness" asperities, of 1-2 orders of magnitude smaller in size. The grooves behave as oil reservoirs, supplying oil for hydrodynamic lubrication. The customary measure of groove size is waviness, which is the "amplitude" (*i.e.*, half of the peak-to-valley depth) of the groove. A schematic is shown in Figure 6-5.

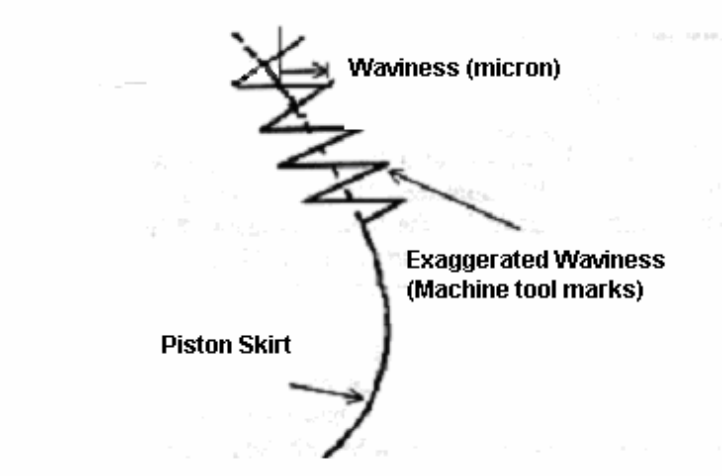

Figure 6-5: **Piston skirt waviness, measured peak-to-peak values**

Figure 6-6 and Figure 6-7 show that friction losses decrease as surface waviness decreases, largely due to a decrease in boundary friction. For a given availability of oil, a piston with deeper machining grooves has more volume to contain the oil – that is, the lubricant can be trapped within the machining grooves instead of staying between the piston and liner. When it is contained within the grooves, the oil is not useful as a lubricant or to support hydrodynamic pressure, and asperity contact occurs. Conversely, when the oil cannot escape into deep machining grooves and is compressed between the piston and liner, hydrodynamic pressure is generated and the piston load can be fully supported on the oil film.

The relation of friction to surface waviness suggests a dependence not only on waviness height, but on the relation of the waviness to oil availability. A smoother piston should require less oil to support hydrodynamic lubrication, while a very wavy piston should require more. Figure 6-8 indicates that this is indeed the case, and that there is a nearly linear relationship between waviness:film-thickness ratio and piston friction. Thus, in cases where very little lubricant is available to the piston a low waviness is preferred, whereas in cases where a large film thickness is possible, a smooth piston is still preferred but a wavier surface is allowable. However, in all cases, a very smooth piston is undesirable, due to factors not included in the present model.

Although skirts with low waviness values appear to produce the lowest friction, extremely smooth surfaces can lead to high friction, wear and sometimes seizure. Extremely smooth surfaces do not retain oil well, so that direct solid-solid contact, if and when it occurs, can be very poorly lubricated and quite severe. Also, the contact surface area may be larger in cases of very smooth surfaces, further contributing to friction and wear. Therefore, friction can be minimized by selecting small but nonzero waviness values, to prevent scuffing. For all other tests in this analysis, a constant waviness of 10 μm was used.

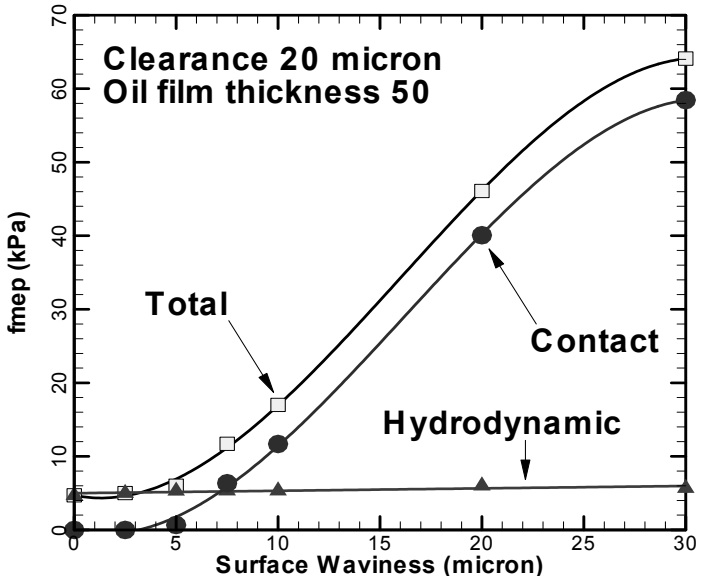

Figure 6-6: Dependence of friction on skirt waviness

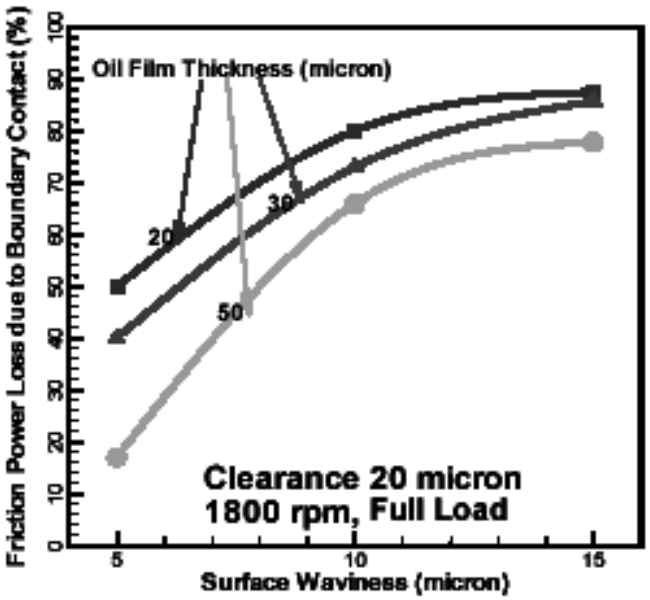

Figure 6-7: Dependence of friction power loss on skirt waviness.

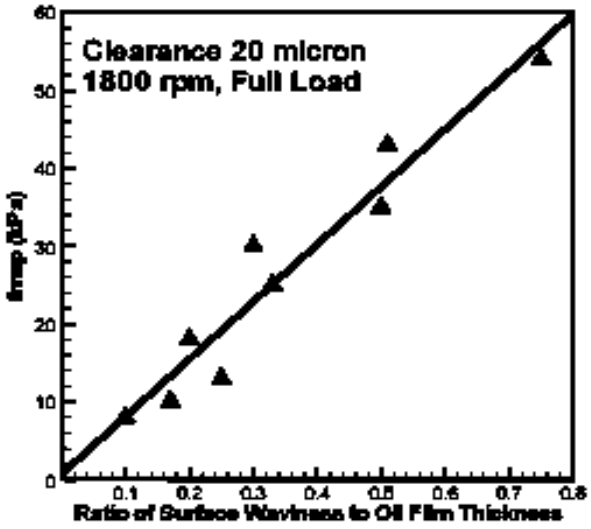

Figure 6-8: Dependence of friction losses on the ratio of waviness to film thickness

In addition to the waviness, the piston surface has a smaller scale roughness, of asperities on the scale of 1μ or less. An analysis of the effect of changing this roughness revealed almost no change in piston fmep with this variable, indicating that the effect of the roughness is dominated by the macroscopic waviness. Since the characteristic length of waviness (*i.e.*, the depth of the machined grooves) is typically an order of magnitude greater than roughness (*i.e.*, the mean depth of the random perturbations from a smooth surface), the effect of waviness on friction loss dominates. In actual operation, however, the peaks of the waves tend to get worn down to the mean line, which gives the piston a much flatter face, as shown in Figure 1-4. In this case, surface roughness may become a primary variable the amount of contact that occurs on the "flat" worn surface will depend on the asperity heights. More work remains to be done in this area.

6.3.4. Skirt Profile

A sensitivity analysis of the effects of piston curvature on skirt-friction was performed by evaluating a variety of polynomial piston-skirt axial profile shapes, shown in Figure 6-9. Each profile was defined by a simple $f(x) = x^n$ polynomial, where x was the vertical distance on the skirt (measured from the mid-point), n was the order of the polynomial, and $f(x)$ was the deviation of the profile from a perfect cylinder (which would be represented on the figure by a vertical face at 200μ). Higher-order polynomials were flatter in the midsection and dropped off dramatically at the extreme points, so that higher-order profiles were flatter overall. When cold, the maximum bulge of each profile was 200 μm, which is the same depth as the actual stock profile. For each profile, the cold skirt-to-liner clearance (measured at the point of maximum bulge to the liner) was kept constant at 20 microns.

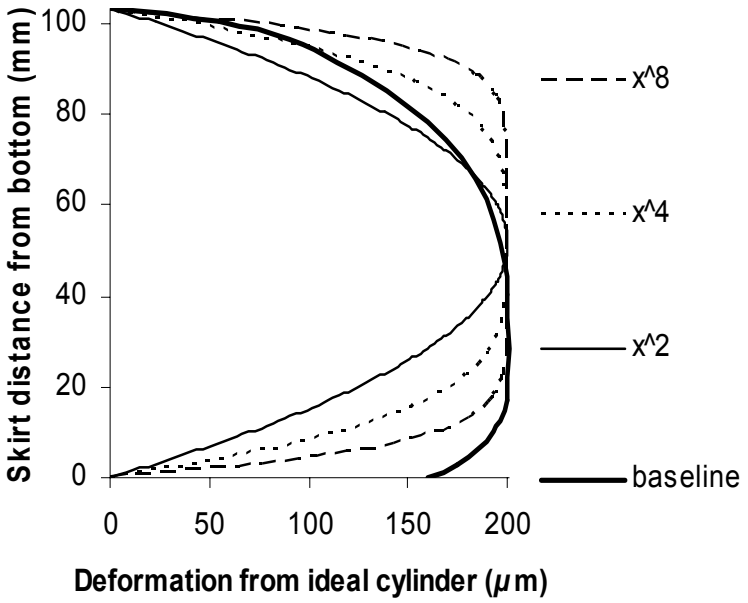

Figure 6-9: Piston profile shapes

As shown in the following figures, changing the "flatness" of the skirt changes both the hydrodynamic and boundary friction of the piston. All results shown are for the major thrust side of the piston, which is of primary interest because a large portion of total cycle friction (including almost all of the boundary friction) is generated there. Several are also shown at 50° after TDC combustion, because hydrodynamic forces are highest at this crank angle. Also, all simulations were run using SAE 40 grade oil. There is an interaction between piston profile and oil viscosity, which is discussed in section 6.3.5, below.

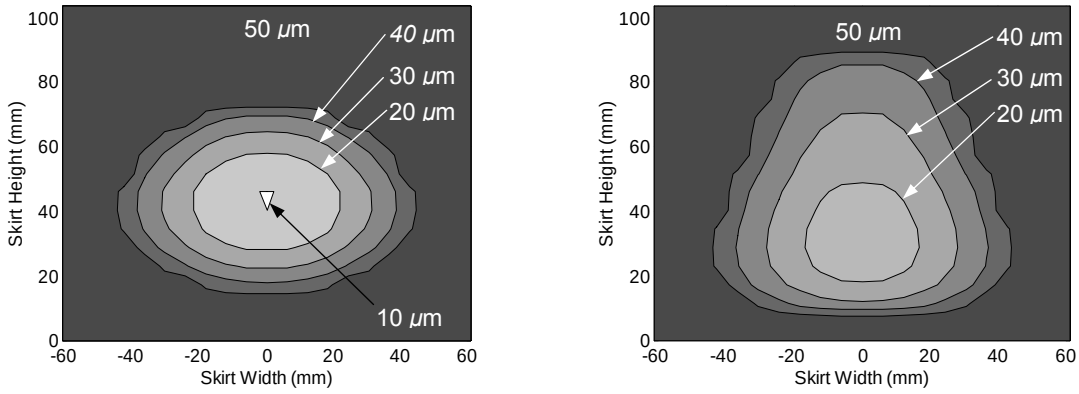

a. sharp-curvature skirt **b. shallow-curvature (flatter) skirt**

Figure 6-10: Oil film thickness for sharp and flat skirts, at 50° ATDC, during expansion

Figure 6-10 shows the effect of a changing skirt profile on the piston wetting. A flatter skirt shows both a larger wetted area and a thicker oil film. The thicker oil film indicates that separation between the piston and liner is increased, decreasing boundary contact or possibly eliminating it entirely. An increase in wetted area size and film

thickness tends to lead to an increase in hydrodynamic friction losses, but this also results in a lower average and peak oil pressures, as is shown in Figure 6-11, which could help reduce hydrodynamic friction. The increase in wetted area and oil film thickness (skirt/liner clearance) is sustained throughout the stroke, as shown in Figure 6-12.

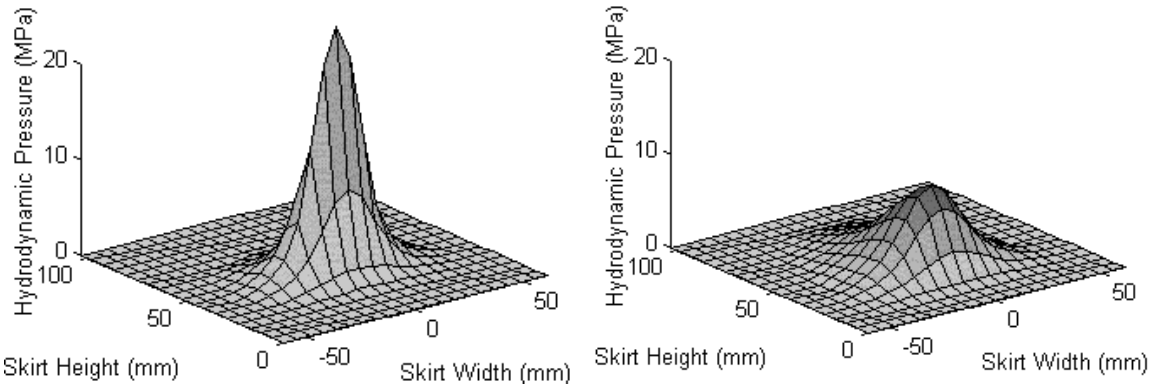

a. sharp-curvature skirt **b. shallow-curvature (flatter) skirt**

Figure 6-11: Pressure maps for sharp and flat skirts, at 50^{o} ATDC, during expansion

In Figure 6-12(a), the skirt-liner clearance for sharper profiles drops significantly below the waviness height, for a large portion of the cycle, meaning that substantial boundary contact is occurring and high friction forces created. For flatter profiles, skirt/liner clearance drops below the waviness height briefly, and only by a small amount, indicating that much less metal-metal contact is taking place. Figure 6-12(b) shows that a piston with a flatter profile experiences more wetting during the entire engine cycle, so that the change in hydrodynamic lubrication is the same throughout.

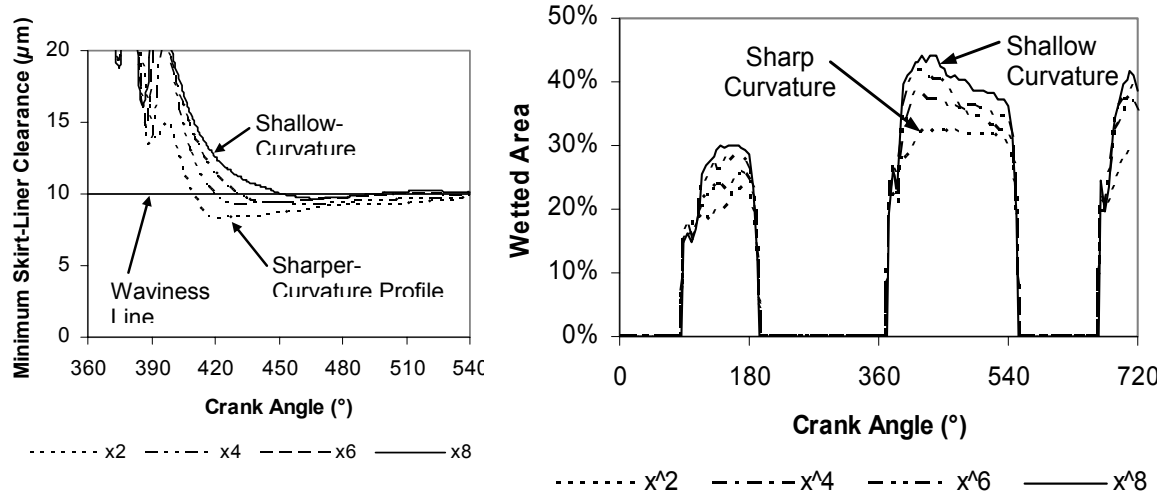

a. Details of profile effect on skirt-liner contact during 360-450° range **b. Percent wetted area for piston on thrust side**

Figure 6-12: Affect of profile on skirt/liner wetting and contact

The change in skirt/liner clearance with piston profile suggests that a sharper profile experiences much more boundary friction than a flatter one. The simulation

confirmed that a flatter piston profile causes a large reduction in boundary friction, along with a slight increase in hydrodynamic friction, as shown in Figure 6-13. Figure 6-13(a) shows that changing the piston profile has a substantial effect on the amount of boundary friction generated, with metal-metal contact almost entirely eliminated for the flattest case. In Figure 6-13(b), a small increase in hydrodynamic friction is shown for flatter profiles, but the change is much smaller than the corresponding change in boundary friction. Figure 6-14 shows the cumulative cycle friction loss with profile, for two different viscosity oils. In both cases, the piston fmep decreases for flatter profiles, with boundary contact decreasing substantially along with smaller increases in hydrodynamic friction. This is the case for both oil viscosities, although the proportion of the changes in hydrodynamic and boundary friction is different for the two cases. The relationship between piston profile and lubricant viscosity is discussed further in the following section.

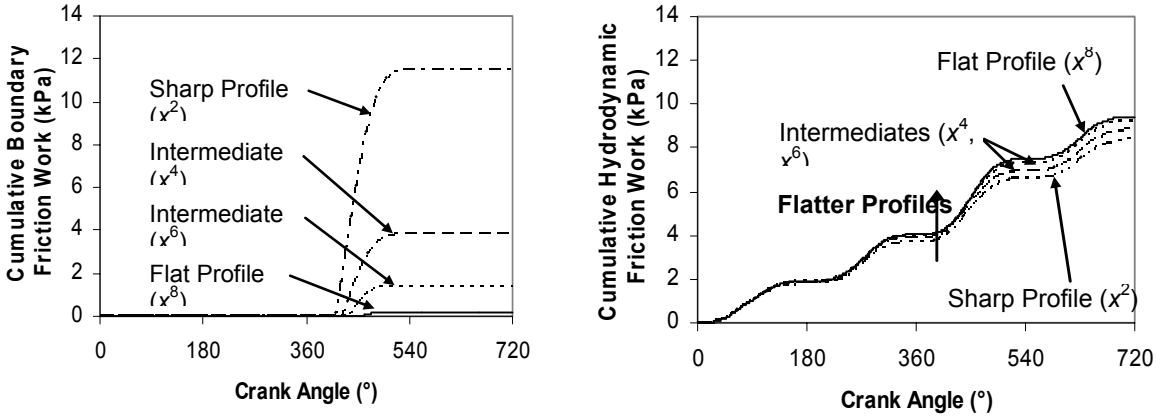

a. boundary friction work

b. hydrodynamic friction work

Figure 6-13: Comparison of cumulative friction work during the cycle, various piston skirt-profiles

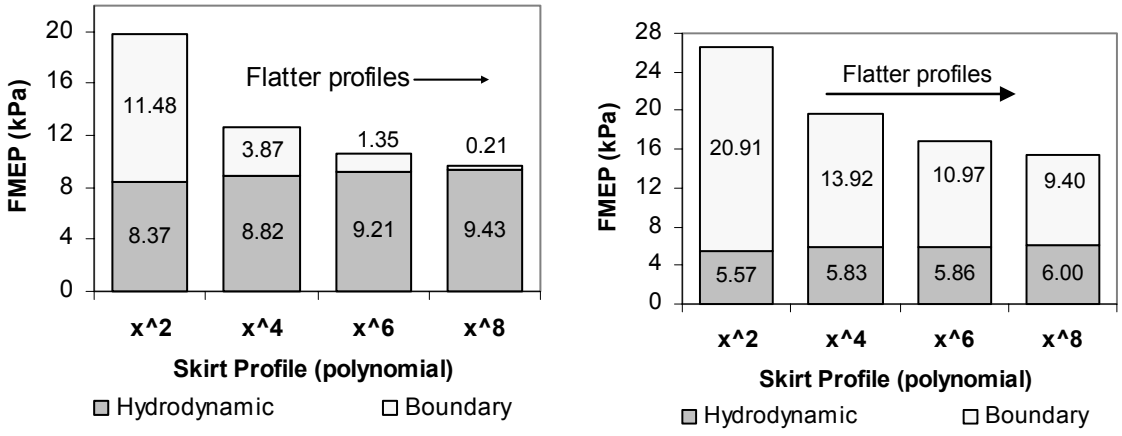

a. high viscosity (SAE-40) oil

b. low viscosity (SAE-20) oil

Figure 6-14: Effect of profile shape on hydrodynamic and boundary friction losses

6.3.5. Lubricant Viscosity

In general, more viscous oils tend to increase hydrodynamic friction, because of the increase in shear stress associated with higher viscosity, but decrease boundary contact, because the thicker oil films supported by highly viscous oils provide greater separation for two surfaces. This is the case for the piston. As oil grade is increased (where the grade is closely correlated to viscosity), the skirt/liner clearance increases, as shown in Figure 6-15. For the most viscous oil, SAE-50, boundary contact is completely eliminated, as indicated by the maintenance of a skirt/liner clearance greater than 10μ, the height of the skirt waviness.

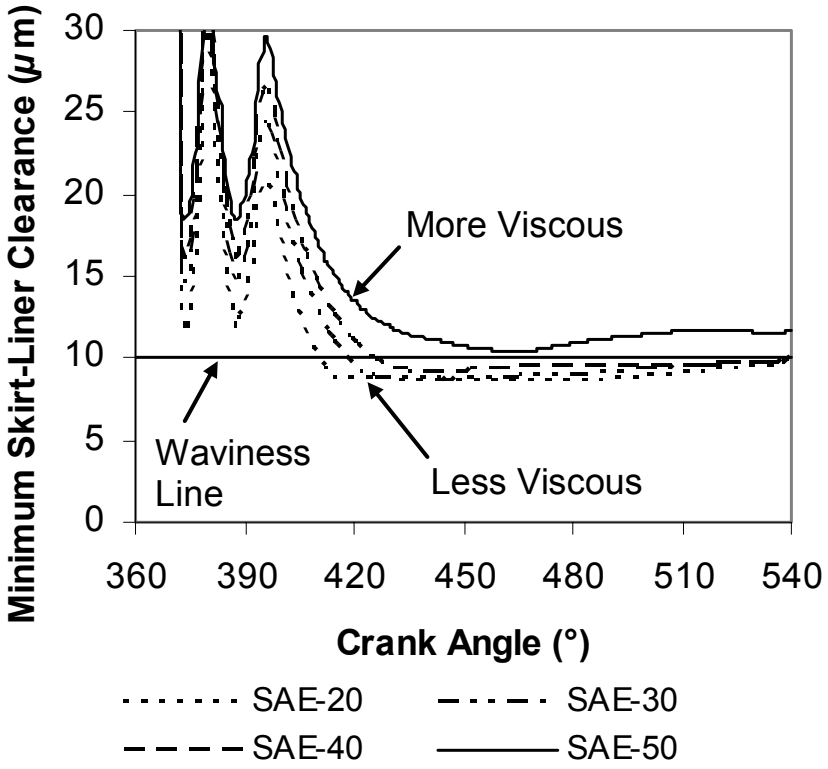

Figure 6-15: Details of viscosity effect on skirt-liner contact during 360^{o}-450^{o} range

As oil viscosity is increased, piston hydrodynamic friction increases, while boundary friction decreases. The effect of changing viscosity on the overall friction depends on the running conditions of the piston – if boundary contact contributes substantially to total piston friction, then increasing lubricant viscosity is likely to reduce overall friction. Conversely, if very little boundary contact is taking place, decreasing lubricant viscosity is more likely to lower total losses – even if asperity contact then increases, it will be outbalanced by the decrease in hydrodynamic friction. The value of the "ideal" oil viscosity, at which friction losses are minimized, is dependent on several factors, including the piston profile.

Figure 6-16 and Figure 6-17 show the dependence of piston friction on viscosity, for two different piston profiles. For a sharply curved profile, increasing viscosity causes

a decrease in friction for all of the oil grades assessed. This is because the sharp profile of the piston causes substantial boundary contact to occur for all viscosities (as described in the preceding section). For the flatter profile, however, a minimum friction is found for SAE-40 oil, where hydrodynamic and boundary friction balance to provide the lowest overall friction.

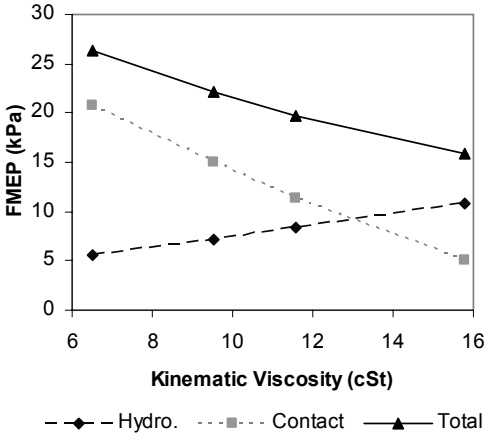

a. Friction change with oil viscosity

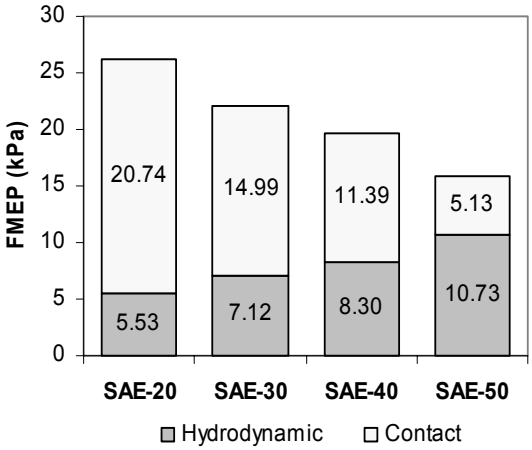

b. Friction change with oil weight

Figure 6-16: Friction change with oil viscosity, sharp curvature profile

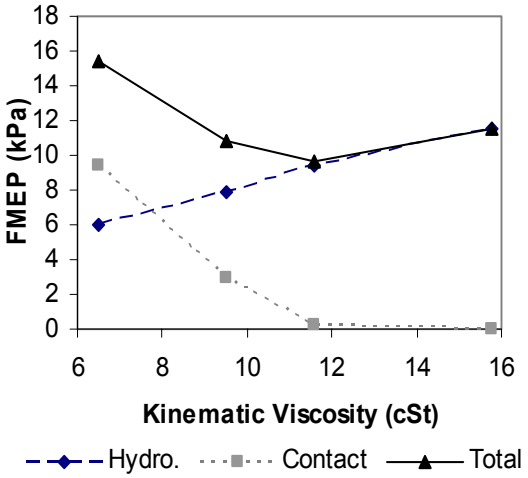

a. Friction change with oil viscosity

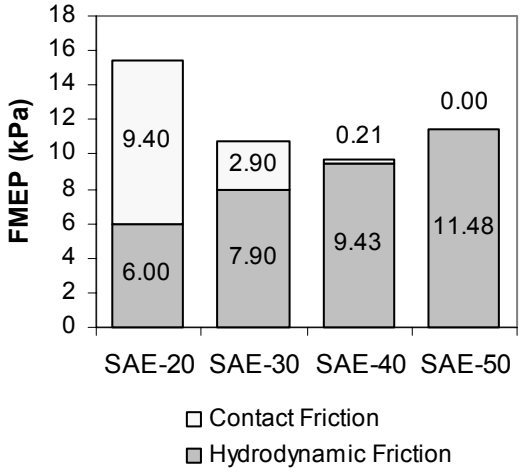

b. Friction change with oil weight

Figure 6-17: Friction change with oil viscosity, shallow curvature profile

6.4. Conclusions and Piston Friction Reduction Strategies

Piston friction arises from a complex combination of design characteristics, material and surface features, oil properties, and engine operating conditions. For the running conditions in the Waukesha engine, the most substantial reduction in friction

arises from reducing boundary contact on the thrust side, which is the source of a large portion of the cycle total. The two most important design parameters identified thus far are oil film thickness and piston surface waviness. Increasing the oil film from 20 to 50 microns can reduce friction by 50%, as shown in Figure 6-4, primarily by providing more separation between the piston and liner, reducing contact friction. Similarly, reducing piston waviness from 10 to 5 microns can also reduce friction loss by 50%, by increasing piston/liner clearance at a given oil supply, as shown in Figure 6-6. While the result of changing both of these parameters clearly will not be 100% reduction in piston friction, substantial friction reduction should be possible.

Other parameters under consideration are the skirt-to-liner clearance, piston profile shape, and lubricant viscosity, all of which may entail friction reductions of 15-30%. Skirt-to-liner clearance can be optimized to reduce friction, either from piston slap, for large clearances, or metal-metal contact, for small clearances. Piston profile shape can also be optimized, primarily by flattening the profile to reduce boundary contact. Lubricant viscosity has a dual effect on piston friction: increasing viscosity decreases boundary friction, but also increases hydrodynamic friction. The viscosity can be optimized to minimize the total, taking into account the piston profile and other factors that contribute to the hydrodynamic/boundary balance.

Many other parameters contribute to piston friction which have not yet been considered. The most important of these is the skirt stiffness. Preliminary investigation indicates that a more flexible skirt can reduce friction, by increasing wetted area and decreasing contact friction. This possibility will be studied further. Also, analysis of the piston and liner surface textures will be carried out, to assess the possibilities for further friction reduction.

(B) EXPERIMENTAL

7. Experimental Validation of Low-Friction Ring Designs

Low-friction piston ring designs proposed as the result of previous research (see 2003-2004 annual report for this project for more details) are currently being tested in a facility at the Engines and Energy Conversion Laboratory at Colorado State University. An instrumented Waukesha VGF 18GL engine is used to measure friction losses with the different proposed ring designs. A summary of the low-friction ring designs is given in Section 7.1, below, and Section 7.4 presents the results of tests that have been performed to date.

7.1. Summary of Low-Friction Designs

New designs for each of the three engine rings are proposed. While the designs for the top and oil control rings directly reduce ring/liner friction, the proposed second ring design does not directly affect friction, but is intended to offset adverse effects from the altered oil control ring. Because most of the ring-pack friction comes from the top and oil control rings (see Figure 3-2) these were the main focus of the friction-reduction strategies.

7.1.1. Top Ring

As was described in Section 3.2, most of the friction between the top ring and liner is generated near TDC of combustion, where high cylinder gas pressures push the ring into the liner with high force. To reduce friction during this period, a skewed barrel top ring is proposed. A schematic of the skewed barrel ring is shown in Figure 7-1.

In the figure, P_1 is the in-cylinder gas pressure, while P_2 is the gas pressure on the second land, which is much lower than P_1 near TDC combustion. The skewed barrel increases the area exposed to the high gas pressure on the front side (facing the liner) of the ring. This gas pressure results in a force pushing the ring away from the liner, which partially balances the high gas pressure on the back of the ring, reducing the net ring/liner force. Reducing the ring/liner force causes a reduction in friction as well as wear in this region.

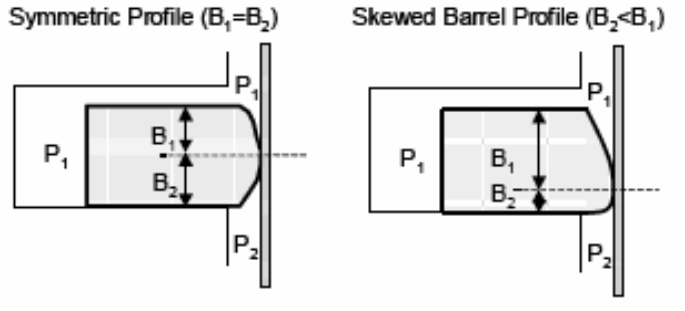

Figure 7-1: Low-friction top-ring design

Figure 7-2 shows the expected reductions in top ring friction as barrel skewness is increased. The x-axis shows "normalized B_2", which is a measure of the height of the ring below the centerline – a smaller B_2 indicates a greater amount of skewness. OS1 and OS2 are two oil supply conditions that have been studied in the ring analysis, and have relatively little effect on top ring friction. As the figure shows, top ring friction decreases approximately linearly with barrel skewness, with possible top ring friction reductions of 30-40% for very skewed barrels. This translates to a total ring-pack friction reduction of ~20%, as shown in Figure 7-3.

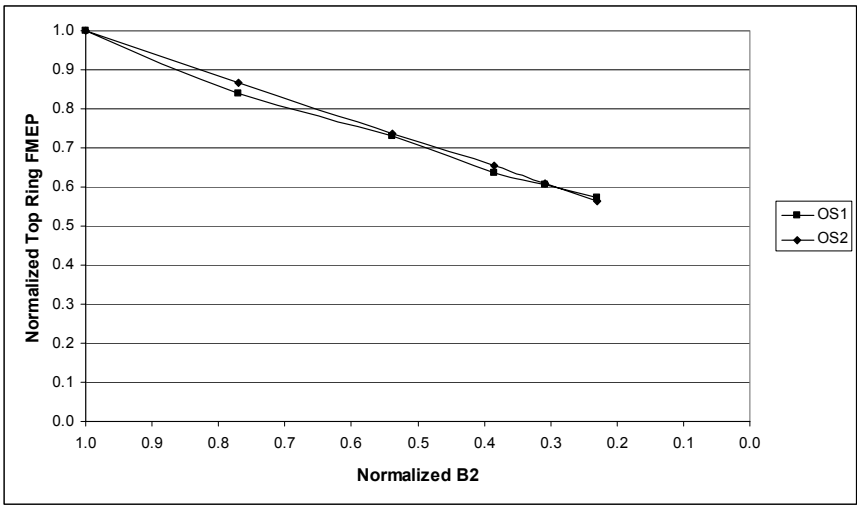

Figure 7-2: Effect of barrel skewness on top ring frictional losses

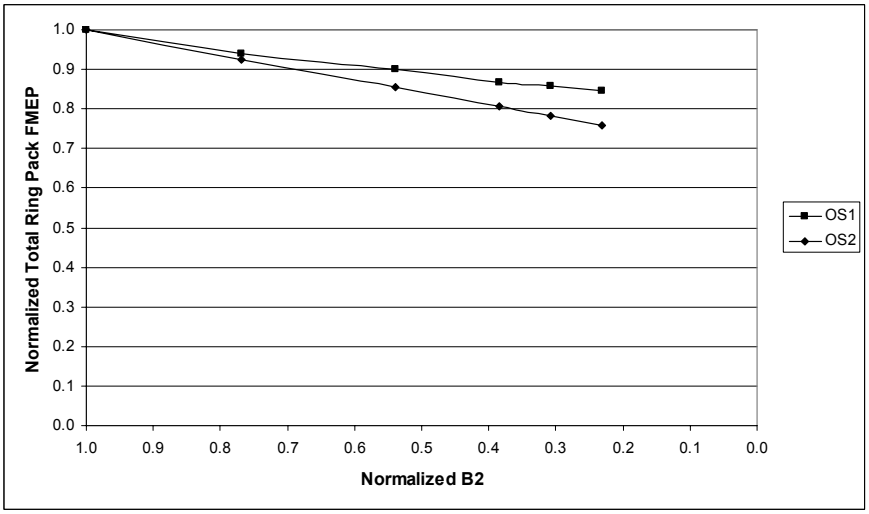

Figure 7-3: Effect of barrel skewness on total ring-pack frictional losses

7.1.2. Oil Control Ring

The main source of frictional losses between the OCR and liner is the high tension in the ring, which is required to ensure the good ring/liner conformability that is required for oil flow control. The high tension causing a high ring/liner force, which

leads to high friction. A reduced tension oil control ring is proposed, to reduce the ring/liner normal force, and thus reduce friction as well. Figure 7-4 and Figure 7-5 show the effect of reducing oil control ring tension. There is a linear decrease of OCR friction as the ring's tension is reduced, with an OCR friction reduction of ~40% possible when the ring tension is reduced by half. This translates to an overall ring-pack friction reduction of ~25%. When the top and oil control ring designs are combined, a ring-pack friction reduction of up to 45% is predicted.

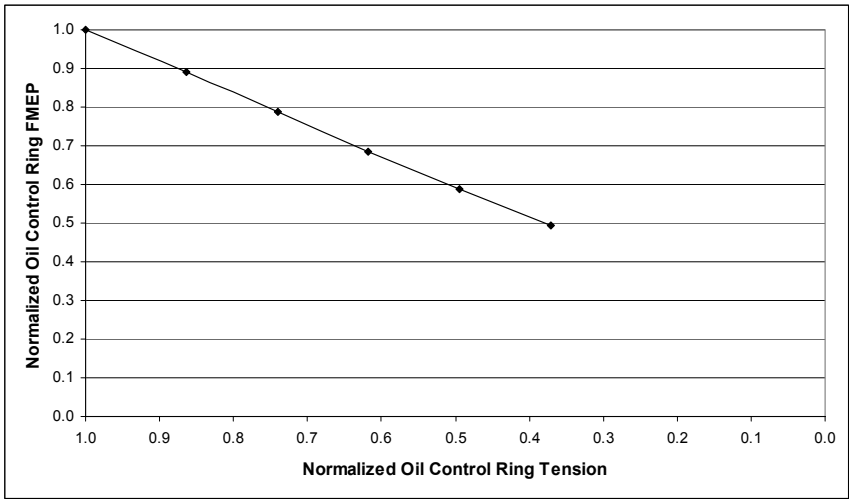

Figure 7-4: Effect of oil control ring tension on OCR frictional losses

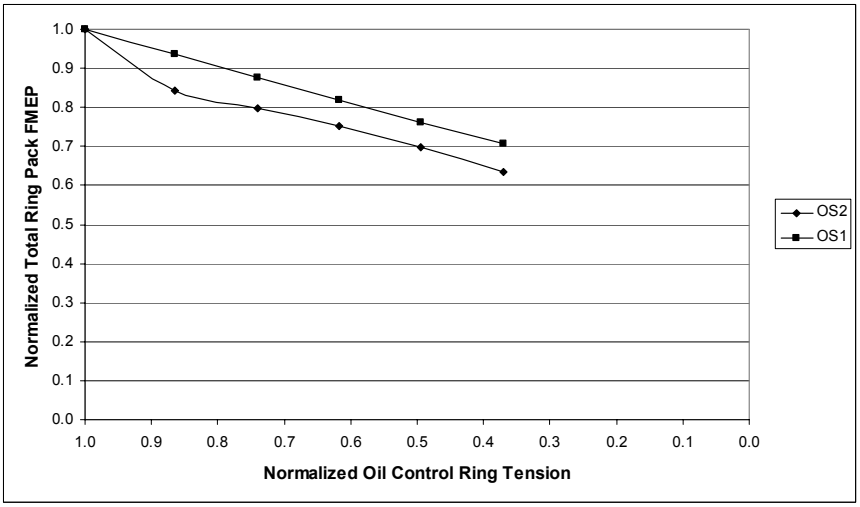

Figure 7-5: Effect of oil control ring tension on total ring-pack frictional losses

7.1.3. Second Ring: Reducing Oil Consumption

Reducing the oil control ring tension can greatly reduce frictional losses, as shown, but this comes at the expense of an increase in oil consumption. The low tension ring is less able to conform to the cylinder liner, and is thus less able to control the film

thickness that is allowed past the ring and into the combustion chamber. A negative twist second ring is proposed to offset this increase in oil consumption.

The benefit expected from the negative twist second ring lies in the ring dynamics, and in particular in the balance between the ring inertia and applied gas pressures near TDC of combustion. Near TDC, the inertia of the ring pulls it upwards – towards the top of the groove – because the piston acceleration is downwards (either the piston is slowing down approaching the TDC position, or it is increasing in speed in the downward direction, after TDC). Gas pressures, conversely, push the ring down, towards the bottom of the groove, because it is higher above the ring than below. The balance between these forces determines where the ring sits in the groove, and whether it is stable. When the ring position is stable there is no effect on oil consumption. When the position is unstable, "ring flutter" can occur, in which the ring moves up and down in the groove for a portion of the stroke, allowing high-pressure gases to blow behind the ring. These high pressure gases can blow oil accumulated behind and below the second ring back down to the crank case, thus reducing oil consumption.

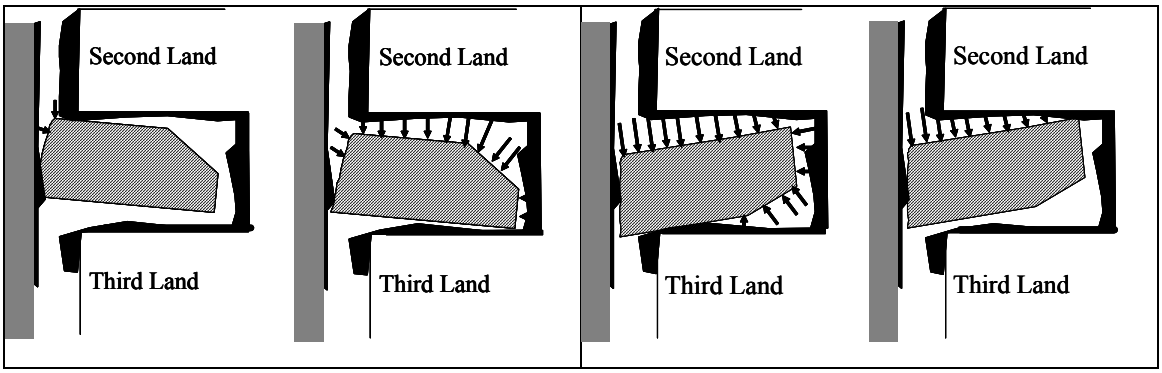

a) Positive Twist – stable.

b) Negative Twist - unstable, encourages 2nd ring flutter.

Figure 7-6: Second-ring designs to reduce oil consumption

Figure 7-6 shows both positive twist and negative twist scraper rings, with the arrows showing net gas pressure. The positive twist case is stable – when the ring is at the top of the groove, the area exposed to the gas pressures is low, so the force pushing down is small. Inertia dominates the force balance and the ring remains at the top of the groove. When the ring is at the bottom, the area exposed to gas pressures is large, and the ring remains pressed to the groove bottom because of high gas forces.

The negative twist case is unstable. When the ring is at the top of the groove, a large area is exposed to the high gas pressure, so the force pushing the ring down is relatively high. If it is great enough to overcome the ring inertia, the ring will be pushed down to the groove bottom. When the ring is at the bottom of the groove, the high-pressure gas exerts a force not only on the top but also on the bottom of the ring, so that the net downward force is reduced. This may allow the ring inertia to bring it back up to the top of the groove, where the cycle begins again.

The ring movement caused by the negative twist allows gas to flow behind the second ring near TDC combustion, blowing accumulated oil back towards the crank case.

It is hoped that this oil consumption reduction mechanism will offset any increases that occur when oil control ring tension is reduced.

7.2. Experimental Test Matrix

In order to validate the model predictions that were described in the previous sections, rings with the reduced friction designs were procured and tested on the Waukesha engine (described in Section 7.3, below). All of the experimental work was conducted at Colorado State University by students and faculty in the Engines and Energy Conversion Laboratory. The experiments were conducted with the primary goal of assessing the friction reduction achieved by the implementation of the reduced friction designs. The sequence of tests is presented in the test matrix Table 7-1 below. The number in parentheses after each test run represents the number of runs of a with the given ring-pack that have been done. More test runs for several already-tested configurations, as well as for the optimized configuration which has not yet been tested, will be performed in the coming 1-2 months.

Table 7-1: Test matrix for low-friction ring-pack designs

Test Run	Top Ring	Second Ring	Oil Control Ring
1. Baseline (2)	Baseline	Baseline	Baseline
2. LTOCR (2)	Baseline	Baseline	Low-tension
3. SBTR (1)	Skewed-barrel	Baseline	Baseline
4. LTOCR&NTSR (1)	Baseline	Negative twist	Low-tension
5. Optimized	Skewed-barrel	Negative twist	Low-tension

7.3. Experimental Set-Up and Procedure

The tests were performed on an instrumented Waukesha VGF 18GL engine, at Colorado State University. The engine is an ARES (Advanced Reciprocating Engine Systems) class engine, which is a high efficiency, low emissions engine typically in the 1 MW range used for power generation. The engine was installed and instrumented in a dynamometer test cell with all typical engine performance measurements (rpm, torque, coolant, lubricant, operating temperatures, etc.) monitored and recorded, along with more specialized measurements made for the purpose of assessing friction reduction. Figure 7-7 shows the installed engine and some of the instruments used.

Specific measurements required for the calculation of frictional losses included in-cylinder pressure from all cylinders, the brake output of the engine, and a precise indication of the piston positions. Kistler 6067C water-cooled pressure transducers were used to measure the pressure in each cylinder. An optical encoder with a precision of 0.1 CAD (crank angle degree) was used to indicate the position of the crank shaft. In order to ensure that this signal did not wander over time, a second optical pick-up was also used, so that the position of the crank shaft and pistons was always accurately known. A MidWest Dynamometer eddy current dyno was used to measure brake output from the engine.

Several other measurements were also recorded during testing. Kistler 6052A pressure transducers were used to measure inter-ring pressure, in order to monitor ring motion. Blow-by and oil consumption measurements were recorded to monitor the effects of component changes on these parameters. A J-Tech Associates VF563B in-line flow meter was used to measure blow-by, and an AVL 403S automatic oil consumption meter was used to measure oil consumption. Engine emissions data was also recorded. A National Instruments DAQ system was used to control and monitor the system, and a Hi-Techniques data acquisition system was used to acquire and record in-cylinder pressure measurements.

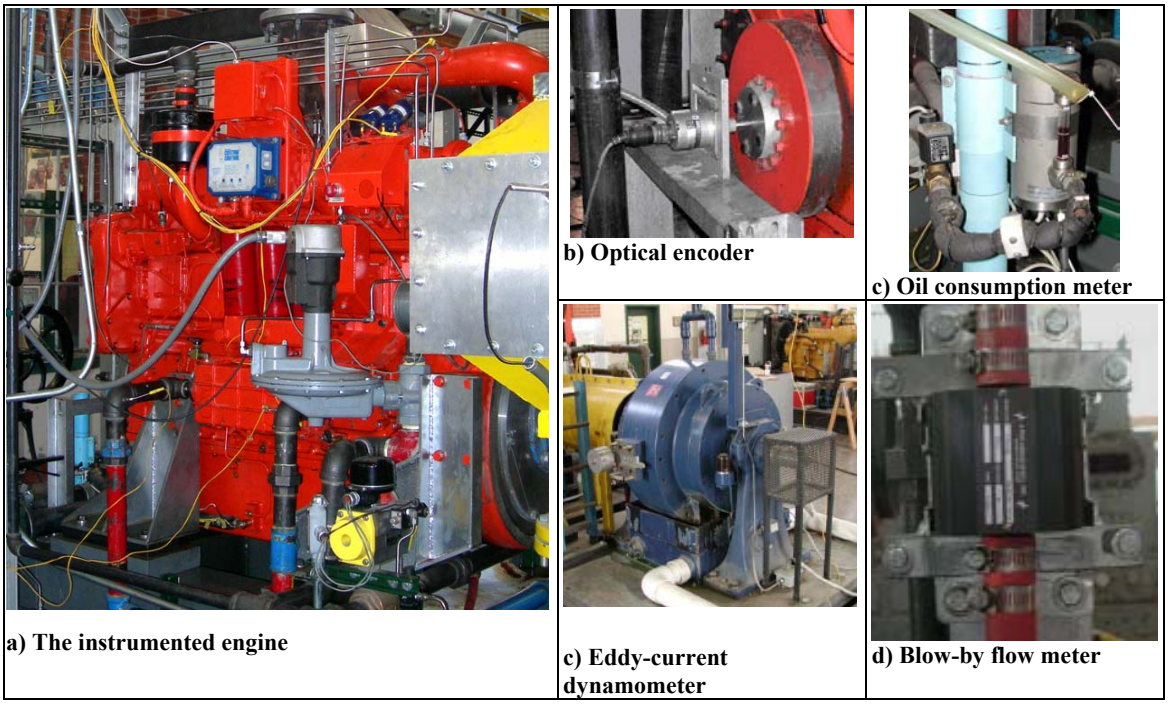

Figure 7-7: Experimental engine set-up

The same testing procedure was followed for all test runs. All rings were previously broken in at Waukesha, Inc., and so no breaking-in procedure was used. For each test run, the first step was to install the correct rings for the given test, followed by a careful engine re-build designed to avoid any unnecessary variability. The engine was then allowed to warm-up, until a stable state was reached. At this point, if required operating conditions were met, the engine was maintained at the stable state for the duration of testing. Once stabilized, the oil consumption measurement was begun, and allowed to continue throughout the testing period. The total time allowed for the oil consumption measurement was 4-5 hours. Other measurements such as blow-by and emissions measurements were also taken continuously during the testing period.

In-cylinder pressure data was taken every 0.1 CAD for each cylinder during data acquisition runs. For each test, the engine was run at four different loads – 70%, 80%, 90%, and 100%, with 100% corresponding to a BMEP of 1100kPa. Two data acquisition runs of 500 engine cycles each recorded at each load. That is, in-cylinder pressure was measured, in each of the six cylinders, with a measurement taken every 0.1CAD, for 1000 engine cycles at each load. These pressure traces were used to

calculate the engine IMEP, which was compared to the output BMEP to calculate engine mechanical losses.

The relationship FMEP = IMEP-BMEP was used to calculate the frictional losses for the engine. Calculations were performed at both MIT and CSU to verify the results. For each cylinder:

$$IMEP \quad \frac{\frac{2\ \pi}{360}\int_{180}^{180} P\ dV}{V_d} \tag{7.1}$$

where IMEP is the gross indicated mean effective pressure, P is the in-cylinder pressure, V is the cylinder volume, and V_d is the total displacement per cylinder. The "dV" term is calculated from the engine speed and geometry, and the known relationship of the engine position to the in-cylinder pressure, as indicated by the two optical position measurements. The relationship between volume and crank angle is:

$$dV = \frac{\pi \cdot B^2}{4}\left\{a \cdot \sin(\theta)[1 + \frac{\cos(\theta)}{[l^2 - a^2 \cdot \sin^2(\theta)]^{1/2}}]\right\} \tag{7.2}$$

where B is the bore, a is the crank radius (stroke/2), l is the stroke length and θ is the crank angle. Calculated IMEP values are compared to the engine BMEP, calculated from the dynamometer output by:

$$BMEP = \frac{4\pi\tau}{V_d} \tag{7.3}$$

where τ is the brake torque. The frictional losses are then calculated as the friction mean effective pressure by:

$$FMEP \quad IMEP \quad BMEP \tag{7.4}$$

where the FMEP calculated represents frictional losses for the entire engine. It is unreasonable to assume that no changes occur in frictional losses due to causes other than changing the piston rings between tests, for example, the tear-down and re-build of the engine inevitably introduces some variation. However, it is assumed that most of the change in FMEP between the baseline and other cases is due to the changed piston-rings, as every effort is made to keep other parameters constant.

7.4. Experimental Results and Comparison to Model

In all cases, the experimental measurements indicated that the friction-reduction ring designs proposed by MIT did in fact cause a reduction in engine friction losses.

Figure 7-8 and Figure 7-9 show frictional losses at each tested load for all of the tests performed to date, test configurations 1-4, as described in Table 7-1. For configurations where several tests have been performed for the same ring set-up, averaged test results are shown. Each of the low-friction rings has been tested

individually, with only the optimized case in which all low-friction rings are used together remaining to be validated. Further tests on some individual-ring test cases will also be run, in order to substantiate the results already obtained.

The figures show that, at all loads, test configurations that use reduced-friction designs show lower friction than the baseline test configuration. The single-barrel top ring (SBTR) shows slightly less friction reduction than the low-tension oil control ring (LTOCR), as predicted by MIT models. The lowest frictional losses were obtained when a combination of the LTOCR and negative-twist second ring (NTSR) were used. This was unexpected, as the NTSR was added to reduce oil consumption, and was not expected to have a large effect on ring-pack friction. The effect of the second ring on oil flow and distribution may have had an impact on top and oil control ring friction that was not predicted by the models. It should also be noted that only one test has been run to date on the LTOCR/NTSR combination of rings. Further testing is planned in the near future, and will further illuminate this finding.

Figure 7-9 shows that the reduced-friction test configurations increase the engine mechanical efficiency by 0.5-1.5%, depending on which test configuration is considered. When the optimized test is performed, in which the SBTR, LTOCR and NTSR are all used together, an additive effect is expected, so that the total increase in efficiency should be even greater for this case. The mechanical efficiency used in Figure 7-9 is defined by:

$$\eta_{mech} = \frac{BMEP}{IMEP} \tag{7.5}$$

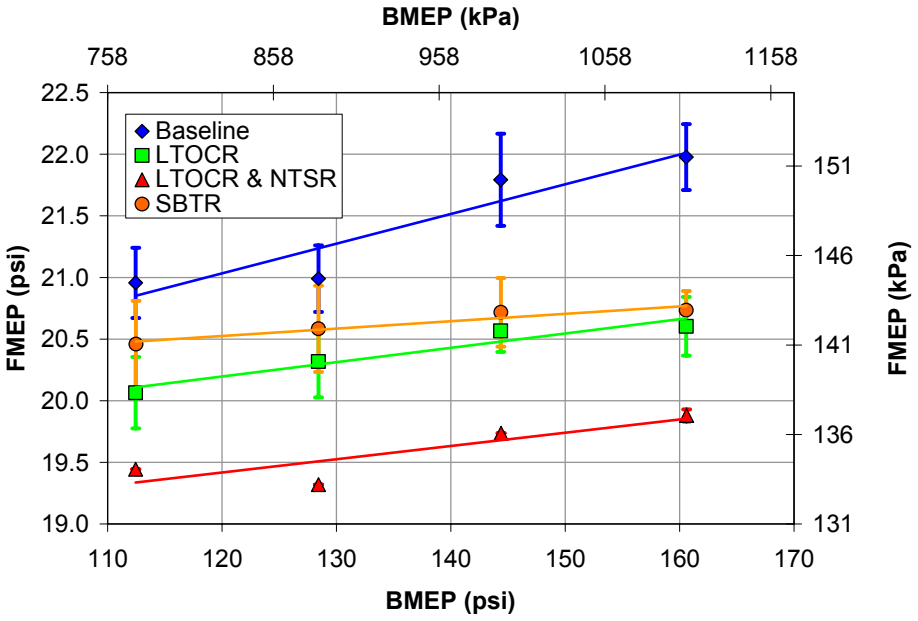

Figure 7-8: FMEP measurements for each test case, as a function of load

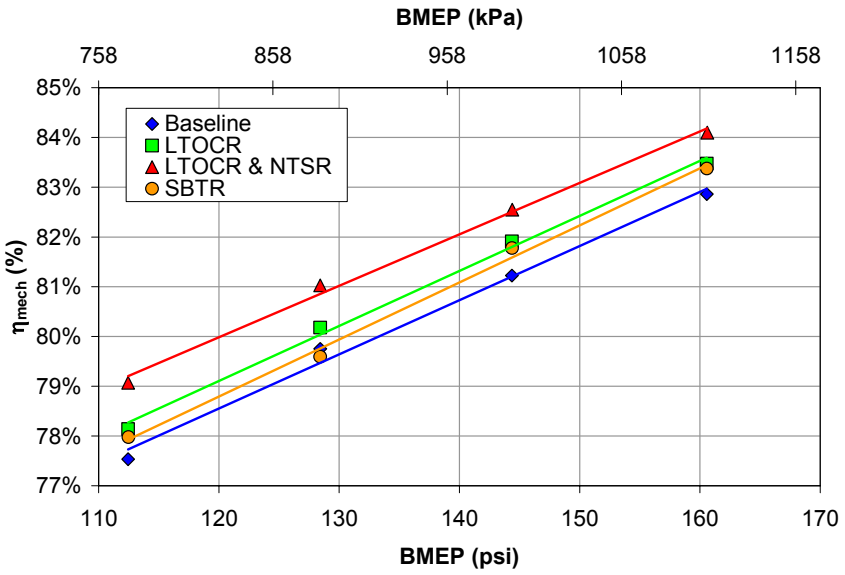

Figure 7-9: Mechanical efficiencies for each test case, as a function of load

Experimental results show larger friction reductions than were predicted by the model, as shown in Figure 7-10. However, the general trend, that the friction-reduction ring designs do reduce friction, is correct. Due to the complexity of the testing system it is not feasible to make a detailed study of the phenomena within the power cylinder that may have contributed to the differences between theory and observation shown. Further testing and model refinement, as well as more controlled testing, should lead to more accurate model predictions in future studies.

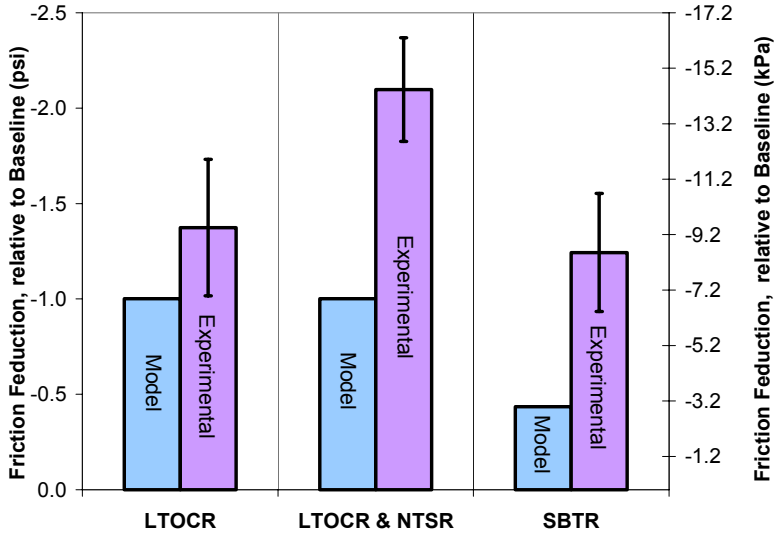

Figure 7-10: Comparison of measured and predicted friction reductions

Oil consumption measurements are also in agreement with the trends predicted. The SBTR has a relatively small effect on oil consumption, as expected. The LTOCR causes a large increase in oil consumption, which was predicted due to the decrease in OCR/liner conformability resulting from the reduced ring tension. The addition of the

NTSR caused a reduction in oil consumption from the case where the low-tension OCR was used alone. Although the second ring modification was not sufficient to reduce oil consumption down to baseline levels, the measured reduction shows that the proposed second ring strategy has the potential to reduce oil consumption, and allow the low tension OCR to be used effectively.

Figure 7-12 shows blow-by flow for each of the test cases. As the figure shows, the effect of the different ring configurations on blow-by is variable. The SBTR configuration shows a slight decrease in blow-by, while the NTSR and LTOCR, together, cause an increase. In all cases the change appears to be relatively minor, however, and is not believed to be a cause for concern.

In general, the in-engine testing has thus far supported the conclusions drawn from the models, and validated friction-reduction ring designs proposed based on those models. The skewed-barrel top ring and low-tension oil control ring have both been shown to reduce friction, compared to baseline rings, when used alone (all other rings kept the same as the baseline configuration). The negative twist second ring has been shown to reduce oil consumption. The optimized test, using all low-friction designed rings, is expected to even further reduce friction, while keeping oil consumption in check.

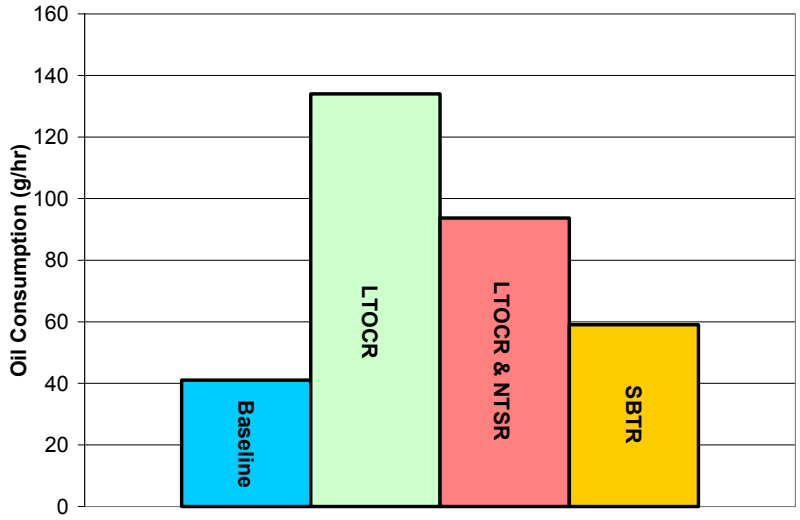

Figure 7-11: Oil consumption measurements for each test case

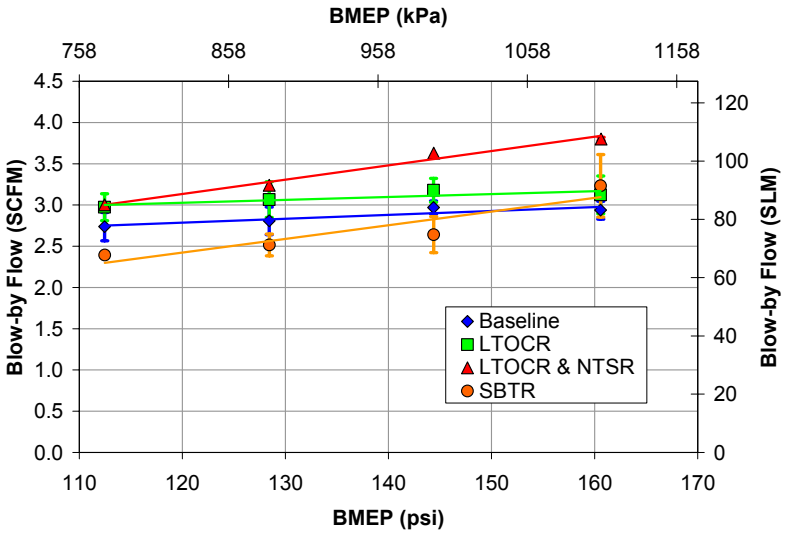

Figure 7-12: Blow-by measurements for each test case

III. SUMMARY AND CONCLUSIONS

The power cylinder is the main contributor to friction power losses in modern internal combustion engines. In this study, work on reducing friction in all power cylinder components was continued, with analyses of lubricant, surface finish, and piston design parameters. Previous analysis and testing of the ring-pack is also ongoing. Results show that there is potential for friction reduction in all of the studied areas.

The focus of this study was on gas-fired reciprocating engines operating in high load, low speed conditions, with specific focus on the Waukesha VGF 18GL engine, which was used as the baseline engine in all studies. Studies on the ring-pack from a previous research phase (2004) indicated that a friction reduction of ~35% was possible with optimized ring designs. In-engine testing supports this conclusion, with all recommended ring designs providing reduced engine friction under standard engine conditions. Further areas of study identified include lubricant, surface treatment, and piston design. These have been analyzed and found to have the potential to reduce friction by 30-50%.

The mechanism of friction reduction in lubricant optimization stems from the lubrication conditions of the rings, during an engine stroke. Near dead-centers, the slow piston speed causes hydrodynamic pressure to be lost and boundary contact to occur, while near mid-stroke, there is relatively little asperity contact and hydrodynamic lubrication dominates. In this mid-stroke region, a minimum frictional loss is reached at a balance between hydrodynamic friction, which increases with lubricant viscosity, and boundary friction, which decreases as viscosity increases. If, lubricant viscosity must be decreased to reach this minimum point, as is the case with the Waukesha engine , there may be a penalty in an increase in boundary friction and wear in the dead-center region. To offset this, lubricant shear rate parameters can be controlled, to maintain high viscosities near dead-centers, while allowing the oil to thin near mid-stroke. Following

this strategy, along with a reduction in lubricant viscosity, a friction reduction of ~12% is predicted for the Waukesha engine ring-pack.

Several surface finish parameters were also studied, including roughness, skewness, and honing cross-hatch angle. A stochastic approach was used, along with an averaged Reynolds equation method using flow factors to account for surface features. Flow factors were calculated using a program developed by Yong Li at MIT. It was found that surface textures that increase resistance to lubricant flow, such as those with low honing angles (honing grooves more perpendicular to flow direction), can reduce friction by allowing the ring load to be supported by hydrodynamic pressure at larger film thicknesses. This serves to reduce asperity contact, and, thus, boundary friction, while not substantially increasing losses due to hydrodynamic friction. It was also found that surfaces with low, negative skewness (more plateau surfaces) can reduce friction by reducing the film thickness at which asperity contact takes place. Combining a low cross-hatch angle and low surface skewness, a friction reduction of ~5% is possible for the baseline engine.

Friction reductions of up to 50% are predicted for optimized piston design, resulting from reducing waviness alone. Pistons with large waviness experience asperity contact at larger film thicknesses, leading to high boundary friction losses. Reducing waviness reduces boundary contact, and thus friction. Other piston parameters were studied and also show the potential to contribute to a reduced friction design, including piston/liner clearance and skirt profile. Lubricant effects were also considered. Several other parameters were identified for future study, including skirt stiffness, surface finish and treatment, and further lubricant study.

Computer models indicate that a total friction reduction of 30-50% is possible through piston, lubricant, and surface optimization. Further consideration must be taken of wear and oil consumption. For example, surfaces of very low skewness may experience scuffing, as has been observed in real engine situations. These possible adverse effects will be fully considered in future analyses. In addition, it should be emphasized that no additional cost would result from the implementation of such designs, and no complex modifications would be needed on existing engine components.

The design strategies developed in this study have promising potential for application in all modern internal combustion engines as they represent simple, low-cost methods to extract significant fuel savings and to reduce harmful environmental damage, without compromising engine performance.

IV. CONTINUING PLANS

Current analyses will be continued and expanded, concurrent with in-engine testing and verification. The piston analysis will be expanded to include the piston skirt stiffness, as well as surface and lubricant effects. Additional surface treatments, such as coatings, and textures, such as micro-dimples, will be considered. Team discussions and University-Industry workshops will be held to ensure that the full potential for friction reduction in these areas will be fully explored, and further areas for study identified.

Design recommendations and low-friction design guidelines will be made, and optimized components tested. Data from the low-friction ring-pack, currently being tested in an improved test-rig at CSU, will be analyzed, and possible design iterations made. Then, mechanical design, lubricant selection, and material effects will be studied as an integrated system. Specific designs of components, lubricant, and material/surface characteristics for a full-scale ARES engine will be recommended, tested and demonstrated. The aggregate improvements will be quantified.

V. ACKNOWLEDGEMENT

This project is sponsored by the United States Department of Energy, Office of Distributed Energy, Advanced Reciprocating Engine Systems (ARES), as part of the Advanced University Reciprocating Engines Program (AUREP) under DOE Cooperative Agreement Number DE-FC26-02NT41339. We appreciate the support of Colorado State University, Dr. Bryan Willson, Ted Bestor, Dr. Rudy Stanglmaier, Kirk Evans, Kris Quillen, and others, in performing the experiment and validation of the results. They are our important university partner in this project. The authors would also like to thank our industrial partner, Waukesha Engine Dresser, Inc., for their support and insight in this study. The authors would like to specifically acknowledge the technical contributions of Ed Reinbold and Rick Donahue of Waukesha, who have worked closely with the MIT team and provided useful input and suggestions throughout the duration of the project. We thank the DOE ARES project monitors, Tom George, Rob Martinez, William Cary Smith, and our technical project monitor Raj Sekar, and in particular the DOE manager and sponsor, Ronald Fiskum for their encouragement and support. Feedback from other industry participants such as Caterpillar and Cummins was very helpful. Prior work and the methodology used in the analyses were supported by related research in the MIT Industrial Consortium on Lubrication in I.C. Engines.

VI. REFERENCES

1. Tian, T., “Modeling the Performance of the Piston Ring-Pack in Internal Combustion Engines,” PhD Thesis, Department of Mechanical Engineering, Massachusetts Institute of Technology, June 1997.
2. Tian, T., Wong, V.W. and Heywood, J.B., “A Piston Ring Pack Film Thickness and Friction Model for Multigrade Oils and Rough Surfaces”, SAE Paper 962032, 1996;

Also in SAE Trans., J. Fuels Lubricants, 1996, 105(4), Pg. 1783-1795
3. Tian, T., Noordzij, L.B., Wong, V.W. and Heywood, J.B., "Modeling Piston-Ring Dynamics, Blowby, and Ring-Twist Effects", ICE - Vol. 27-2, 1996 ASME Fall Technical Conference, Vol. 2, pp. 67-80, Fairborn, Ohio, Oct. 1996
4. Tian, T., "Dynamic Behaviors of Piston Rings and their Practical Impact. Part 1: Ring Flutter and Ring Collapse and their Effects on Gas Flow and Oil Transport", ImechE 2002, Pg. 209-227
5. Tian, T., "Dynamic Behaviors of Piston Rings and their Practical Impact. Part 2: Oil Transport, Friction and Wear of Ring/Liner Interface and the Effects of Piston and Ring Dynamics", ImechE 2002, Pg. 229-247
6. Smedley, G., "Piston Ring Design for Reduced Friction in Modern Internal Combustion Engines," M.S. Thesis, Department of Mechanical Engineering, Massachusetts Institute of Technology, May 2004.
7. Smedley, et. al., "Friction Reduction via Piston and Ring Design for an Advanced Natural-Gas Reciprocating Engine," Proceedings of ICEF04 ASME Internal Combustion Engine Division, #ICEF2004-879.
8. Richardson, D.E., "Review of Power Cylinder Friction for Diesel Engines", Internal Report, Cummins Engine Company
9. Nakada, M., "Piston and Piston Ring Tribology and Fuel Economy", Proceedings of International Tribology Conference, Yokohama, 1995
10. Ting, L.L., "A Review of Present Information on Piston Ring Tribology", SAE Paper 852355, 1985
11. Hill, S.B. and Newman, B.A., "Piston Ring Designs for Reduced Friction", SAE Paper 841222, 1984
12. McGeehan, J.A., "A Literature Review of the Effects of Piston and Ring Friction and Lubricating Oil Viscosity on Fuel Economy", SAE Paper 780673, 1978
13. Cullen, Joao A. and Frodsham, Gary M., "Reduced Cross Section Compression Rings for Diesel Engines", SAE Paper 971146, 1997
14. Graphic from: http://www.roymech.co.uk/Useful_Tables/Tribology/Liquid_Lubrication.htm
15. Hu, Y., Cheng, S., Takayuki, A., Kobayashi, and Y., Aoyama, S., "Numerical Simulation of Piston Ring in Mixed Lubrication – A Nonaxisymmetrical Analysis", Transactions of the ASME, Journal of Tribology, Vol. 116, July 1994, Pg. 470-478.
16. Greenwood, J.A. and Tripp, J.H., "The Contact of Two Nominally Flat Rough Surfaces," Proc. Inst. Mech. Engrs., Vol. 185, pp.625-633.
17. Wong, V., Tian, T., Lang, H., Ryan, J., Sekiya, Y., Kobayashi, Y. and Aoyama, S., "A Numerical Model of Piston Secondary Motion and Piston Slap in Partially Flooded Elastohydrodynamic Skirt Lubrication", International Congress and Exhibition, Detroit, MI, Paper 940696, (1994).
18. Mufti, R. and Priest, M., "Experimental Evaluation of Piston-Assembly Friction Under Motored and Fired Conditions in a Gasoline Engine," ASME Journal of Tribology, Vol. 127, 2005, pp. 826-836.
19. Mainsah, E., Greenwood, J.A. and Chetwynd, D.E., Metrology and Properties of Engineering Surfaces, Springer Verlag, London: 2001.

20. Patir, N. and Cheng, H.S., "Application of Average Flow Model to Lubrication Between Rough Sliding Surfaces," Transactions of the ASME, Journal of Lubrication Technology, Vol. 101, April 1979, pp. 220-229.
21. McCool, J.I., "Comparison of Models for the Contact of Rough Surfaces," Wear, 107, 1986.
22. Hegemeier, T., Stewart, M., "Some Effects of Liner Finish on Diesel Engine Operating Characteristics," SAE paper 930716, 1993.
23. Jeng, Y., "Impact of Plateaued Surface on Tribological Performance," Tribology Transactions, 39, 354-361, 1996.
24. Jocsak, J., "The Effects of Surface Finish on Piston Ring-pack Performance in Advanced Reciprocating Engine Systems", M.S. Thesis, Department of Mechanical Engineering, Massachusetts Institute of Technology, June 2005.
25. Jocsak, J., Wong, V.W. and Tian, T., "The Effects of Cylinder Liner Finish on Piston Ring-Pack Friction," Proceedings of ICEF04 ASME Combustion Engine Division, 2004, Paper # ICEF2004-952.
26. Jocsak, J. et al., "Analyzing the Effects of Three-Dimensional Cylinder Liner Surface Texture on Ring-Pack Performance with a Focus on Honing Groove Cross-Hatch Angle," Proceedings of ICEF05, ASME Combustion Engine Division, 2005, Paper #ICEF2005-1333.
27. Hamilton, D.B., Walowit, J.A. and Allen, C.M., "A Theory of Lubrication by Microasperities", ASME J. Basic Eng., vol. 88, pp. 177-185, 1966.
28. Anno, J.N., Walowit, J.A. and Allen, C.M., "Microasperity Lubrication", ASME Journal of Lubrication Technology, vol. 90, pp. 351-355, 1968.
29. Anno, J.N., Walowit, J.A., and Allen, C.M., "Load Support and leakage from Microasperity-Lubricated Face Seals", ASME Journal of Lubrication Technology, vol. 91, pp. 726-731, 1969.
30. Tian, H., Saka, N., Suh, N., "Boundary Lubrication Studies on Undulated Titanium Surfaces", Tribology Transactions, vol. 32, pp. 289-296, 1989.
31. Kovalchenko, A., Ajayi, O., Erdemir, A., Fenske, G., Etsion, I., "The Effect of Laser Surface Texturing on Transitions in Lubrication Regimes During Unidirectional Sliding Contact", Tribology International, vol. 38, pp. 219-225, 2005.
32. Siripuram, R. and Stephens, L., "Effect of Deterministic Asperity Geometry on Hydrodynamic Lubrication", ASME Journal of Tribology, vol. 126, pp. 527-534, 2004.
33 Etsion, K., Burstein, L., "A Model for Mechanical Seals with Regular Microsurface Structure", Tribology Transactions, vol. 39, pp. 677-683, 1996.
34 Ronen, A., Etsion, I., and Kligerman, Y., "Friction Reducing Surface-Texturing in Reciprocating Automotive Components", Tribology Transactions, vol. 44, pp. 359-366, 2001.
35 Ryk, G., Kligerman, Y., and Etsion, I., "Experimental Investigation of Laser Surface Texturing for Reciprocating Automotive Components", Tribology Transactions, vol. 45, pp. 444-449, 2002.
36 Varenberg, M., Halperin, G. and Etsion, I., "Different Aspects of the Role of Wear Debris in Fretting Wear", Wear, vol. 252, pp. 902-910, 2002.

37 Zhao, J., Sadeghi, F. and Nixon, H., "A Finite Element Analysis of Surface Pocket Effects in Hertzian Line Contact", ASME Journal of Tribology, vol. 122, pp. 47-54, 2000.
38 Moughon, L., and Wong, V.W., "Effects of Lubricant and Piston Design on Reciprocating Engine Friction," Proceedings of ICEF2005, ASME Combustion Engine Division, 2005, Paper #ICEF2005-1343.
39 Mansouri, S.H., and Wong, V.W., "Effects of Piston Design Parameters on Piston Secondary Motion and Skirt-Liner Friction," SAE Paper 2004-01-2911, 2004.

APPENDIX A: DERIVATION OF FUNDAMENTAL EQUATIONS

A.1 Reynolds Equation

The Reynolds equation is used in both the piston and ring simulations to model the behavior of the lubricant. It is based on the fundamental conservation of momentum relationships of the Navier-Strokes equations (A.1) and conservation of mass, or continuity (A.2):

Conservation of Momentum (Navier-Stokes Equations):

x-direction:

$$\rho\left(\frac{\partial u}{\partial t}+u\frac{\partial u}{\partial x}+v\frac{\partial u}{\partial y}+w\frac{\partial u}{\partial z}\right)=-\frac{\partial p}{\partial x}+\mu\left(\frac{\partial^2 u}{\partial x^2}+\frac{\partial^2 u}{\partial y^2}+\frac{\partial^2 u}{\partial z^2}\right)+\rho X$$

y-direction:

$$\rho\left(\frac{\partial v}{\partial t}+u\frac{\partial v}{\partial x}+v\frac{\partial v}{\partial y}+w\frac{\partial v}{\partial z}\right)=-\frac{\partial p}{\partial y}+\mu\left(\frac{\partial^2 v}{\partial x^2}+\frac{\partial^2 v}{\partial y^2}+\frac{\partial^2 v}{\partial z^2}\right)+\rho Y \qquad \text{(A.1)}$$

z-direction:

$$\rho\left(\frac{\partial w}{\partial t}+u\frac{\partial w}{\partial x}+v\frac{\partial w}{\partial y}+w\frac{\partial w}{\partial z}\right)=-\frac{\partial p}{\partial z}+\mu\left(\frac{\partial^2 w}{\partial x^2}+\frac{\partial^2 w}{\partial y^2}+\frac{\partial^2 w}{\partial z^2}\right)+\rho Z$$

Conservation of Mass:

$$\frac{d\rho}{dt}+\frac{\partial}{\partial x}(\rho u)+\frac{\partial}{\partial y}(\rho v)+\frac{\partial}{\partial z}(\rho w)=0 \qquad \text{(A.2)}$$

where ρ is the lubricant density, u, v and w are the flow speeds in the x, y and z directions, respectively, μ is the lubricant dynamic viscosity, and X, Y and Z are external forces acting on the lubricant. With the origin on the surface of interest, the x-axis is

taken along the axis of the cylinder, the y-axis is in the radial direction and the z-axis is as in the tangential direction.

Several simplifying assumptions can be made for both the piston and ring cases:

1. The thickness of the fluid film in the y-direction (radially) is much smaller than in the x and z directions, $h << L_x, L_z$. Then curvature of the film can be ignored.

2. There is negligible pressure variation across the oil in the y-direction: $\frac{p}{y} \quad 0$.

3. Flow is laminar. An approximate Reynolds' number, with typical values, is on the order of: Re $\frac{VD}{\nu} \sim \frac{10\frac{m}{s} * 1e^{6}}{10e^{6}} \quad 1$

4. No external forces act on the fluid film, then $X \quad Y \quad Z \quad 0$.

5. Fluid inertia is small compared to viscous shear – as demonstrated by the low Reynolds numbers involved. Then LHS terms in Eq. (A.1) can be neglected.

6. All velocity gradients are negligible compared to $\frac{\partial u}{\partial y}, \frac{\partial w}{\partial y}$.

With the above assumptions, Eq. (A.1) reduces to:

$$\frac{1}{\mu}\frac{\partial p}{\partial x} = \frac{\partial^2 u}{\partial y^2}$$
$$\frac{1}{\mu}\frac{\partial p}{\partial z} = \frac{\partial^2 w}{\partial y^2} \qquad \text{(A.3)}$$

Then, the following boundary conditions can be applied, to define a no-slip condition between the fluid and two surfaces, (U is the relative speed between the two translating surfaces, h is the separation between the surfaces):

$$u(y=0) = 0$$
$$u(y=h) = U$$
$$w(y=0) = 0 \qquad \text{(A.4)}$$
$$w(y=h) = 0$$

Integration of Eq. (A.3) and application of the above boundary conditions yields the following result:

$$u = \frac{1}{2\mu}\frac{\partial p}{\partial x} y(y-h) + \frac{h-y}{h} U$$
$$w = \frac{1}{2\mu}\frac{\partial p}{\partial z} y(y-h) \qquad \text{(A.5)}$$

Substitution of Eq. (A.7) into the expression for conservation of mass given by Eq. (A.2) yields:

$$\frac{\partial}{\partial y}(\rho v) = -\frac{\partial}{\partial x}(\rho u) - \frac{\partial}{\partial z}(\rho w) \qquad \text{(A.6)}$$

The following boundary conditions are then applied, which link the radial movement of the fluid with the radial movements of the two surfaces.

$$v(y=0)=\frac{\partial h}{\partial t}$$
$$v(y=h)=0 \qquad \text{(A.7)}$$

Now, integrating Eq. (A.6) with respect to y and applying the boundary conditions, and assuming an incompressible lubricant, yields:

$$\frac{\partial}{\partial x}\left(\frac{h^3}{\mu}\frac{\partial p}{\partial x}\right)+\frac{\partial}{\partial z}\left(\frac{h^3}{\mu}\frac{\partial p}{\partial z}\right)=6U\frac{\partial h}{\partial x}+12\frac{\partial h}{\partial t} \qquad \text{(A.8)}$$

This is the two-dimensional Reynolds Equation for incompressible lubricants. For the case of the piston, the full 2-D equation must be used to account for fluid distribution between the piston skirt and liner. For the rings, however, a simplified relationship can be used.

A.1.1: 1-Dimensional Reynolds Equation – Rings

In the case of the piston rings, the two-dimensional Reynolds equation can be further simplified to a 1-D case, if it is assumed that negligible fluid flow takes place around the circumference of the ring. Then, Eq. A.8 can be simplified to:

$$\frac{}{x}\ \frac{h^3}{\mu}\frac{p}{x}\quad 6U\frac{h}{x}\ \ 12\frac{h}{t} \qquad \text{(A.9)}$$

This relationship is used to study lubrication conditions on one part of the ring.

A.2 Shear Stress and Volumetric Flow Rate of Oil

The same relationships given above in equations A.1 and A.2 are used to derive the shear stress and volumetric flow rate of the oil. The derivation given below is the 1-D case, based on Eq. A.9, for simplicity in demonstrating the concepts. However, the method of derivation is applicable to multi-dimensional cases, including both piston and rings.

Beginning again with Eqs. A.3, and the boundary conditions given in A.4, an expression for the axial velocity of lubricant flow is obtained:

$$u\quad \frac{1}{2\mu}\frac{p}{x}y(y\quad h)\quad \frac{h\quad y}{h} \qquad \text{(A.10)}$$

It should be noted that performing the integration in this way assumes that the viscosity is not a function of the distance from the liner in the cross-flow direction. However, for a shear-thinning fluid, the viscosity is a function of the local shear rate, which is given by the rate of change of the velocity in the cross-flow direction. Although

many oils are shear-thinning fluids, it has been shown in [1] that accurate results can be obtained for these oils by approximating the viscosity as the piston speed divided by the average distance between the nominal lines defining the ring and liner surfaces. Therefore, the above integration is still valid even in these cases.

Shear stress is given by:

$$\tau(x) = \mu \left. \frac{\partial u}{\partial y} \right|_{y=0} \tag{A.11}$$

Then, using Eq. (A.10):

$$\tau(x) = \frac{\mu U}{h} - \frac{h}{2}\frac{dp}{dx} \tag{A.12}$$

The volumetric flow rate can also be derived using the above results:

$$Q(x) = \int_0^h u(y)dy \tag{A.13}$$

Using Eq. (A.10):

$$Q(x) = -\frac{h^3}{12\mu}\frac{dp}{dx} + \frac{Uh}{2} \tag{A.14}$$

A.3 Piston Dynamics: Equations of Motion

The equations of motion for the piston are derived from x and y direction force balances and momentum balance given in section II.2.6.1, with parameters given in Table 2-1. From the force and momentum balance relationships, two terms can be defined which do not depend on piston contact:

$$F_\sigma \quad (F_g \quad \hat{F}_{IP} \quad \hat{F}_{IC} \qquad F_{qj})\tan\phi \qquad F_{rj} \tag{A.15}$$

$$M_s \quad M_{PP} \quad F_g C_p \quad F_{IC} C_g \quad C_p \quad F_{qj} \qquad F_{rj} I_j \tag{A.16}$$

Then, including the following relationships:

$$M_{IP} \quad M_{IC} \qquad I_{PP}\left(\frac{\ddot{e}_t \quad \ddot{e}_b}{L}\right) \tag{A.17}$$

$$F_{IP} \qquad m_{PP} \; \frac{\ddot{e}_t \quad a(\ddot{e}_b \quad \ddot{e}_t)}{L} \tag{A.18}$$

$$F_{IC} \quad m_{Pis}(\ddot{e}_t \quad b(\ddot{e}_b \quad \ddot{e}_t) \tag{A.19}$$

the equations of motion given in section II.2.6.1 are derived, and re-presented below:

$$\begin{matrix} m_{PP}(1 \quad \frac{a}{L}) \quad m_{Pis}(1 \quad \frac{b}{L}) & m_{PP}\frac{a}{L} \quad m_{Pis}\frac{b}{L} & \ddot{e}_t & F_\sigma & F_s\delta_s \quad F_f \tan\phi \\ \frac{I_{Pis}}{L} \quad m_{Pis}(a \quad b)(1 \quad \frac{b}{L}) & m_{Pis}(a \quad b)\frac{b}{L} \quad \frac{I_{Pis}}{L} & \ddot{e}_b & M_s & F_s y_s \delta_s \quad M_f \end{matrix} \tag{A.20}$$

Then, $\ddot{e}_t$ and $\ddot{e}_b$, the piston eccentricities, are functions of themselves, their time derivatives, and the terms defined in A.10 and A.11:

$$\ddot{e}_t \quad F_\sigma(t) \quad G_1(e_t, \dot{e}_t, e_b, \dot{e}_b, t) \tag{A.21}$$

$$\ddot{e}_b \quad M_s(t) \quad G_2(e_t, \dot{e}_t, e_b, \dot{e}_b, t) \tag{A.22}$$

These equations are solved for the piston position and tilt as a function of time, iteratively with the hydrodynamic relationships given in section II.2.6.2.

APPENDIX B: METRICS FOR EVALUATING FRICTION REDUCTION

B.1. Determination of FMEP in the Friction Models

FMEP - friction mean effective pressure - is a measure of the work done by friction normalized by the engine's displaced volume. It is a useful metric with which to compare the performance of different engines in a way that removes the effect of engine or component size. In this study, it provides a simple metric used to evaluate and compare the performance of different piston ring designs.

The determination of the friction force is determined by the model for hydrodynamic, mixed and pure boundary lubrication conditions, and is described in Section 2. Friction work losses for a cycle can then be determined by integrating this friction force over the distance traveled by the piston, for an engine cycle. Dividing this total friction work loss per cycle by the displaced volume gives FMEP:

$$FMEP \quad \frac{\int_{cycle} F_f \, dx}{V} \tag{B.1}$$

where F_f is the ring/liner friction force, for a given ring, x is the axial direction (direction of piston movement) and V is the displaced volume for an engine cycle. This integration is performed numerically by the friction model.

B.2. Determination of FMEP from Experimental Measurements

FMEP is determined experimentally from three key measurements: gas pressure inside the cylinders; piston positions during engine operation; and the output brake power of the engine. The in-cylinder pressure and piston position data are used to calculate the net IMEP – indicated mean effective pressure – in each cylinder. The IMEP is a measurement of the work delivered to the piston by the cylinder gases. The brake power data is used to calculate BMEP – brake mean effective pressure – for the engine. The BMEP is a measurement of the output work from the engine, normalized by engine volume.

Calculations were performed at both MIT and CSU to verify the results. For each cylinder:

$$IMEP \quad \frac{\frac{2\ \pi}{360}\int_{360}^{360} P\ dV}{V_d} \tag{B.2}$$

where IMEP is the net indicated mean effective pressure, P is the in-cylinder pressure, V is the cylinder volume, and V_d is the total displacement per cylinder. The net imep is used so that any changes in pumping work are not taken into account in the FMEP calculation, eliminating one source of variability in mechanical losses. The "dV" term is calculated from the engine speed and geometry, and the known relationship of the engine position to the in-cylinder pressure, as indicated by the two optical position measurements. The relationship between volume and crank angle is:

$$dV = \frac{\pi \cdot B^2}{4}\left\{a \cdot \sin(\theta)[1 + \frac{\cos(\theta)}{[l^2 - a^2 \cdot \sin^2(\theta)]^{1/2}}]\right\} \tag{B.3}$$

where B is the bore, a is the crank radius (stroke/2), l is the stroke length and θ is the crank angle. A mean of IMEP values for each cylinder was obtained, and compared to the BMEP, calculated from the dynamometer output by:

$$BMEP = \frac{4\pi\tau}{V_d} \tag{B.4}$$

where τ is the brake torque. The mechanical losses, not including pumping work, are then calculated as the friction mean effective pressure by:

$$FMEP \quad IMEP \quad BMEP \tag{B.5}$$

where the FMEP calculated represents frictional losses for the entire engine. It is unreasonable to assume that no changes occur in frictional losses due to causes other than changing the piston rings between tests, for example, the tear-down and re-build of the engine inevitably introduces some variation. However, it is assumed that most of the change in FMEP between the baseline and other cases is due to the changed piston-rings.

B.3. Error Analysis of Experimental Results

For each of the rings that were tested, a statistical analysis was conducted to determined whether or not a reduction in the mean FMEP was achieved. Although testing conditions were kept as constant as possible, it is impossible to eliminate cycle to cycle variation of combustion pressures, so that there was variation between cycle to cycle IMEP measurements over the course of all tests. Data was taken for a large number of cycles (1000 cycles for each test point) to reduce the effects of this variability. Variability in other measurements, such as BMEP, were also present, but this variation was much smaller than the variability introduced by cycle to cycle combustion changes.

The propagation of the variability in measured cylinder pressure values was accounted for using a general equation that is used to determine the error as a result of a calculation. For a function of two variables, $f(x_1,x_2)$, if the errors in the independent variables were Δx_1 and Δx_2, the error as a result of an operation is determined by:

$$\Delta f(x_1, x_2) = \sqrt{\left(\frac{\partial f}{\partial x_1}\Delta x_1\right)^2 + \left(\frac{\partial f}{\partial x_2}\Delta x_2\right)^2} \qquad \text{(B.6)}$$

This relationship was used to calculate the propagated error in measured FMEP values. The large number of samples taken allowed this error to be relatively small compared to the FMEP values calculated, so that the changes in FMEP measured were shown to be statistically significant.